CSSB
Centre for Structural
Systems Biology

BNITM
Bernhard-Nocht-Institut für Tropenmedizin

Identification and localization of putative SPM3 associated proteins in *Plasmodium falciparum* gametocytes

Dissertation

With the aim of achieving a doctoral degree at the Faculty of Mathematics, Informatics and Natural Science

Department of Biology
University of Hamburg

Submitted by
Korbinian Niedermüller

Hamburg, 2025

1st Supervisor: Tim-Wolf Gilberger

2nd Supervisor: Michael Filarsky

Date oft he Disputaion: 12.12.2025

Eidesstattliche Versicherung:

Hiermit versichere ich an Eides statt, die vorliegende Dissertationsschrift selbst verfasst und keine anderen als die angegebenen Hilfsmittel und Quellen benutzt zu haben.

Sofern im Zuge der Erstellung der vorliegenden Dissertationsschrift generative Künstliche Intelligenz (gKI) basierte elektronische Hilfsmittel verwendet wurden, versichere ich, dass meine eigene Leistung im Vordergrund stand und dass eine vollständige Dokumentation aller verwendeten Hilfsmittel gemäß der Guten wissenschaftlichen Praxis vorliegt. Ich trage die Verantwortung für eventuell durch die gKI generierte fehlerhafte oder verzerrte Inhalte, fehlerhafte Referenzen, Verstöße gegen das Datenschutz- und Urheberrecht oder Plagiate.

Affidavit

I hereby declare and affirm that this doctoral dissertation is my own work and that I have not used any aids and sources other than those indicated.

If electronic resources based on generative artificial intelligence (gAI) were used in the course of writing this dissertation, I confirm that my own work was the main and value-adding contribution and that complete documentation of all resources used is available in accordance with good scientific practice. I am responsible for any erroneous or distorted content, incorrect references, violations of data protection and copyright law or plagiarism that may have been generated by the gAI.

Hamburg, den Unterschrift

Erläuterungen zur Nutzung von generativer KI (gKI) in der Dissertation

Ich versichere, dass ich generative Künstliche Intelligenz (KI)-Tools nur in dem Umfangverwendet habe, der mit der Prüferin/dem Prüfer/den Prüfenden vereinbart wurde.

Ich versichere, dass ich mich Internetquellen oder KI-Anwendungen nur in der unten ausgewiesenen Form bedient habe. Alle Stellen, die wörtlich oder sinngemäß aus Veröffentlichungen entnommen wurden, sind als solche kenntlich gemacht.

Ich versichere, dass ich mich KI-Tools lediglich als Hilfsmittel bedient habe und in der vorliegenden Arbeit mein gestalterischer Einfluss überwiegt. Ich bin mir bewusst, dass die Nutzung maschinell generierter Texte keine Garantie für die Qualität von Inhalten und Text gewährleistet.

Ich verantworte die Übernahme jeglicher von mir verwendeter maschinell generierter Textpassagen vollumfänglich selbst und dokumentiere im folgenden listenartig, für welche Aufgaben ich KI-Tools genutzt habe.

In der hier vorliegenden Arbeit habe ich gKI-Systeme wie folgt genutzt:

-Korrekturlesen mit Schwerpunkt Grammatik und Vokabular

-Erstellen von Fließtexten aufbauend auf Stichpunkten

-Optimierung der Lesbarkeit

Ich versichere, alle Nutzungen vollständig angegeben zu haben. Mir ist bekannt, dass fehlende oder fehlerhafte Angaben als Täuschungsversuch gewertet werden können. Zudem bin ich bereit, auf Nachfrage meine Vorgehensweise (z. B. durch Arbeitsnotizen, Prompts oder mündliche Erläuterungen u.Ä.) offen zu legen.

Hamburg,

Korbinian Niedermüller

Table of contents

Image Index

Table Index

Abbreviation

Table 1: Abbreviations

General abbreviations		Protein abbreviations	
AAPs	Apical Annuli Proteins	**AMA1**	Apical Membrane Antigen 1
AF594	Alexa Fluorophore 594nm	**ARA1**	Apical Ring Associated protein 1
APR	Apical Polar Ring	**ARK1/3**	Aurora-Related Kinase 1/3
BC	Basal Complex	**CDPK1**	Calcium Dependent Protein Kinase 1
CP	Centriolar Plaque	**CPAP**	Centrosomal P4.1-Associated Protein
DAPI	4',6-diamidino-2-phenylindole	**CSP**	Circumsporozoite Protein
DHE	Dihydroethidium (Hydroethidine)	**DHHC1**	Aspartate-Histidine-Histidine-Cysteine palmetyl transferase
DIC	Differential interference contrast	**EB1**	End-Binding protein 1
DNA	Deoxyribonucleic acid	**EBA175**	Erythrocyte Binding Antigen 175
Dpi	Days post induction	**EMP1**	Erythrocyte Membrane Protein 1

EM	Electron Microscopy	**GAPM**	Glideosome Associated Protein with multiple Membrane spans
FKBP	FK506-binding protein	**GDV1**	Gametocyte Development factor 1
FRB	FKBP-rapamycin binding	**GEXP19**	Gametocyte Exported Protein 19
GDP	Guanosine Diphosphate	**GPA**	Glycophorin A
ger	German	**HP1**	heterochromatin Protein 1
GFP	Green Fluorescent Protein	**KIC11**	Kelch 13 Interacting Candidate 11
GlcNAc	N-Acetyl-Glucosamine	**MIC2**	Microneme Protein 2
GlmS	glucosamine-6-phosphate riboswitch	**MSP**	Merozoite Surface Protein
GTP	Guanosine Triphosphate	**MTIP**	Myosin Tail Interacting Protein
IDC	Intraerythrocytic Development Cycle	**PhIL1**	Photosensitized INA-Labelled protein 1
IMC	Inner Membrane Complex	**PIP**	PhIL1 Interacting Protein
ISC	IMC Suture Component	**PKRP**	Protein Kinase Related Protein
ISP	IMC Sub-compartment Protein	**RH1**	reticulocyte-binding homolog 1
ITN	Insecticide Treated Nets	**RON**	Rhoptry Neck protein
kDa	kilo Daltons	**SAS**	spindle assembly abnormal protein
KO	Knock Out	**SPM1**	Subpellicular Microtubule protein 1
LIMMA	Linear Models for Microarray Data	**SPM3**	Subpellicular Microtubule protein 3
logFC	logarithmic Fold Change	**TBCCD1**	Tubulin Binding Cofactor Containing 1
MAP	Microtubule Associated Protein	**TRAP**	thrombospondin-related anonymous protein
mRNA	Messenger RNA		
MT	Microtubule		
MTOC	Microtubule Organization Center		
nucMT	nuclear Microtubule		
PCR	Polymerase Chain reaction		
PFA	Paraformaldehyde		
PI3P	Phosphatidylinositol 3-Phosphate		
PPM	Parasite Plasma Membrane		
PV	Parasitophorous Vacuole		
PVM	Parasitophorous Vacuolar Membrane		
RBC	Red Blood Cell		
RBCM	Red Blood Cell Membrane		
RNA	Ribonucleic Acid		
SLI	Selection Linked Integration		
SLS	Suture Like Structures		
SPMT	Subpellicular Microtubule		
SPN	Subpellicular Network		
TGD	Targeted Gene Disruption		
TMD	Transmembrane Domain		

TOG-domain	Tumor Over-expressed Gene-domain
TSC	transverse suture component
TuTr	Tubulin Tracker (deep red)
WHO	World Health Organization
WT	Wilde Type
yTuRC	y Tubulin Ring Complex

Publications

Niedermüller, K.; Piwon, N.; Mesen-Ramirez, J. P.; Liffner, B.; Fernandes, C. F.; Farias, G. B.; Alder, A.; Löw, C.; Wilson, D. W.; Gilberger, T-W. An atlas of novel microtubule associated proteins in the malaria parasite *Plasmodium falciparum*. mBio 2025 (under revision)

Pietsch, E.; **Niedermüller, K**.; Gilberger, T-W.; Burda, P-C. Disruption of a *Plasmodium falciparum* patatin-like phospholipase delays male gametocyte exflagellation. Mol. Microbiol. 2024 Mar;121(3):529-542. doi: 10.1111/mmi.15211. Epub 2023 Dec 22.
PMID: 38131156

Pietsch, E.; Ramaprasad, A.; Bielfeld, S.; Wohlfarter, Y.; Maco, B.; **Niedermüller, K**.; Wilcke, L.; Kloehn, J.; Keller, M. A.; Soldati-Favre, D.; Blackman, M. J.; Gilberger, T-W.; Burda, P-C. A patatin-like phospholipase is important for mitochondrial function in malaria parasites. mBio 2023 Dec 19;14(6):e0171823. doi: 10.1128/mbio.01718-23. Epub 2023 Oct 26.
PMID: 37882543

Note of Thanks

I would like to express my sincere gratitude to Prof. Tim Gilberger for providing me with the invaluable opportunity to write my dissertation. It was a truly enriching experience to delve into such a fascinating field of research under his guidance. I am particularly grateful for the freedom he granted me to pursue my work in my own way. The time spent working under his supervision was truly amazing.

I also extend my thanks to Prof. Michael Filarsky for his co-supervision of my dissertation and for his crucial role in steering my scientific endeavors in the right directions.

My sincere appreciation goes to Dr. Paul-Christian Burda and Dr. Joelle Mesen-Ramirez for their excellent training and supervision in the laboratory. I am also thankful for their constant input and unwavering support.

I would like to thank my BNITM-internal co-supervisors, Dr. Joachim Matz and Dr. Tobias Spielmann, for their time and invaluable assistance throughout this project.

Furthermore, I wish to acknowledge our international collaborators, especially Danny Wilson, Noa Dahan, Ron Dzikowski, and Mathew Dixon, for their insightful scientific discussions and for always being receptive to my ideas and interpretations.

Finally, a big thank you to the entire Gilberger Group at the CSSB, as well as the Matz and Bachman groups at the BNITM. Thank you very much for three amazing years filled with hard work, dedication, and perseverance, but also with a great deal of joy, laughter, and collaborative spirit.

Abstract

Malaria is a tropical disease caused by protozoan parasites of the genus *Plasmodium* and its various subspecies. The most severe form of malaria, malaria tropica, is caused by *Plasmodium falciparum*. *P. falciparum* holds a unique position among other human infecting *plasmodium* species, generating falciform (crescent-shaped) gametocytes, which are essential for transmission to mosquitoes. Despite extensive research efforts, the underlying cellular mechanisms and biological rationale for the formation of these distinctive falciform gametocytes remain poorly understood.

The major morphological changes observed during gametocytogenesis are thought to be driven by two structural components: the inner membrane complex (IMC) and the underlying subpellicular microtubules (SPMTs). These cytoskeletal structures are supposed to be crucial for the elongation, shaping, and rigidity of the developing gametocyte.

Recent research identified PfSPM3, a subpellicular microtubule-associated protein, as an essential factor in gametocyte development. It has been hypothesized that PfSPM3 may facilitate the connection between the IMC and the SPMTs.

To further explore this potential function, we employed a BioID proximity labeling approach using PfSPM3 as bait to identify putative interaction partners. This approach revealed 133 as “enriched hits” annotated proteins of which we classified 26 as likely SPM3 interacting candidates. To characterize their roles during gametocytogenesis, we generated GFP-fusion constructs to localize these candidates in a stage-specific and subcellular context. This localization screen led to the identification of

i) four proteins that colocalized with microtubules in gametocytes, suggesting potential structural or regulatory functions within the SPMT network,

ii) four proteins that predominantly localized to the tips of the subpellicular microtubules, three of which also showed a clear centriolar plaque localization in asexual parasites and

iii) six proteins with a suture-like localization pattern across the gametocyte.

Notably, the protein PF3D7_1449100 localized not only in a suture-like pattern but also at the microtubule tips in both gametocytes and asexual stages.

Functional disruption of PF3D7_1003400 led to the formation of abnormally shaped gametocytes arrested at Stage III, suggesting a critical role in maintaining structural integrity during early gametocyte maturation.

This thesis provides a comprehensive overview of protein localization during *P. falciparum* gametocytogenesis. By identifying novel structural and regulatory components involved in this essential life cycle stage, this work lays a foundation for future investigations into the molecular mechanisms of gametocyte maturation and offers valuable insights that may inform future strategies for blocking malaria transmission at the sexual stage.

Zusammenfassung

Malaria ist eine Tropenkrankheit, die jährlich mehrere Hunderttausend Todesopfer fordert Malaria ist eine Tropenkrankheit, die durch einzellige Parasiten der Gattung *Plasmodium* verursacht wird. Die schwerste Form der Malaria, die Malaria tropica, wird durch *Plasmodium falciparum* ausgelöst. Nur diese Art bildet sichelförmige (falciforme) Gametozyten – ein besonderes Stadium des Parasiten, dass für seine Übertragung auf Moskitos unerlässlich ist. Trotz umfangreicher Forschung sind die zu Grunde legenden Mechanismen und die biologische Bedeutung dieser sichelförmigen Gametozyten unzureichend geklärt.

Es wird angenommen, dass die wesentlichen morphologischen Veränderungen, die während der Gametozytogenese beobachtet werden, durch zwei strukturelle Komponenten angetrieben werden: den inneren Membrankomplex (inner membrane compley, IMC) und die darunterliegenden subpellikulären Mikrotubuli (subpellicular microtubule, SPMTs). Diese Zellstrukturen sind möglicherweise entscheidend für die Elongation, Formgebung und Rigidität des sich entwickelnden Gametozyten.

Neuste Forschungsergebnisse haben PfSPM3, ein mit subpellikulären Mikrotubuli assoziiertes Protein, als einen essenziellen Faktor in der Gametozytenentwicklung identifiziert. Es wird vermutet, dass PfSPM3 eine Verbindung zwischen dem IMC und den SPMTs darstellen könnte.

Um diese potenzielle Funktion weiter zu untersuchen, haben wir einen BioID-Proximity-Labeling-Ansatz genutzt. Dabei diente PfSPM3 als Köder, um potenzielle Interaktionspartner aufzuspüren. Dieser Ansatz enthüllte 133 als „angereicherte Treffer“ klassifizierte Proteine, von denen wir 26 als wahrscheinliche SPM3-Interaktionskandidaten einstuft haben. Um ihre Rolle während der Gametozytogenese zu untersuchen, haben wir GFP-Fusionskonstrukte für jeden Kandidaten generieret, um deren Position in einem stadien-spezifischen und subzellulären Kontext zu bestimmen. Dieses Lokalisierungs-Screening führte zur Identifizierung von:

i) vier Proteinen, die in Gametozyten mit Mikrotubuli kolokalisieren, was auf potenzielle strukturelle oder regulatorische Funktionen innerhalb des SPMT-Netzwerks hindeutet,

ii) vier Proteinen, die vorwiegend an den Spitzen der subpellikulären Mikrotubuli lokalisiert sind, und von denen drei eine deutliche Zentriolen-Lokalisation in asexuellen Parasiten zeigen, und

iii) sechs Proteinen mit einem Suture-ähnlichen Lokalisierungsmuster in Gametozyten.

Bemerkenswerterweise lokalisierte das Protein PF3D7_1449100 nicht nur in spezialisierten Bereichen des IMCs in den Gametozyten, sondern auch an deren Mikrotubuli-Enden. Dieses Lokalisation konnte auch in den asexuellen Stadien gezeigt werden. Zusätzlich führte die funktionelle Inaktivierung von PF3D7_1003400 zur Bildung

abnormal geformter Gametozyten, die im Stadium III arretierten waren. Dieses deutet auf eine kritische Rolle dieses Proteins bei der Aufrechterhaltung der strukturellen Integrität während der frühen Gametozyten-Entwicklung hin.

Diese Arbeit bietet einen umfassenden Überblick über die Lokalisation ausgewählter Proteine während der Gametozytogenese in *P. falciparum*. Durch die Identifizierung neuer struktureller und regulatorischer Komponenten, die an diesem essentiellen Lebenszyklus-Stadium beteiligt sind, legt diese Arbeit eine Grundlage für zukünftige Untersuchungen der molekularen Mechanismen der Gametozyten-Entwicklung und bietet wertvolle Einblicke, die zukünftige Strategien zur Blockierung der Malariaübertragung im sexuellen Stadium beeinflussen könnten.

Chapter 1: Introduction

1.1 Background Malaria

Malaria is a life-threatening tropical disease caused parasites of the genus *Plasmodium*, which are transmitted through the bite of an infected female *Anopheles* mosquito (1). The disease remains one of the most significant global health challenges, particularly in tropical and subtropical regions (2; 3).

In 2023, an estimated 263 million cases of malaria were reported worldwide, leading to approximately 597,000 deaths. Alarmingly, over 70% of these fatalities occurred in children under the age of five (3). These figures are 55% higher than the targets set by the World Health Organization for malaria eradication by 2025, highlighting the challenges in achieving global malaria control goals (4).

Currently, nearly half of the global population is at risk of malaria infection. The burden of the disease remains disproportionately high in Africa, where 95% of all malaria cases (approximately 246 million) were recorded in 2023. Nigeria alone accounted for nearly one-third of cases (25.9%) and deaths (30.9%), underscoring the regional disparity in disease prevalence (Fig. 1) (3).

Malaria is a disease with a wide spectrum of clinical manifestations, ranging from mild to severe cases. In its early stages, malaria is often difficult to diagnose due to its nonspecific symptoms, which include fever, fatigue, and headaches. However, one of the most characteristic features of human malaria infections is the presence of periodic fever episodes, which result from the synchronous asexual replication of *Plasmodium* parasites within red blood cells. The timing of these fever cycles varies depending on the *Plasmodium* species responsible for the infection (5; 6).

Malaria tertiana (ger.: *Dreitagsfieber)* is a relatively mild form of malaria characterized by fever paroxysms occurring every 48 hours. This form is caused by *Plasmodium vivax* and *Plasmodium ovale* (7; 8; 9). A distinct feature of *P. vivax* infections is their ability to cause relapses due to the presence of dormant liver-stage parasites known as hypnozoites. These hypnozoites can remain in the liver for weeks, months, or even years before reactivating and initiating another symptomatic episode of malaria, making eradication of the infection particularly challenging (10).

Malaria quartana (ger.: *Viertagsfieber*) is the least common form of malaria and is characterized by fever paroxysms occurring every 72 hours. This form is caused by *Plasmodium malariae* (7; 8). Unlike *P. vivax*, *P. malariae* does not form hypnozoites and therefore does not cause relapses. However, infections with *P. malariae* can persist for years, sometimes even decades, due to its ability to remain at low levels in the bloodstream without causing overt symptoms (11).

Figure 1: Global distribution of malaria.
Schematic map depicting the global distribution of Malaria, based on the WHO world malaria report 2023.

The most severe form of malaria, known as malaria tropica, is caused by *Plasmodium falciparum*. Unlike the other types of malaria, malaria tropica does not typically exhibit a regular fever periodicity. Instead, it is associated with high parasite loads and severe complications, collectively termed complicated malaria (12). This life-threatening form of the disease can lead to cerebral malaria (malaria-related encephalitis) (13), placental malaria in pregnant women (14), severe anemia, multi-organ failure (15), and, if left untreated, death. The severity of *P. falciparum* infections is largely attributed to its ability to cause cytoadherence, wherein infected red blood cells adhere to blood vessel walls, leading to blockages in microcirculation and severe organ damage (16). While cytoadherence is mostly associated with *P. falciparum*, it has been reported in other species as well (17; 18).

Efforts to combat malaria have been ongoing for decades. The global malaria eradication programs, initiated by the WHO in 1947, significantly reduced the number of endemic countries (3; 19). However, in recent years, malaria cases have resurged due to various factors, including climate change (20), increased global travel (21), socio-political instability (22), and the growing resistance of *Plasmodium* parasites to antimalarial drugs (23), as well as insecticide resistance in mosquito vectors (24).

Preventive measures such as insecticide-treated bed nets (ITNs), indoor residual spraying (IRS), and chemoprophylaxis using artemisinin play a critical role in malaria control (19). In addition, vaccination has emerged as a promising tool for reducing mortality, especially in children. Currently, two malaria vaccines, RTS,S/AS01 (Mosquirix) (25) and R21/Matrix-M (26), are recommended by the WHO for use in endemic regions (19).

RTS,S is a recombinant protein-based vaccine composed of two main components: a repeat (R) and a T-cell epitope (T) derived from the *Plasmodium falciparum* circumsporozoite protein (CSP), fused with the surface antigen (S) of the hepatitis B virus. Although this vaccine provides partial protection, its efficacy wanes over time, leading to a moderate reduction in malaria incidence and mortality (25; 27).

In contrast, R21 is an improved version of RTS,S that utilizes similar CSP components but omits the excess hepatitis B surface antigen. Instead, it incorporates the adjuvant Matrix-M, which enhances immune response and is also used in the Novavax COVID-19 vaccine (28). R21 has demonstrated a higher efficacy of approximately 77% and induces significantly higher antibody levels compared to RTS,S, making it a more promising candidate for large-scale deployment (29).

Despite these advances, challenges remain in the widespread implementation of malaria vaccines, including production scalability, delivery logistics, and sustained funding for immunization programs (4). A multifaceted approach integrating vaccination, vector control, early diagnosis, and effective treatment will be essential to achieving global malaria eradication goals in the coming decades (19).

1.2 Human malaria parasites

Malaria is caused by protozoan parasites, which infect both humans and non-human hosts. Among the five *Plasmodium* species known to infect humans, *P. falciparum* and *P. vivax* are the most prevalent. *P. falciparum* is primarily responsible for malaria cases in African countries, while *P. vivax* is more common in Asia and South America. The other three human-infecting species—*P. malariae*, *P. knowlesi*, and *P. ovale*—occur less frequently but still contribute to the global malaria burden (3).

In addition to human-infecting *Plasmodium* species, there are more than 200 non-human *Plasmodium* species that infect vertebrates from reptiles, birds to rodents and primates (Fig. 2) (30). Notably, the rodent malaria parasite *P. berghei* has been extensively used in laboratory research due to its suitability for experimental studies on malaria pathogenesis and drug development (31; 32; 33).

Besides *P. berghei, P. falciparum* is one of the most well-studied *Plasmodium* species due to its high virulence and global impact. This has led to extensive research into its biology, pathogenesis, and potential therapeutic interventions. Unlike other malaria forms, malaria tropica does not exhibit a strictly periodic fever cycle, making its clinical diagnosis more challenging (16; 12).

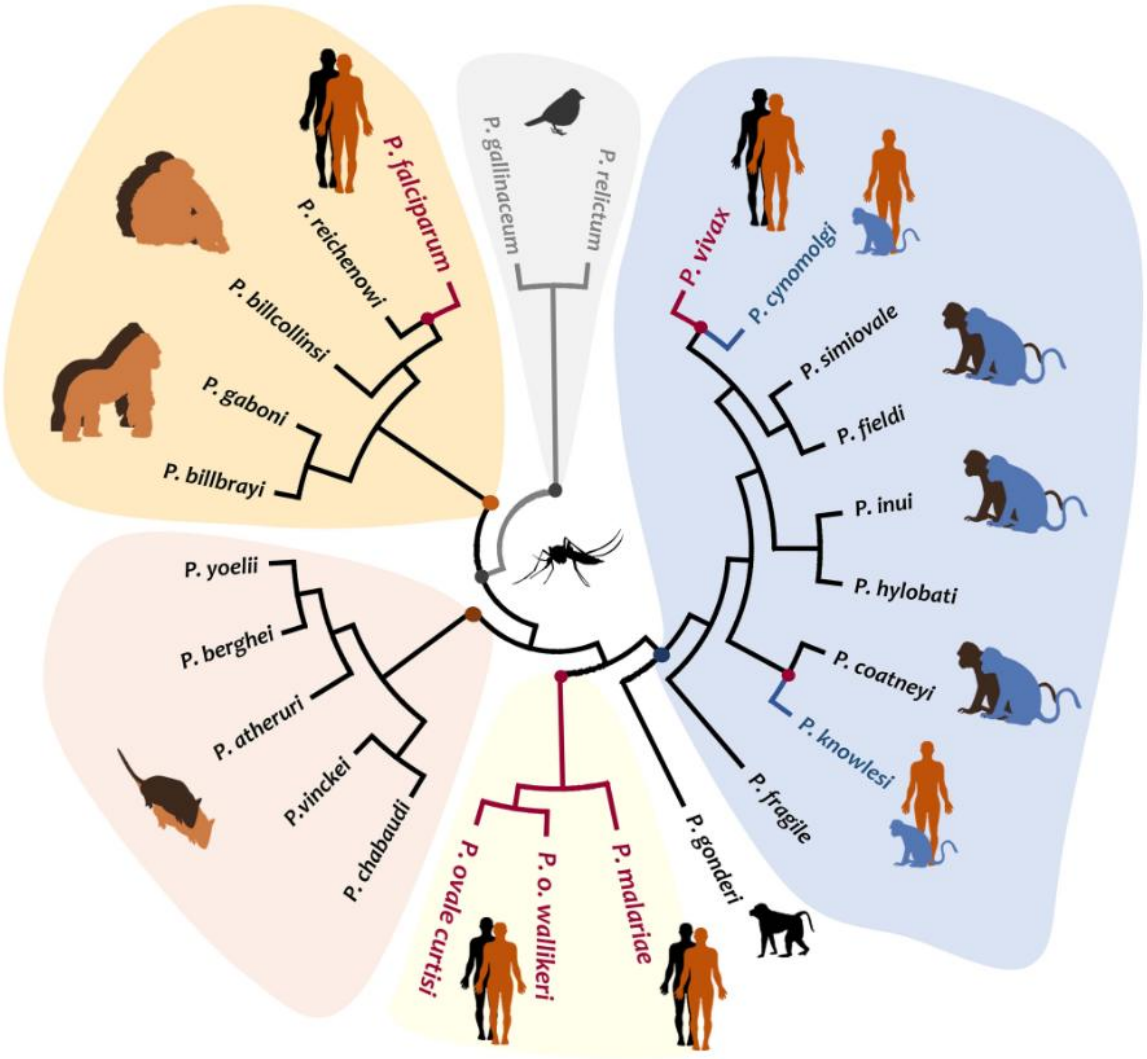

Figure 2: Phylogenetic tree of the Malaria parasite.
Phylogenetic representation of the genus Plasmodium and their different host species. Highlighted in red are the major human infecting plasmodium species. The subspecies *Laverania* is depicted in the upper left corner. (34)

Phylogenetically, *P. falciparum* belongs to the Laveranian clade (35), which also includes *P. billcollinsi*, *P. billbrayi*, *P. gaboni*, *P. gora* (*P. adleri*), *P. gorb* (*P. blackloci*), and *P. reichenowi* (Fig. 2) (36). Laveranian parasites are characterized by a higher repertoire of PEXEL motifs containing proteins, which facilitate protein export essential for their survival within host cells (37). Additionally, they are the only *Plasmodium* species known to form falciform gametocytes, a distinct feature of *P. falciparum* that aids in transmission via mosquitoes (35; 38).

P. vivax, the second most prevalent *Plasmodium* species, causes malaria tertiana. While *P. vivax* is less lethal than *P. falciparum*, it poses a significant public health concern in Asia and South America, where it is the predominant cause of malaria (3). Its ability to form dormant liver-stage hypnozoites contributes to relapsing infections, making its eradication particularly challenging (10).

1.3 Plasmodium falciparum life cycle

P. falciparum exhibits a complex life cycle, alternating between its human host and the *Anopheles* mosquito vector (Fig. 3). Asexual replication and the generation of sexual precursors occur exclusively in human red blood cells (RBCs), whereas gametogenesis and sexual replication require transmission into the mosquito vector (39; 40).

Our understanding of the pre-erythrocytic stage of *P. falciparum* is primarily inferred from observations in *P. berghei* and *P. yoelii*, with limited direct information available for *P. falciparum* itself (33; 41).

The life cycle initiates when a mosquito blood meal introduces a small number of sporozoites (10-100 in P. yoelii) into the human skin (42; 43). A small portion of these sporozoites remain at the site of inoculation, where they may develop into skin exoerythrocytic forms (44; 45). The remaining sporozoites enter the bloodstream and travel to the liver, where they traverse Kupfer cells (46; 47), endothelia cells and multiple hepatocytes (48) within transient vacuoles before ultimately invading a hepatocyte (49). This invasion is facilitated by CSP (50) and thrombospondin-related anonymous protein (TRAP) (51).

Within the hepatocyte, the liver-stage parasite (52) undergoes extensive asexual replication, producing thousands of merozoites within a single infected cell (53; 54). Upon rupture of the hepatocyte, the merozoites are released into the bloodstream, where they invade RBCs, initiating the intraerythrocytic developmental cycle. Here, the parasite undergoes asexual replication, generating 16–32 daughter merozoites per cycle (55; 56; 57), which subsequently infect new RBCs. This erythrocytic cycle, along with the periodic rupture of infected RBCs, is responsible for most malaria-associated symptoms, including fever, anemia, and systemic inflammation (58).

A small proportion of the merozoites commit to sexual development, differentiating into either male or female gametocytes (59). In *P. falciparum*, gametocytogenesis occurs over five distinct morphological stages and takes approximately 10–12 days to complete (60). During this process, immature gametocytes are sequestered in the bone marrow and only mature stage V gametocytes reappear in peripheral circulation (61), where they can be ingested by another mosquito during a blood meal.

Inside the mosquito midgut, gametocytes mature into male (micro-) and female (macro-) gametes (62). Following fertilization, they form zygotes, which subsequently transform into motile ookinetes. These ookinetes migrate into the midgut wall and develop into oocysts. Over the course of approximately two weeks, each oocyst undergoes sporogony, eventually rupturing to release thousands of sporozoites into the mosquito's body cavity. These sporozoites then migrate to the salivary glands, where they become ready for transmission to another human host during the mosquito's next blood meal, perpetuating the cycle of infection (63).

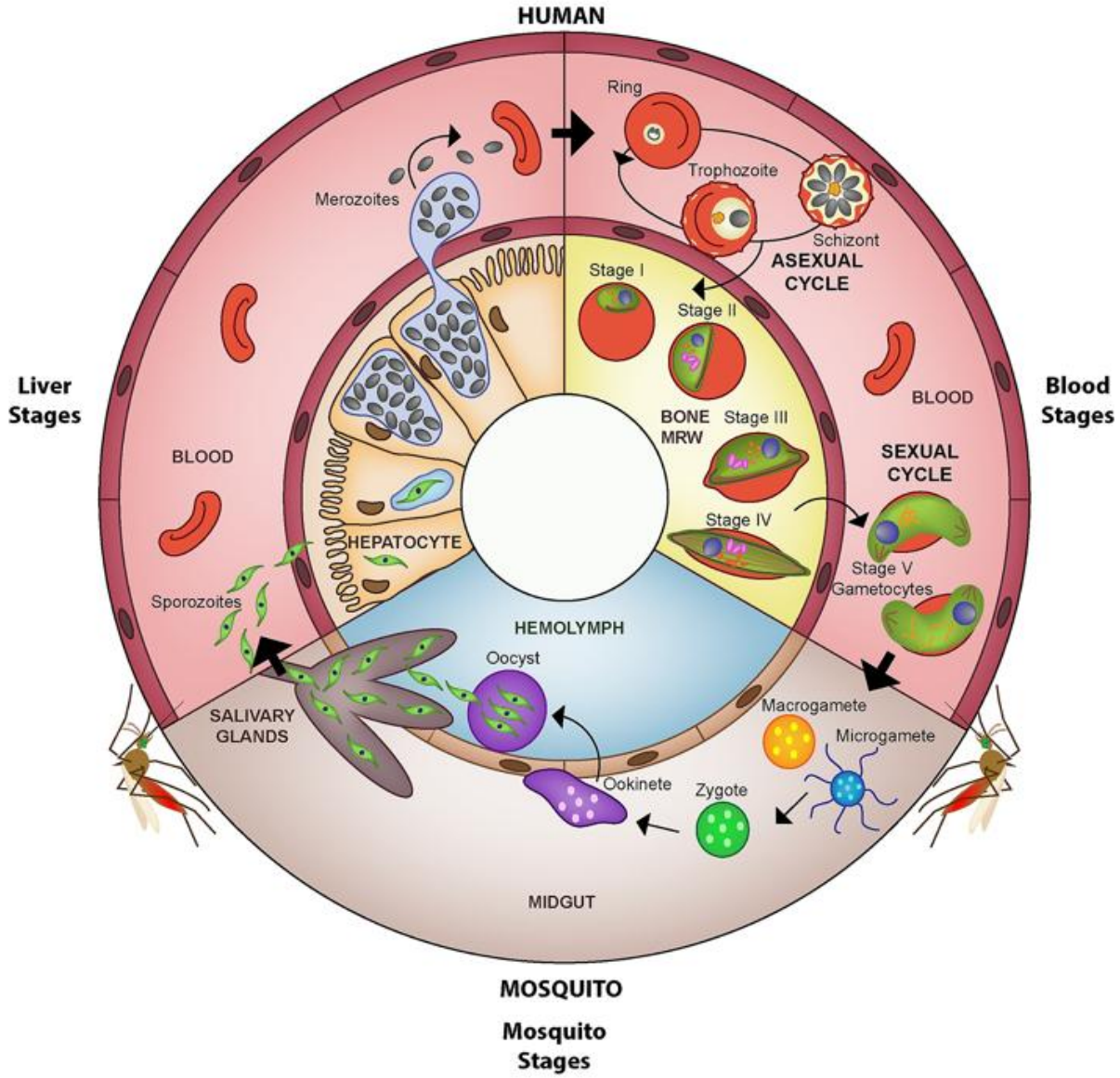

Figure 3: Plasmodium falciparum life cycle

Schematic representation of the *Plasmodium falciparum* Life cycle. The infection starts with the bite of an infected mosquito, injecting mobile sporozoites into the human host. The sporozoites travel via the bloodstream towards the liver, where they invade and replicate inside hepatocytes, forming thousands of daughter-merozoites. Eventually, the merozoites are released into the bloodstream, to invade erythrocytes and start the intraerythrocytic or asexual replication cycle. A small portion of asexual parasites commit to form male or female gametocytes, the sexual precursor cells of P. falciparum. Gametocyte maturation occurs over five morphological distinct stages, taking place in the bone marrow. Mature gametocytes are released back into the bloodstream and are eventually taken up by a blood feeding mosquito. Inside the mosquito midgut, the female gametocytes form macrogametes, while the male gametocytes undergo three rounds of genomic replication to from 8 mobile microgametes. The microgamete fuses with the macrogamete into a zygote, which eventually transforms into an ookinete. The ookinete penetrates the mosquito's midgut cell wall and undergoes sporogony to form thousands of sporozoites. The sporozoites are released into the hemolymph, where they travel towards the mosquito salivary glands, ready to initiate the cycle again. (64)

1.4 The Intraerythrocytic development cycle

The intra-erythrocytic development cycle (IDC, Fig. 4) is particularly significant, as it is responsible for the clinical manifestations of malaria. The IDC begins when a merozoite invades an erythrocyte using specialized surface proteins.

The first contact between am Merozoite and RBC is a primary and reversible attachment to the RBC surface. The attachment is mediated by merozoite surface proteins (MSPs) (65), which interact with erythrocyte surface proteins such as Band 3, glycophorin A (GPA), and heparin-like polysaccharides (66; 67) (68). Once attached, the merozoite reorients itself, positioning its apical end toward the erythrocyte (69).

Invasion is initiated by the interaction of erythrocyte-binding antigen 175 (EBA175) with GPA (70; 71) and *P. falciparum* reticulocyte-binding homolog 1 (PfRH1) with an unknown receptor (72). These interactions trigger a calcium flux within the merozoite, leading to the secretion of rhoptry contents via the invasion secretion machinery (73; 74; 75).

Rhoptry proteins (RON-2, -4, -5) are inserted into the RBC plasma membrane, facilitating the formation of a tight junction by binding to apical membrane antigen 1 (AMA1). This tight junction irreversibly anchors the merozoite to the RBC surface (76; 77; 78).

The tight junction is then actively translocated over the merozoite by an actomyosin motor complex known as the glideosome (79). This complex generates the mechanical force required for invasion (80; 81). The myosin A heads are anchored within the parasite by interactions with inner membrane complex (IMC) proteins such as GAP40, GAP45, and GAP50 via myosin tail-interacting protein (MTIP) (82; 83; 84; 85; 86). The IMC itself is a double-membrane structure underlying the parasite plasma membrane (87). Actin filaments, on the other hand, are connected to the cytoplasmic tail domains of membrane proteins via aldolase tetramers, which help transmit the glideosome-generated force to the erythrocyte (88; 89). Although widely accepted, this model has been recently challenged (90; 91; 92).

As the parasite moves into the RBC, the tight junction migrates toward the basal end of the parasite, translocating its components. During invasion, the parasite pushes the host cell membrane inward, forming a protective parasitophorous vacuole (PV) around it, which shields the parasite from host immune defenses (93; 94; 95). Once completely inside the PV, the content of the dense granules are released, marking the beginning of an extensive remodeling of the host cell (96; 97; 98).

Within the PV, the newly internalized merozoite assumes a characteristic ring shape for approximately 20 hours. This early intra-erythrocytic stage is metabolically quiescent (99) and represents the only blood-stage form typically observed in *P. falciparum* blood smears (100; 101). While historically considered a passive phase, recent studies indicate high protein expression and export activity, which set the stage for significant morphological and functional changes in later stages (102; 103; 104).

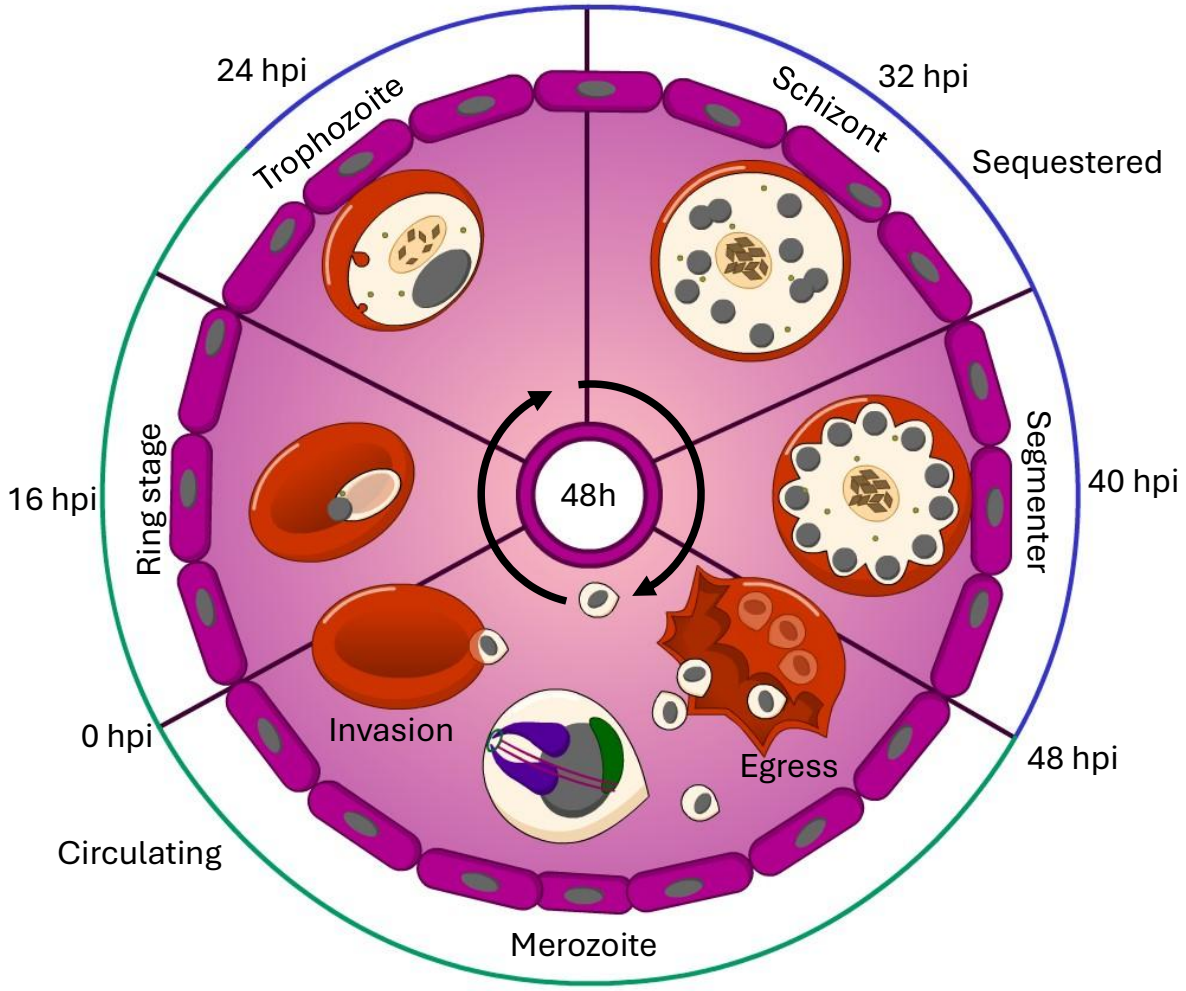

Figure 4: Plasmodium asexual replication cycle.
Schematic depicting the asexual replication cycle of P. falciparum. Following invasion of a erythrocyte by a merozoite, the merozoite transforms into ring stage parasite. After ca. 24h, the parasites become metabolically active, entering the trophozoite stage. During this stage, the parasites expresses and exports specific surface proteins, to adhere the erythrocyte to the endothelia wall to evade splenic clearance. Once the nucleus starts to divide, the parasite has reached the schizont stage, where it undergoes multiple rounds of DNA replication to form up to 32 daughter nuclei. After ca. 40h, the parasites start to segment the individual merozoites, which are eventually released in a process called egress. The free merozoites travel via the bloodstream to invade fresh erythrocytes to start the cycle again. Figure generated using Adobe Animate.

After 20 hours, the ring stage transitions into the trophozoite stage, the primary metabolic phase (105; 106). Here, the parasite extensively degrades host hemoglobin (107), which is taken up via a specialized feeding groove known as the cytostome (108). This stage also involves extensive remodeling of the host RBC (101), including the formation of Maurer's clefts (109; 110; 111), which facilitate the export of parasite-derived proteins such as *P. falciparum* erythrocyte membrane protein 1 (PfEMP1) (112). PfEMP1 plays a crucial role in cytoadherence, enabling infected RBCs to evade splenic clearance (113; 114). Additionally, trophozoites increase in size in preparation for the schizont stage (101), and hemozoin, a byproduct of hemoglobin digestion, begins to accumulate within the

parasite's food vacuole (115). Late-stage trophozoites complete the first round of DNA replication, marking the transition to the schizont stage (116).

During the schizont stage (36–44 hours post-invasion), the parasite undergoes up to five rounds of asynchronous DNA replication and mitosis without cell division (117), a process known as schizogony (118). In addition to nuclear replication, organelles such as micronemes, rhoptries, and the apicoplast undergo extensive replication (119). The parasite's mitochondrion expands into a tubular network, supplying energy for these processes (120).

At approximately 40 hours, the parasite initiates segmentation, a specialized form of cytokinesis in which individual nuclei and organelles are distributed into daughter merozoites (121; 122). This process relies on two key structures: the basal complex and the IMC. The basal complex forms at the posterior end of the developing merozoite, opposite the apical complex. It guides the leading edge of the IMC and is thought to function as a docking site for cytoskeletal elements involved in abscission. The IMC provides structural support, ensuring the proper shape of the developing merozoites (123; 124; 125; 126; 127; 128).

Ultimately, the parasite ruptures the RBC membrane in a process known as egress, releasing daughter merozoites into circulation to propagate the infection (129; 130). The cyclical destruction of RBCs by *Plasmodium* is directly responsible for the characteristic paroxysmal symptoms of malaria, including fever, chills, and anemia (58).

Egress is a rapid and highly regulated process driven by both parasite and host-derived factors. Minutes before egress, the PV membrane (PVM) undergoes rounding (131), and the segmented merozoites rearrange into a flower-like structure around the hemozoin crystal. PVM rupture occurs first, granting the merozoites increased motility, followed by perforation of the RBC membrane (132; 133). High-speed video microscopy has revealed that RBC membrane rupture initiates at a single point, causing the membrane to tear open while curling outward, ultimately expelling the newly formed merozoites into circulation (132; 133; 134).

1.5 Gametocytogenesis

While asexual replication occurs in the human host, the malaria parasite requires transmission back to the mosquito for sexual replication and genetic recombination (Fig. 5) (135). To facilitate transmission, a subset of blood-stage parasites undergo sex-specific differentiation, a process that occurs in less than 1% of the parasites (136; 137).

Sexual differentiation involves an initial commitment phase (138), a second sexual conversion phase (139; 140), followed by an extended developmental phase (141). The classical model of sexual commitment suggests that commitment occurs during the trophozoite stage preceding the cycle in which differentiation takes place (138). However, recent studies indicate that commitment can also occur within the same cycle (140). The

key regulatory event initiating sexual commitment is the transcriptional activation of the AP2-G gene locus (142; 143).

In asexual parasites, the AP2-G locus is epigenetically silenced by heterochromatin formation, maintained by heterochromatin protein 1 (HP1) (144). In *Plasmodium falciparum*, the activation of AP2-G is facilitated by gametocyte development 1 (GDV1), which binds to and inactivates HP1, effectively reducing HP1 levels and favoring AP2-G expression (145; 146; 147). Once activated, AP2-G amplifies its own expression through a positive feedback loop, leading to high AP2-G expression levels in committed parasites (142; 148). The rate of sexual commitment is highly responsive to environmental conditions, including high parasitemia, hemoglobinopathies, metabolic signaling, hormones, and drug treatment (149; 150; 151; 152).

Upon commitment, parasites undergo a second cell fate decision, differentiating into either male or female gametocytes (139). Notably, all daughter merozoites from a single committed schizont develop exclusively into either male or female gametocytes, never a mixture (140). Because *Plasmodium* parasites are haploid and lack sex chromosomes, sex determination cannot rely on chromosomal differences. Nonetheless, competent clones are capable of producing both fertile male and female gametocytes, suggesting an epigenetic basis for sex differentiation (153; 154; 147; 155).

While several sex-specific genes have been identified through genomic screens in *P. berghei* (156; 157; 158), the precise molecular mechanisms governing sex determination in *P. falciparum* remain unknown. During their maturation, male and female gametocytes progress through five morphologically distinct stages, each requiring approximately two days to complete (159; 38). Including the initial sexual commitment phase, which takes an additional two days, the entire process of gametocytogenesis spans 12 to 14 days, culminating in the production of mature gametocytes.

During development, stage II to IV gametocytes are sequestered in the bone marrow, shielding them from immune clearance and unfavorable conditions in circulation (61; 160). Only mature stage V gametocytes re-enter the bloodstream, where they coexist with early asexual-stage parasites and are available for uptake by a mosquito during a subsequent blood meal (161).

Stage I gametocytes are morphologically similar to late-stage asexual parasites. Like their asexual counterparts, they degrade hemoglobin and modify the host cell interior without undergoing DNA replication (162). During this stage, nuclear microtubules begin to expand from the centriolar plaque, elongating the nucleus (163).

The transition to Stage II is marked by the emergence of the IMC as a thin stripe beneath the parasite plasma membrane (164; 165). The IMC initially forms in proximity to the centriolar plaque, which acts as a microtubule organizing center (MTOC) in gametocytes (163). The IMC extends along one side of the parasite and serves as a scaffold for the assembly of subpellicular microtubules (SPMT, Fig. 6, A i) (124; 163). Together, the IMC and SPMTs constitute a specialized elongation apparatus that initiates the morphological

transformation of the round Stage I gametocyte into the lemon-shaped Stage II gametocyte (166; 167).

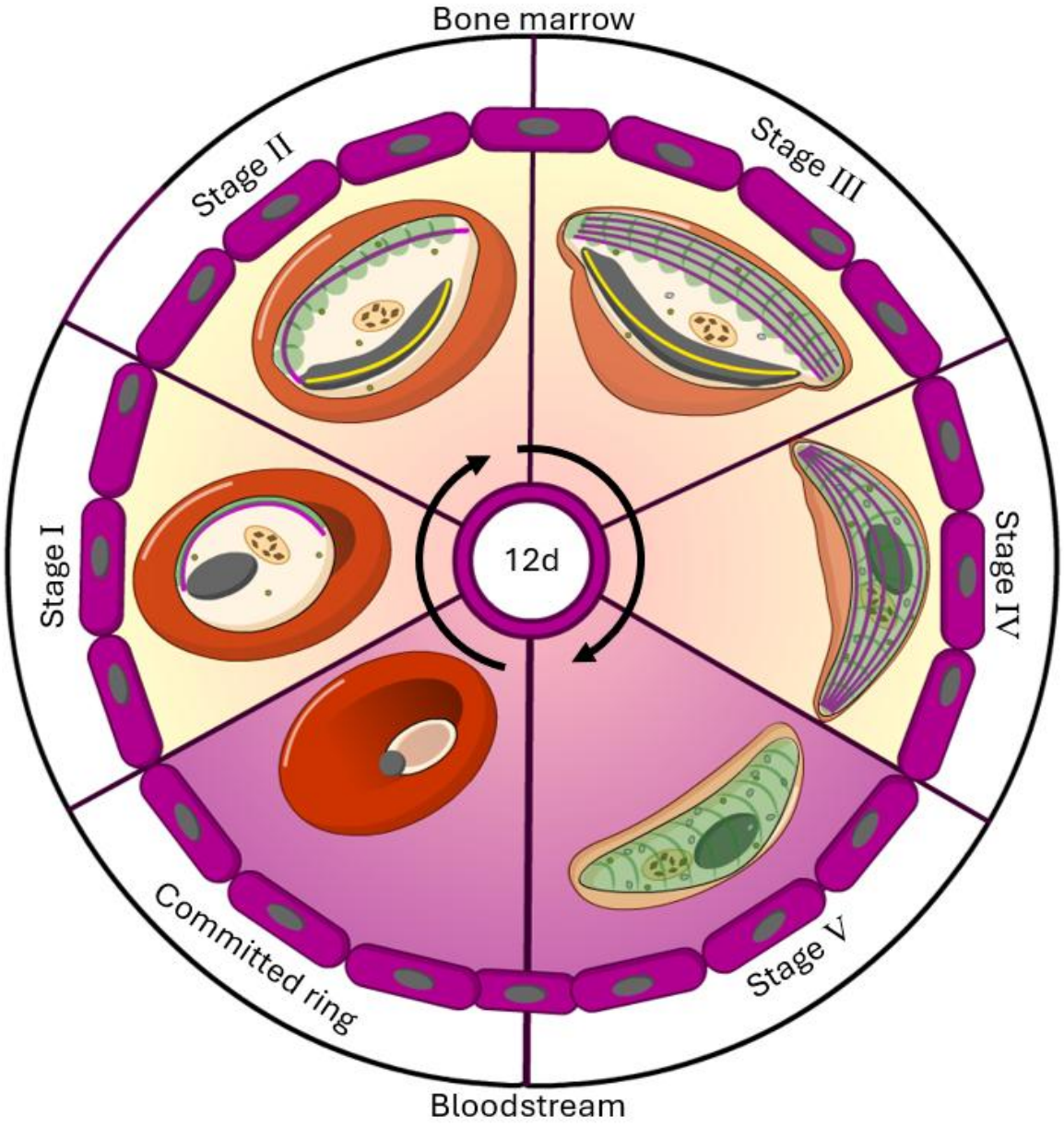

Figure 5: Gametocytogenesis of P. falciparum.
Schematic illustrating the maturation of P. falciparum gametocytes. A small portion of asexual parasites commit to form gametocytes. These committed rings start to grow and transform into Stage I gametocytes. Stage I gametocytes are egg-shaped, with an single microtubule (MT) strand (magenta) growing from the centriolar plaque, supported by the initial inner membrane complex (IMC, green). Stage II gametocytes are lemon-shaped, which is caused by the elongation of the IMC and the underlying subpellicular microtubule (SPMT, magenta), additionally, nuclear microtubules (nucMT, yellow) polymerize, elongating the nucleus (grey). In stage III gametocytes, the number of the SPMTs starts to increase, forming a MT sheet, which is expanded by the lateral growing IMC. In this stage, the sutures between the individual IMC plates are clearly visible (dark green). In stage IV gametocytes, the parasite is maximally elongated, with pointy ends and the nucMTs are depolymerized, leading to a shrinking nucleus. This crescent shape is name giving for the genus *P. falciparum*. In stage V, the SPMTs are depolymerized, leading the parasite in a sausage-like shape. Figure generated using Adobe Animate.

By Stage III, the IMC has expanded laterally, forming rectangular plates connected by proteinaceous fibers known as sutures (Fig. 6, A ii) (168; 169; 123). Concurrently, additional microtubules are incorporated into the SPMT sheet, leading to the formation of an elongated, hotdog-shaped parasite (164; 170). At this stage, a thickened protrusion emerges at the ends of the parasite. The nuclear microtubules reach maximal elongation (163)

In Stage IV, the gametocyte attains maximal elongation, reaching approximately 12µm in length (171). The ends of the SPMTs interconnect, forming pointed extensions that protrude against the RBC membrane, which is reduced to a thin layer around the parasite (172). Due to physical constraints imposed by the RBC membrane, the parasite begins to bend, resulting in the characteristic banana-like shape. A flattened extension of the RBC membrane, known as Laveran's bib, forms between the two ends of the gametocyte. At this stage, hemoglobin ingestion is completed (172), and the mitochondrion develops into an extensive tubular network. Unlike in asexual parasites, the mitochondrion in gametocytes exhibits a cristae-rich structure, and evidence suggests the presence of multiple mitochondria (173; 174). Additionally, nuclear microtubules are depolymerized, leading to nuclear condensation (163).

During the transition to Stage V, SPMTs are depolymerized, resulting in a sausage-shaped gametocyte (175). Late-stage male and female gametocytes are morphologically similar, though male gametocytes exhibit a more dispersed hemozoin distribution and fewer osmophilic bodies (38; 174). The increased deformability of Stage V gametocytes enables their circulation back in the bloodstream, allowing their uptake by a feeding mosquito (160).

1.6 Structural dynamics driving gametocyte elongation

Gametocytogenesis in *P. falciparum* involves profound morphological transformations that are orchestrated by a specialized elongation machinery. Central to this process is the IMC (123), a key structural component that, together with the PPM, forms a distinct cortical structure known as the pellicle (166). The IMC is a conserved feature among motile and invasive stages of the parasite, including merozoites, gametocytes, ookinetes, and sporozoites, where it consists of flattened membrane sacs (alveoli) beneath the PPM (38; 176; 177).

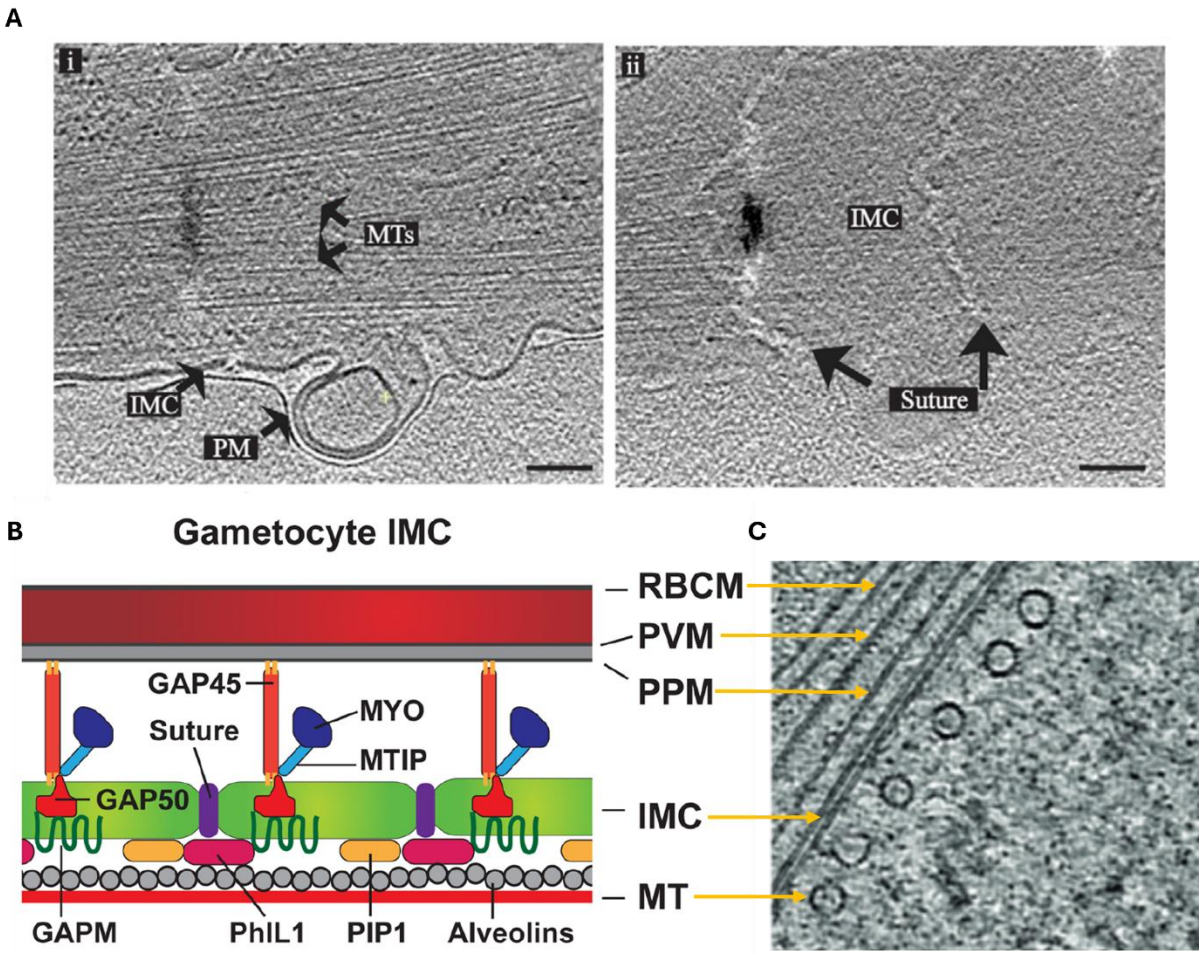

Figure 6: The inner membrane complex and the structure of the pellicle.
Structural composition of the parasite pellicle in Plasmodium gametocytes. **(A)** Electron microscopy images of (i) the subpellicular microtubules (SPMT) and (ii) the inner membrane complex (IMC)-sutures. **(B)** Schematic depicting the composition of the pellicle. The pellicle consists of the parasite plasma membrane (PPM) and the cisternal IMC. The IMC is connected to the PPM via glideosome associated proteins (GAP). Another part of the glideosome is the actin network beneath the PPM, connected to the IMC via myosin motor proteins (MYO, MTIP). Beneath the IMC lies the alveolin and SPMT network, connected to the IMC by unknown proteins. **(C)** Cryo-Electron microscopy cross section illustrating the different layers of the parasite pellicle and SPMTs. Adapted from (169; 178; 170)

In asexual parasites, IMC formation begins in the early schizont stage following multiple rounds of genome replication (179). During segmentation, the IMC works in tandem with the basal complex to facilitate cytokinesis, ensuring proper packaging of nuclei and organelles into individual daughter merozoites (180; 181; 125). Unlike the continuous IMC structure in asexual parasites, gametocytes exhibit a segmented IMC, composed of rectangular plates connected by proteinaceous fibers known as sutures (182; 168). These IMC plates provide a scaffold for the mechanical stability and elongation of the gametocyte (164; 166; 163).

Mature gametocytes possess 11–13 IMC plates (166; 123), with central plates measuring ~400nm in width and capping plates at the parasite's extremities extending up to ~800nm (167). The suture spacing between IMC plates is approximately 100nm (168). While several IMC-associated proteins have been identified, including members of the GAP (183), GAPM (180), alveolin (184), and ISP (185; 186) families, as well as key regulators such as CDPK1 (187), PhiL1 (188), and PIP (167), only two suture-specific proteins—Pf3D7_1345600 (MAL13P1.228, from here referred as 228) (123) and DHHC1 (189)—have been characterized in *P. falciparum* thus far.

Comparative studies in *T. gondii* reveal that gametocytes in this related apicomplexan contain at least 12 IMC suture-associated proteins, classified into IMC suture components (ISC) and transverse suture components (TSC) (190; 191). The conservation and functional relevance of these proteins in *Plasmodium* remain to be fully elucidated.

The IMC is intimately linked to the PPM through multiple protein interactions, forming a structural complex that integrates with the actomyosin motor system (175), collectively referred to as the glideosome (Fig. 6, B) (192; 79). In sporozoites and asexual parasites, the glideosome is a crucial component for parasite motility and host cell invasion, relying primarily on actomyosin-mediated force generation (193; 194). It is anchored to the IMC via GAP40 and MTIP, which interact with MyoA, a key myosin motor protein (82; 83; 84; 85; 86). MyoA activity enables the movement of actin filaments, which in turn transmit mechanical forces through transmembrane proteins such as MIC2 and TRAP (195; 80). These interactions facilitate gliding motility in invasive parasite stages, though the precise function of the glideosome in gametocytes remains unclear.

The IMC is supported by a network of specialized microtubules known as subpellicular microtubules (164; 166), which play a pivotal role in shaping the developing gametocyte. In stage IV gametocytes, SPMTs form a tight, corset-like structure beneath the IMC plates (167; 170), running perpendicular to their orientation. The spacing between individual SPMTs ranges from ~10 to 25nm (164), while the uniform distance between the IMC and SPMTs is approximately 18nm, suggesting a well-regulated connection between these structures. The number of SPMTs varies across different life stages: Merozoites possess 2 to 4 SPMTs, whereas ookinetes have 60, sporozoites 14 and gametocytes 21 SPMTs (170).

In *P. falciparum*, gametocyte SPMTs exhibit extreme stability and possess a diameter of 27–38nm, with 13 to 18 tubulin subunits (170). Unlike motile and invasive stages such as merozoites, ookinetes, and sporozoites, gametocytes lack a defined apical complex or polar ring, which typically serve as MTOCs (196; 197). Instead, recent studies indicate that SPMT nucleation occurs at two distinct sites: The outer centriolar plaque, a bipartite MTOC embedded within the nuclear membrane and from the nascent IMC, where SPMT assembly may be initiated independently of the nuclear structures (167; 163).

Cryo-electron microscopy (cryo-EM) studies have further revealed that, in contrast to other parasite stages, SPMTs in gametocytes exhibit mixed polarity, with no consistent plus-end or minus-end orientation. Despite this apparent randomness, the overall SPMT polarity within an individual gametocyte maintains a near 1:1 distribution. This suggests a balance in structural forces that contribute to the characteristic elongation of the gametocyte (170).

SPMT-driven elongation continues until the gametocyte reaches its mature, crescent-shaped morphology, constrained within the host RBC. The physical distortion of the RBC, while maintaining membrane integrity, is a hallmark of gametocyte maturation. In stage V gametocytes, SPMTs undergo depolymerization, leading to a transition from a rigid to a more flexible cell state, facilitating reentry into the bloodstream for transmission to the mosquito vector (175).

In addition to the IMC and SPMTs, an additional structural element, the subpellicular network (SPN), contributes to gametocyte rigidity. The SPN is composed of a dense network of alveolins (184; 198), which are intermediate filament-like proteins that line the cytoplasmic face of the IMC (199; 123). These filaments, measuring 8–10nm in diameter, are arranged in a regularly spaced meshwork that reinforces the mechanical stability of the IMC and its associated structures (184; 200).

Thirteen alveolins have been identified in *P. falciparum* (PfIMC1a–1m) (117), all containing one or more conserved alveolin-repeat domains (199). These proteins are thought to contribute to the elasticity and resilience of the gametocyte pellicle, potentially mediating interactions between the IMC and SPMTs (198; 177; 201).

The transformation of *P. falciparum* gametocytes from a rounded stage I morphology to the elongated, crescent-shaped stage IV form is a complex process governed by the coordinated action of the IMC, SPMTs, and SPN. Despite recent advances, several key questions remain unresolved, including the precise mechanisms of IMC plate formation, the molecular basis of suture assembly, and the regulatory pathways controlling SPMT nucleation and depolymerization. Future studies integrating high-resolution imaging, proteomics, and genetic perturbation approaches will be instrumental in further elucidating these processes, ultimately enhancing our understanding of *Plasmodium* gametocyte biology and its implications for malaria transmission.

1.7 Microtubule function, structure and dynamics

MTs are cytoskeletal polymers that play a fundamental role in eukaryotic cell architecture, intracellular transport, and cell division (202; 203; 204). They are composed of linear strands called protofilaments, which are assembled from α/β-tubulin heterodimers (205; 206). Typically, 13 protofilaments associate laterally to form a hollow cylindrical microtubule with a diameter of approximately 15–25nm (202; 207). The arrangement of α- and β-tubulin within protofilaments generates intrinsic microtubule polarity (208), which is essential for their dynamic behavior and directional interactions with molecular motors and associated proteins.

The polarity of MTs is a defining feature that governs their function. The plus (+) end is more dynamic and undergoes frequent growth and shrinkage (209), whereas the minus (−) end is typically more stable and anchored to MTOCs, such as centrosomes or the nuclear envelope (210; 211).

MT dynamics are characterized by phases of polymerization, depolymerization, and rescue (regrowth) (202). This dynamic instability allows microtubules to rapidly explore the intracellular environment, interact with organelles, exert mechanical forces, and coordinate with the actin cytoskeleton (212; 213; 214). On a larger scale, MTs are involved in fundamental cellular processes, including migration, differentiation, cell division, polarization, morphogenesis, and host cell invasion in certain parasites (215).

MT growth occurs primarily at the plus end, where α/β-tubulin dimers are added to the existing polymer (209). Although polymerization can also occur at the minus end, it proceeds at a significantly slower rate (216). The assembly process is regulated by the binding and hydrolysis of guanosine triphosphate (GTP) within the tubulin proteins (217). In the cell, soluble tubulin dimers exist in a GTP-bound state (218). Upon incorporation into the MT lattice, β-tubulin undergoes GTP hydrolysis, converting tubulin-GTP into tubulin-GDP. The GDP-bound tubulin is less stable, leading to an inherent structural instability within the microtubule (219).

At the growing MT tip, a small region of unhydrolyzed tubulin-GTP forms a stabilizing GTP cap. If the GTP cap is lost due to insufficient GTP-tubulin incorporation, the MT undergoes a transition from growth to rapid disassembly, a process known as catastrophe. This shortening continues until either complete depolymerization occurs or a new GTP cap is re-established, leading to a rescue phase and renewed polymerization (219).

EM studies have led to the development of three primary models of MT assembly, each describing distinct mechanisms for how tubulin subunits are incorporated at the growing MT tip: The first model describes MT growth by short, straight protofilaments composed of pre-assembled α/β-tubulin heterodimers that are added to the plus end. This direct stacking of protofilaments enables the elongation of the MT in a linear manner (220). The second model suggests that newly formed protofilaments initially assemble into a sheet-like structure at the tip of the growing MTs. As polymerization continues, the lateral edges of the protofilament sheet gradually close, resulting in the formation of the hollow cylindrical tube (221). The third model proposes that curved protofilaments are incorporated into the growing MT tip, similar to how depolymerizing MTs peel apart during disassembly. The curvature of the protofilaments straightens as they integrate into the MT lattice, facilitating elongation (222).

Although MTs are highly conserved structures across eukaryotic cells, yet in apicomplexan parasites such as *Plasmodium*, they exhibit unique adaptations that distinguish them from those in other organisms (179; 223). Notably, *Plasmodium* tubulin is more closely related to plant tubulin than to human tubulin, suggesting a distinct evolutionary trajectory (224; 225). In apicomplexans, two major subsets of microtubules contribute to cellular organization and function: SPMTs and spindle microtubules (223).

SPMTs are essential structural components that provide mechanical support and shape to apicomplexan cells (226). They originate from the apical polar ring (APR), a specialized MTOC, and extend in a spiral pattern along the inner side of the IMC (196). This distinctive arrangement stabilizes the parasite's shape and supports cellular processes such as motility and host cell invasion (192).

SPMTs exhibit remarkable stability compared to canonical eukaryotic microtubules. They resist depolymerization under conditions that typically disrupt microtubules, such as exposure to polymerization-inhibiting agents or cold treatment (227; 228). Additionally, unlike most eukaryotic MTs, which are composed of 13 protofilaments (229), SPMTs in apicomplexans consist of 9 to 16 protofilaments (179). This deviation from the standard architecture may contribute to their enhanced stability and structural rigidity (170).

Spindle MTs in apicomplexan parasites mediate nuclear division during both asexual and sexual replication. These MTs are nucleated from the centriolar plaque (CP) (230), a non-canonical MTOC embedded within the nuclear membrane (231). Unlike in many eukaryotic cells, where centrosomes with centrioles serve as the primary MTOCs for spindle formation, centrioles appear to be absent in *Plasmodium,* or their presence has yet to be identified (232; 233). Despite this, *Plasmodium* maintain robust mitotic and meiotic spindle dynamics, indicating that they rely on alternative microtubule-nucleating mechanisms.

Although tubulin can spontaneously polymerize when its concentration exceeds a critical threshold (234), most cells require specific nucleation factors to regulate this process. MT nucleation occurs at designated subcellular sites known as MTOCs, which facilitate the initiation, stabilization, and anchoring of MTs (235).

The centrosome is the best-characterized MTOC in eukaryotic cells (236). It is a non-membrane-bound organelle composed of a pair of centrioles surrounded by a pericentriolar matrix (237). Classically, the centrosome serves as the primary site of MT nucleation, with microtubule minus ends anchored at the centrosome via the γ-tubulin ring complex (γ-TuRC), while plus ends extend outward toward the cell periphery (235).

In contrast, apicomplexan parasites and especially *Plasmodium,* employ two unique MTOCs adapted to their specialized cellular structures and life cycle. Besides a conventional centrosome, they utilize distinct MTOCs such as the APR or the CP.

The CP is a non-centrosomal MTOC found in *Plasmodium* parasites and plays a critical role in regulating MT dynamics during cell division and parasite development (179). Structurally, it appears as a bipartite, electron-dense complex, with one portion embedded within the nucleus and the other extending into the cytoplasm (232; 230; 231; 238). Although essential to cellular processes, the precise protein composition of the CP remains largely unclear. Current insights are primarily derived from microscopy studies that have identified a limited number of CP-associated proteins—such as γ-tubulin (239; 240), centrin (241; 242; 118), SAS4/6, and CPAP (243; 244; 245; 246)—which localize to the CP and are believed to support its role in microtubule nucleation. Given its key involvement in processes like cell division, gametogenesis, and MT organization, there is

growing interest in uncovering the full molecular makeup and functional mechanisms of the CP.

The APR is a key cytoskeletal structure in *Plasmodium*, forming part of the apical complex, a defining feature of Apicomplexan parasites (247). Located at the apical end of the cell, the APR serves as a non-centrosomal MTOC that anchors and organizes SPMTs, which help maintain cell shape and are essential for parasite motility and host cell invasion (196; 179). Unlike classical centrosomes, the APR remains tightly associated with IMC (248; 170), resembling a cap-like structure which embeds the minus ends of the SPMTs (249). Though its precise molecular composition is not fully resolved, several proteins, including components of the tubulin network and structural proteins like ARA1, APR2 and AAPs (apical annuli proteins), have been implicated in APR function in *Plasmodium* (250; 251; 247). The APR is particularly important during the invasive stages of the parasite's life cycle, such as sporozoites and merozoites, highlighting its role in facilitating host cell entry and pathogenesis.

In *P. falciparum* gametocytes, the organization and nucleation of SPMTs display significant deviations from those observed in other invasive life cycle stages such as merozoites or sporozoites (Fig. 7). One of the most notable differences is the absence of the APR, a well-characterized MTOC in asexual stages that serves as the anchoring platform for SPMTs. The lack of an APR in gametocytes necessitates a distinct mechanism for SPMT nucleation and spatial organization.

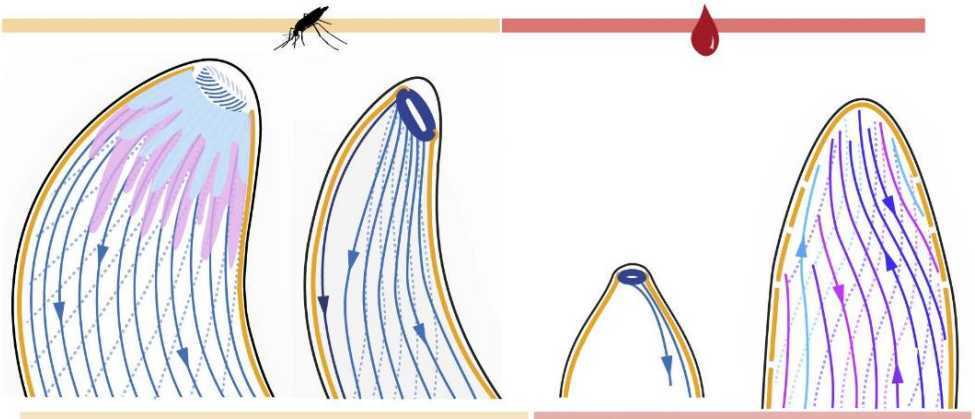

	Ookinete	Sporozoite	Merozoite	Gametocyte
Apical polar ring	yes	yes	yes	no
"+/-" polarity set	yes	yes	yes	no
Inner luminal helix	yes	yes	no	no
Seam orientation set	yes	yes	?	no
Protofilament number set	yes	yes	yes	no
L-shaped tubulin conoid	yes	no	no	no

Figure 7: Nucleation and organization of the SPMTs across different life cycle stages.
Schematic summarizing the different SPMT characteristics and compositions in the *P. falciparum* life cycle stages ookinete, sporozoite, merozoite and gametocyte. (170)

Fluorescence microscopy studies have demonstrated that the first strand of SPMTs in gametocytes appears to nucleate concurrently with the nucMTs from the CP (163), suggesting a potential, albeit initial, role for the CP in coordinating early microtubule dynamics. However, this function seems limited to early gametocyte stages, as other investigations propose that SPMT nucleation occurs from ncMTOCs embedded within the growing IMC during gametocyte development (167). These ncMTOCs appear to operate independently of canonical centrosome structures, underscoring a gametocyte-specific cytoskeletal organization. Despite these advances, the precise molecular mechanism of SPMT nucleation in gametocytes remains unresolved.

Interestingly, the lack of a uniform MT polarity in mature gametocytes implies the existence of at least two spatially distinct ncMTOCs positioned at both ends of the parasite (170). This is further supported by ultrastructural observations in stage IV gametocytes, where SPMTs consistently terminate at defined points or circular structures at both poles of the cell, with no MTs extending beyond these boundaries (167; 163; 252). Such bipolar termination suggests localized nucleation and/or anchoring hubs, yet to date, no proteins have been identified that definitively function as ncMTOC components for SPMTs in the gametocyte context.

In the absence of clear knowledge regarding SPMT nucleation sites, our understanding of how these SPMTs are anchored to the IMC or its associated sutures—and how they are guided along the curved parasite body—remains speculative. Cryo-EM studies have shown that SPMTs consistently maintain a ~18nm distance from the IMC, implying the existence of a proteinaceous linker or scaffold bridging the two structures (170). However, these studies did not reveal any electron-dense material between the IMC and SPMTs, complicating efforts to visualize such connections directly. Earlier work suggested that the SPMTs may instead be tethered to the IMC sutures (166), which could explain the difficulty in resolving discrete linking structures in EM, given the complexity and overlap of membrane and cytoskeletal elements at these junctions.

Another outstanding question concerns the developmental interplay between the IMC and the SPMTs during gametocyte maturation. It remains unclear whether the IMC acts as the anchoring platform that spatially organizes and stabilizes the growing MTs, or whether the MTs themselves act as a structural scaffold that guides the expansion and shaping of the IMC. Current data support a model in which the IMC and SPMTs are tightly interdependent: disruption of either structure adversely affects the assembly and maintenance of the other, suggesting a reciprocal, co-regulatory relationship (167; 252). This mutual dependence highlights the finely tuned coordination required for proper gametocyte morphogenesis and reinforces the importance of deciphering the molecular mediators that link cytoskeletal and membrane systems in these transmission-stage parasites.

We recently characterized PfSPM3, a novel protein associated with the SPMTs, which was identified through a BioID assay using the IMC protein PhiL1 as bait (253). Using conditional gene inactivation and gene truncation we could show that PfSPM3 is dispensable in asexual stages of the parasite, but its absence during gametocytogenesis results in the formation of morphologically abnormal gametocytes (254).

Further investigations revealed that this abnormal morphology is due to early disturbance of the SPMT network during gametocyte development. Along these observations we further showed with electron microscopy that in SPM3 deficient sporozoites (using the rodent *P. berghei*) the SPMT-IMC interconnection was altered (254). These findings support the hypothesis that PfSPM3 plays a crucial role in facilitating the connection between the IMC and the SPMTs.

Notably, PfSPM3 does not contain a transmembrane domain and its putative interaction with the inner membrane of the IMC is unclear. Therefore, we propose that PfSPM3 functions as part of a larger protein complex, acting as a tether to mediate and stabilize the interaction between the SPMTs and the IMC.

With this thesis, we aim to:

1. Identify novel PfSPM3 interacting proteins important for gametocytogenesis.

2. Localize potential candidates within a cellular context during gametocytogenesis.

3. Probe into their possible function by miss-localizing the proteins into the nucleus.

Chapter 2: Results

2.1 previous work

To identify potential PfSPM3 interacting proteins, that might be involved in the formation of a tethering complex, we performed a BioID proximity labeling assay using PfSPM3 as bait. We first generated a transgenic cell line by endogenously fusing the BirA* biotin ligase and a GFP tag to the C-terminus of PfSPM3, utilizing the selection linked integration (SLI) system (255). The resulting PfSPM3-BirA*-GFP construct (Fig. 8 A) was transfected into an NF54/iGP background, which enables robust induction of sexual commitment with a conversion rate of approximately 70% (256).

The correct genomic integration of the construct was confirmed by PCR, and fluorescence microscopy verified the expected localization of the fusion protein in gametocytes. As assumed, we observed GFP signals co-localizing with the subpellicular microtubules (SPMT) in gametocytes (Fig. 8 B, upper row), consistent with previous observations of PfSPM3 localization (254).

To determine whether PfSPM3-BirA*-GFP could biotinylate proximal proteins, we induced gametocytogenesis as described before (256), supplemented the culture medium with 0.15mM biotin for 8h. The PFA-fixed cells were then labeled with streptavidin-conjugated AF594 and anti-GFP antibodies. In the transgenic cell line, we detected a robust AF594 signal co-localizing with the anti-GFP signal (Fig. 8 B, lower row), indicating that the biotin ligase was active and successfully biotinylated proteins in the vicinity of the bait protein.

After confirming correct integration, expression and biotinylation, gametocytogenesis was induced again and 8 days post-induction (dpi), the culture was supplemented with 0.15mM biotin for 24 hours. Biotinylated proteins from three independent biological replicates were affinity-purified from parasite lysates using streptavidin-coated Sepharose beads and subsequently identified through mass spectrometry as described before (253).

Given that BirA*-dependent biotinylation in the absence of additional biotin has been reported in *Plasmodium*-infected cells, we included parental NF54/iGP parasites as a negative control for subsequent mass spectrometry analysis (257).

Quantitative analysis of protein enrichment, comparing results between biotin-supplemented parasites and NF54 wild-type controls, identified 181 proteins that were enriched at least twofold (logFC ≥ 1) relative to the NF54/iGP control.

Our bait protein, PfSPM3, was the second most enriched protein in our dataset (logFC = 2.7). Additionally, we identified another known SPMT-interacting protein, PfSPM1 (logFC = 1.7), and the microtubule (MT) associated protein PfEB1 (logFC = 2.0) among the top 50 enriched proteins, validating the quality of the BioID assay (Fig. 8 C).

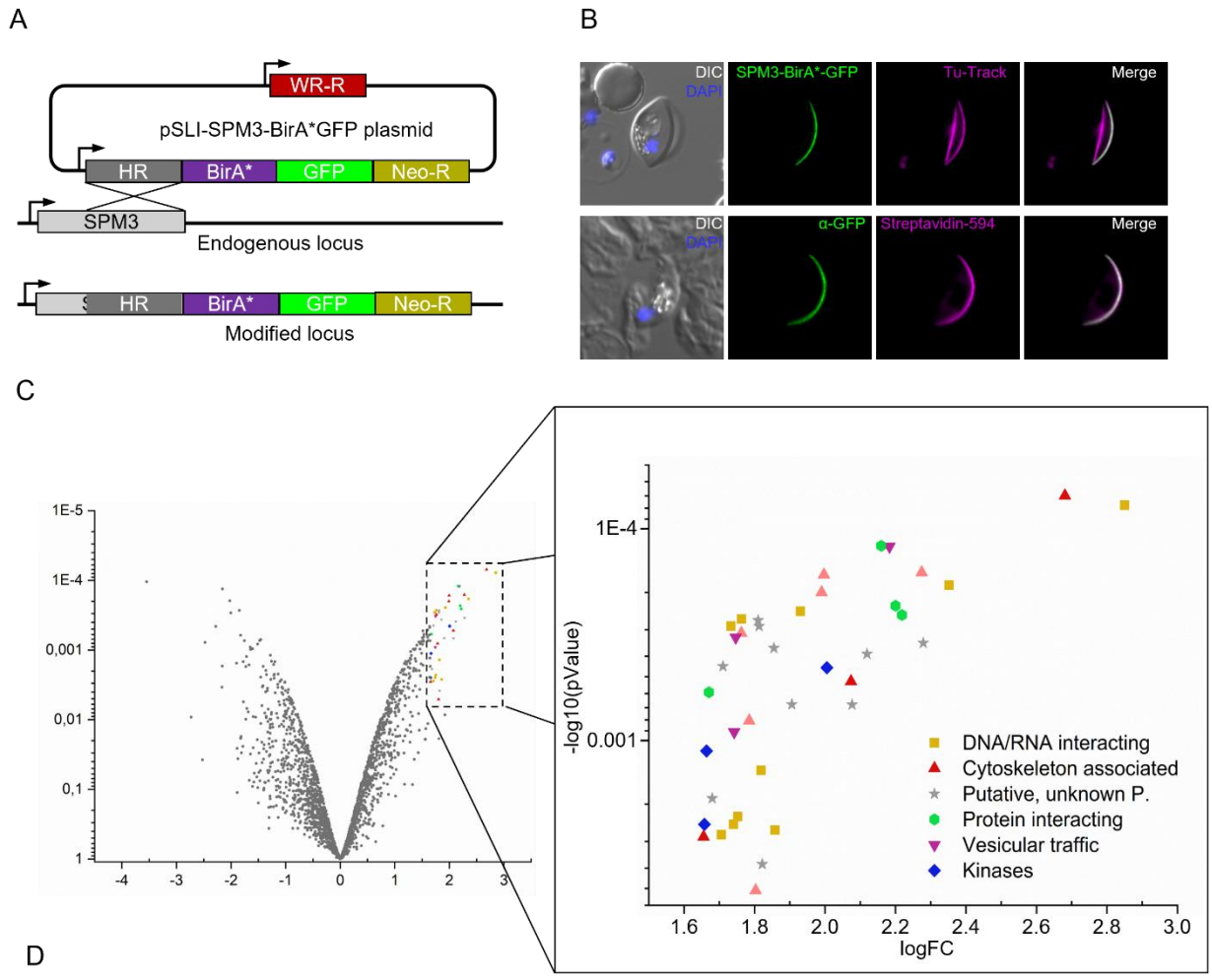

Protein interacting	
GeneID	LogFC
PF3D7_0510800	2.2
PF3D7_0604500	2.2
PF3D7_1142100	2.2
PF3D7_1416200	1.7

Cytoskeleton associated	
GeneID	LogFC
PF3D7_1327300	2.7
PF3D7_1449100	2.3
PF3D7_0307300	2.1
PF3D7_0111000	2.0
PF3D7_1245100	2.0
PF3D7_1322200	1.8
PF3D7_1203300	1.8
PF3D7_0909500	1.7

Putative, unknown proteins	
GeneID	LogFC
PF3D7_1027000	2.3
PF3D7_1003400	2.1
PF3D7_0928100	2.1
PF3D7_0805100	1.9
PF3D7_1416600	1.9
PF3D7_0111400	1.8
PF3D7_0924600	1.8
PF3D7_1114900	1.7
PF3D7_1036900	1.7

DNA/RNA interacting	
GeneID	LogFC
PF3D7_0419600	2.8
PF3D7_1128200	2.4
PF3D7_0927200	1.9
PF3D7_1317300	1.9
PF3D7_0105700	1.8
PF3D7_0919900	1.8
PF3D7_0518700	1.8
PF3D7_0706500	1.7
PF3D7_0930400	1.7
PF3D7_1224300	1.7

Vesicular traffic	
GeneID	LogFC
PF3D7_1423700	2.2
PF3D7_1408800	1.7
PF3D7_1110500	1.7

Kinases	
GeneID	LogFC
PF3D7_1356800	2.0
PF3D7_0311400	1.7
PF3D7_1420600	1.7

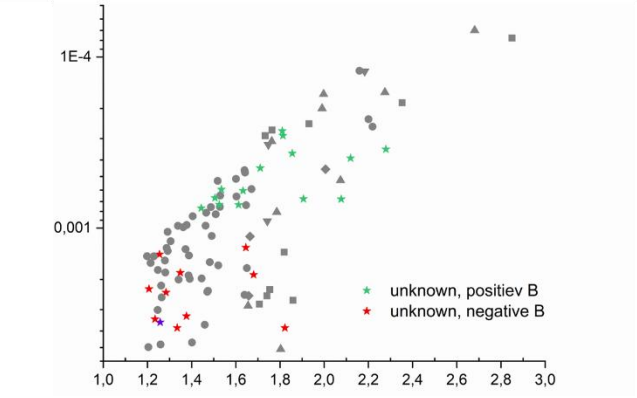

F

Putative, unknown proteins	
GeneID	LogFC
PF3D7_1423500	1.8
PF3D7_0704000	1.6
PF3D7_0529800	1.6
PF3D7_0825900	1.6
PF3D7_1417100	1.5
PF3D7_0522100	1.5
PF3D7_1019100	1.5
PF3D7_0705100	1.4
PF3D7_0504800	1.3

Figure 8: Identification and classification of putative PfSPM3 interacting candidates using BioID.

(A) Schematic representation of the SLI-based single-cross-over homologous recombination approach resulting in a *SPM3-birA*-GFP* fusion of the endogenous locus. **(B)** First row: Colocalization of SPM3-BirA*GFP with the microtubule in life cells. SPM3 was endogenously tagged with BirA*GFP (green) and microtubule were visualized with Tubulin Tracker deep red (magenta). Second row: Colocalization of biotinylated proteins with SPM3-BirA*GFP. SPM3-BirA*-GFP (mouse anti-GFP, green) parasites were fixed in 4%PFA and biotinylated proteins were visualized using streptavidin-594 (red). Nuclei were stained with Hoechst-33342 (blue). **(C)** Volcano-plot showing proteins identified over three replicas via mass spectrometry. SPM1 was chosen as a cut of value for further analysis. The zoom in shows the top 41 enriched proteins labeled according to their predicted function (258). **(D)** Table showing the top 41 proteins from D, grouped according to their predicted molecular function with their respective logFC value. **(E)** Scatter plot showing the 100 most enriched proteins. Conserved, unknown proteins with are positive B-value (green) and negative B-value (red) are highlighted accordingly. **(F)** Table showing conserved, unknown proteins which were additionally chosen for tagging with their respective logFC value.

2.2 Selection of putative candidate proteins

Using the logarithmic fold change (logFC) from PfSPM1 as a cut-off for further analysis, we selected 41 proteins. To refine the candidate list further, we categorized these proteins based on their predicted cellular functions using annotations from PlasmoDB (258). The proteins were grouped into the following categories: proteins involved in protein interactions (4), cytoskeletal-interacting proteins (8), putative proteins with unknown function (9), DNA/RNA-interacting proteins (10), vesicular traffic (3) and kinases (3) (Fig. 8 D).

Since our goal was to focus on putative PfSPM3-interacting proteins, we prioritized the cytoskeletal-interacting proteins and proteins involved in protein interactions for further analysis. From the group of cytoskeletal-interacting proteins, we excluded the following based on published literature: PfKinesins-8 (PF3D7_0111000, (259)) and -13 (PF3D7_1245100, (260)), PfEB1 (PF3D7_0307300, (261)), and PfSPM1 (PF3D7_0909500, (262)). Additionally, we excluded PF3D7_1142100 (KIC11, (263)) and PF3D7_1416200 (metacaspase-3, (264)) from the group of proteins involved in protein interactions from further investigations.

To expand this list of putative interactors, we included uncharacterized proteins within our dataset to our downstream analysis: Among the top 100 enriched proteins from our BioID analysis, we identified 25 putative unknown proteins. To refine our selection, we excluded proteins with a negative B-value in the Linear Models for Microarray Data (LIMMA) analysis (Fig. 8 E). When using LIMMA analysis, the B-value indicates the log-odds, that a gene is differentially expressed, adjusted for multiple testing. A positive B-value is an indicator that the expression level of the selected gene is significantly different from the control condition. This reduces the list of putative, unknown proteins to 14 candidates, 8 of which had already emerged in our previous analysis (Fig. 8 F).

In addition to these, we incorporated PF3D7_0529800, a protein identified by our collaborators as essential in asexual stages and localized to the centriolar plaque (Spielmann, T.; personal communication). We also included PF3D7_0311400 (protein kinase related protein, PKRP), which previous studies from our lab showed localizes to the inner membrane complex (IMC) in asexual stages and to the sutures in gametocytes (253; 265). Furthermore, PF3D7_1423500 and PF3D7_1036900 were added due to their high fold-change values (>1.7). This selection process resulted in a final list of 24 candidate proteins.

2.3 Phylogenetic analysis of the candidate proteins

To further explore the evolutionary conservation of these candidate proteins, we conducted a phylogenetic analysis, comparing their sequence similarities across multiple *Plasmodium* species (Fig. 9). As controls, we included PfSPM3 (PF3D7_1327300), the bait of our BioID dataset, as well as β-Tubulin (PF3D7_1008700), a highly conserved cytoskeletal protein. Our analysis revealed that all selected proteins are highly conserved within *Plasmodium*, suggesting a specialized role in the biology of *P. falciparum* and its closest relatives.

Further analysis of the evolutionary conservation of candidate proteins revealed intriguing patterns regarding their distribution within the *Plasmodium* genus and across related haemosporidian parasites. Notably, proteins predicted to contain functional domains demonstrated a higher sequence coverage across haemosporidian species compared to those lacking recognizable domains. This observation is consistent with the idea that conserved domains often indicate essential, preserved biological functions across evolutionary lineages.

When extending the comparison beyond the haemosporidia order, the conservation markedly dropped. In fact, only the control gene β-tubulin showed significant sequence similarity, with a low e-value, when compared with more distantly related organisms.

Interestingly, roughly one-third of the selected candidate proteins (PF3D7_0604500, PF3D7_1027000, PF3D7_0928100, PF3D7_1416600, PF3D7_0111400, PF3D7_0924600, PF3D7_1423500, PF3D7_0205100, PF3D7_0825900, PF3D7_1417100, PF3D7_1019100, PF3D7_0705100) exhibited high sequence conservation restricted to the *Laverania* clade, a subgroup within the haemosporidia order that includes *Plasmodium falciparum* and other ape infecting plasmodium parasites, forming falciform gametocytes. This clade-specific conservation pattern suggests that these proteins may have evolved to mediate functions particularly relevant to host–parasite interactions within hominid hosts. An additional three candidates (PF3D7_1322200, PF3D7_0510800, PF3D7_1114900) demonstrated a high conservation throughout the broader haemosporidia order, suggesting roles in more conserved, perhaps fundamental aspects of parasite biology.

Among all 28 candidates, two proteins stood out as peculiar cases. The first, PKRP (PF3D7_0311400), displayed notably low sequence coverage outside *P. falciparum*, yet maintained a surprisingly low e-value in distant comparisons. This pattern suggests that while PKRP may be largely unique to *P. falciparum*, specific motifs or structural elements are sufficiently conserved to retain detectable homology in other *Plasmodium* species. It raises the possibility that PKRP represents a specialized adaptation in *P. falciparum*, potentially associated with its unique virulence factors or host immune evasion strategies.

The second notable outlier was PF3D7_0504800, which was found to be highly conserved across nearly all *Plasmodium* species examined, with the conspicuous exception of *P. berghei*, a rodent malaria parasite widely used as a laboratory model. The absence of this protein in *P. berghei* is intriguing and might hint at a function critical for human or primate-specific infection, possibly relating to differences in host cell invasion, or transmission dynamics between human- and rodent-infecting parasites. The lack of this protein in *P. berghei* could also reflect fundamental biological differences in the gametocyte or sporozoite stages, where host specificity plays a decisive role.

2.4 Generation of GFP fusion cell lines

To validate the selected candidates putative PfSPM3 association, we first focused on determining their subcellular localization in gametocytes. For this purpose, we generated transgenic cell lines for each protein by endogenously fusing a GFP tag to the C-terminus of the respective gene, using the SLI-system (255). This resulted in the expression of a target protein – GFP fusion protein in the parasite.

For prospective functional studies, we used a SLI plasmid were the encoded GFP was additionally flanked by two FKBP coding domains on each side and an additional open reading frame for the mis-localizer to enable the knock-sideways (KS) of the candidate (255). However, since the nuclear localization signal based knock sideways (NLS-KS) system is ineffective for transmembrane domain (TMD)-containing proteins (255), we employed an alternative strategy for the two candidates, PF3D7_0704000 and PF3D7_1003400. For these proteins, we generated a transgenic cell line where a C-terminal mNeon tag was introduced, followed by a GlmS ribozyme sequence (266). This system allows for post-transcriptional gene knockdown by triggering mRNA degradation upon the addition of glucosamine (267).

The resulting constructs were transfected into an NF54/iGP parasites, which enables robust gametocyte induction by the addition of shield1 (256). We verified the correct integration of the tagging constructs by genomic PCR and analyzed the expression and localization of the fusion proteins using life cell fluorescence microscopy.

Figure 9: Phylogenetic analysis of selected candidates.

Graphical representation of the presence or absence of orthologues for 28 selected proteins from the *Pf*SPM3 proxiome across 13 species of *Plasmodium* or other eukaryotes was determined using pBLAST. Query coverage indicated by circle size and alignment significance (*E*-value) indicated from 0 (dark blue) to ~175 (yellow).

In total, we successfully generated functional transgenic cell lines for 15 candidate proteins. However, we were unable to construct the necessary plasmids for three candidates (PF3D7_0205100, PF3D7_1019100, PF3D7_1417100) and failed to establish stable transgenic lines for six others (PF3D7_0825900, PF3D7_0928100, PF3D7_1036900, PF3D7_1114900, PF3D7_1423500, PF3D7_0311400).

2.5 Localization of candidate proteins

To determine the localization of these proteins in gametocytes, we induced gametocytogenesis by stabilizing GDV1 overexpression through the addition of Shield-1 to the culture medium (256). After one full replication cycle (on day 3 post gametocyte induction), we supplemented the medium with 50mM N-Acetyl-D-Glucosamine (GlcNAc) for 5 days to eliminate all non-committed parasites (256). Beginning on day 5 post-induction, we monitored gametocyte development by capturing fluorescence microscopy images every two days. To assess protein localization in relation to the microtubule cytoskeleton, we simultaneously stained the gametocytes with Tubulin Tracker deep red (TuTr).

The NF54/iGP cell line expresses GFP-tagged GDV1 under an inducible promoter leading to some background fluorescence signal. In early asexual stages and Stage I gametocytes, GDV1-GFP formed distinct DNA-associated puncta. However, as gametocytogenesis progressed beyond Stage II, the GDV1 signal became less structured, appearing as a diffuse background fluorescence in later stages.

The subsequent localization analysis of our selected candidate proteins revealed a variety of distribution patterns within the gametocyte cellular architecture, particularly in relation to the MT network (overview in Fig. 10). To systematically categorize these localization patterns, we classified our findings into four distinct groups based on their spatial association with the microtubules.

The first group (par. 2.4) includes all proteins (PF3D7_1027000, PF3D7_0510800, PF3D7_0704000, PF3D7_0709400) that do not fit into any category. This group primarily consists of proteins with diffuse, unspecific localization patterns or proteins whose precise subcellular distribution could not be reliably determined. Some of these proteins may exhibit weak or transient interactions with cellular structures, or their localization may depend on additional factors such as stage-specific modifications or interactions with other proteins.

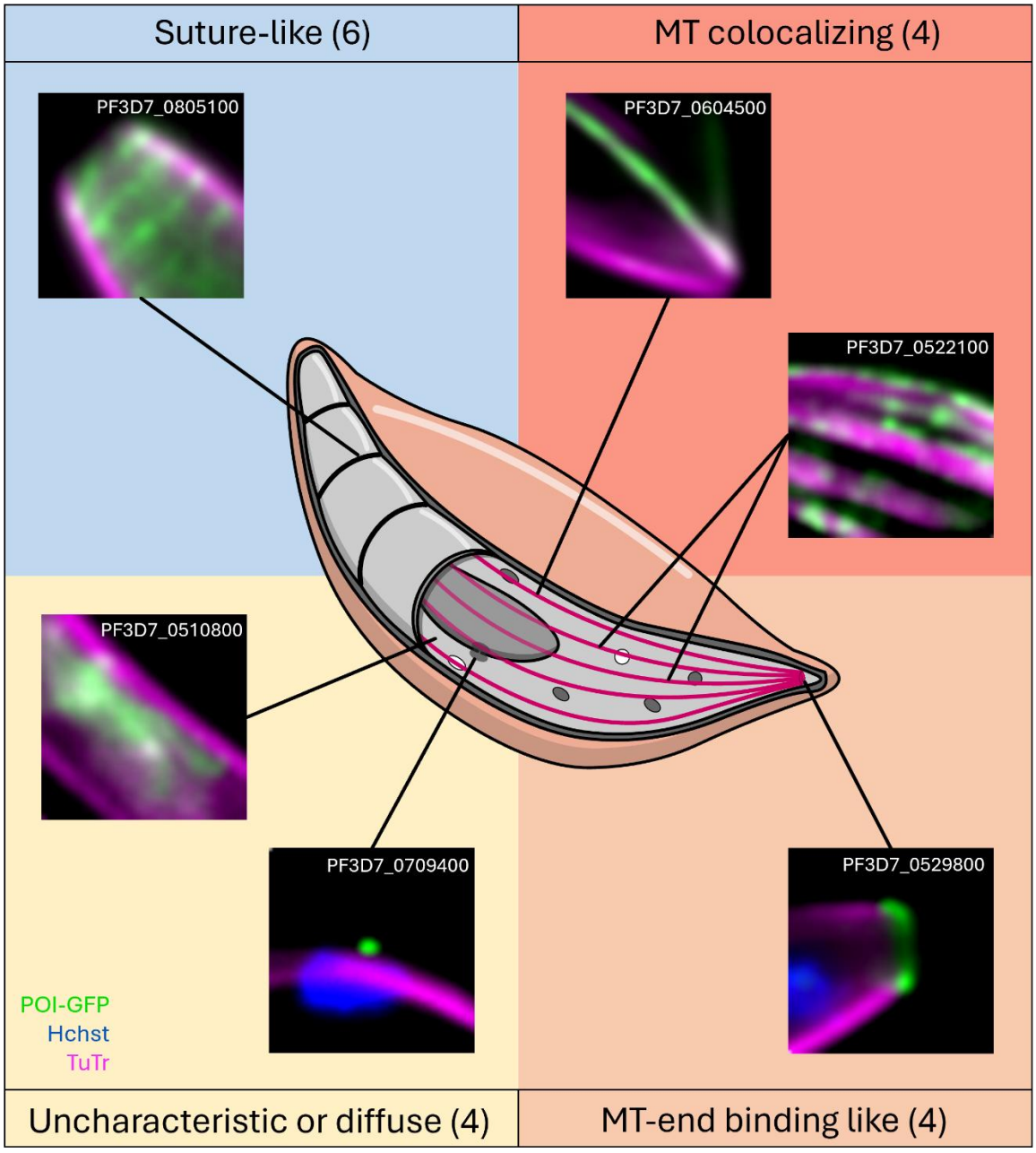

Figure 10: Localization atlas of selected PfSPM3 interacting candidates.
The successfully tagged proteins were categorized based on their subcellular localization during gametocytogenesis. The schematic in the middle depicts a stage IV gametocyte with the SPMTs in magenta and representative fluorescence microscopy images arranged around it. Beginning in the upper right corner, four proteins showed a colocalization with on or multiple microtubules. A set of four proteins showed a distinct localization towards the tip of the SPMTs. Four proteins showed either a diffuse cytoplasmatic or uncharacteristic localization within the gametocytes. The last six proteins showed a suture like localization. Representative pictures of the cell lines were taken every two days starting 72h after gametocytogenesis induction. The GeneID of the proteins in the representative images are depicted on the top of the images. POI-GFP-fusion protein (green), the microtubules were visualized with Tubulin Tracker-deep red (magenta) and the DNA was stained with Hoechst (blue). Hchst: Hoechst33342; MT: Microtubule; POI-GFP: Protein of interest-green fluorescent protein; TuTr: Tubulin Tracker deep red.

The second group (par. 2.5) comprises proteins (PF3D7_0111400, PF3D7_0924600, PF3D7_0604500, PF3D7_0522100) that predominantly co-localize with the Tubulin Tracker signal throughout gametocytogenesis. These proteins may play a direct role in regulating MT stability, bundling, or interactions with other cellular structures. Their consistent association with the MT cytoskeleton suggests they may be integral to the maintenance of the elongated gametocyte shape and cytoskeletal integrity.

The third group (par. 2.6) consists of proteins (PF3D7_0504800, PF3D7_0705100, PF3D7_0529800, PF3D7_1322200) that exhibit a dual localization pattern: a concentrated dot-like signal adjacent to the nucleus, reminiscent of the centriolar plaque (CP), as well as additional signal enrichment at the distal ends of the microtubule network. This suggests a potential role in MT organization or centrosome-associated functions, which could be relevant for structural transitions during gametocyte elongation. The localization of these proteins to the MT tips further hints at a possible involvement in microtubule dynamics, such as stabilization, polymerization, or anchoring of the SPMT network to other cellular components.

The fourth group (par. 2.7) includes proteins (PF3D7_1003400, PF3D7_0805100, PF3D7_1416600, PF3D7_1449100, PF3D7_1203300) that appear as striped patterns running perpendicular to the Tubulin Tracker signal. This localization pattern closely resembles the arrangement of the IMC sutures, suggesting that these proteins may be somehow associated with the sutures. Given the suspected role of sutures in maintaining IMC structure and integrity (166; 124), proteins within this category could be involved in stabilizing the gametocyte pellicle or regulating cytoskeletal interactions during gametocyte maturation.

In the following paragraphs more detailed analysis of the specific localization pattern in relation to the microtubules of the individual fusion protein are given.

2.6 Proteins showing a diffuse or uncharacteristic localization

This group includes the proteins PF3D7_1027000, PF3D7_0510800, PF3D7_0704000 and PF3D7_0709400, which displayed either a diffuse cytoplasmic signal or could not be clearly assigned to a specific cellular structure. While PF3D7_0704000 and PF3D7_0510800 exhibit a uniform distribution throughout the cytoplasm (Fig. 11 A, B), PF3D7_1027000 and PF3D7_0709400 show a punctate localization pattern that were difficult to categorize definitively (Fig. 11 C, D).

The first two proteins, Pf3D7_0704000 (Fig. 11 A) and Pf3D7_0510800 (Fig. 11 B), exhibit a diffuse cytoplasmic localization throughout gametocyte maturation. Pf3D7_0704000 is a 393kDa protein containing eight predicted transmembrane domains. Pf3D7_0510800 is a 73kDa protein, predicted to contain a WD40 repeat domain at its C-terminal end.

The third protein in this group, Pf3D7_1027000 (Fig. 11 C), appears as one or multiple dots in close proximity to the DNA signal in all gametocyte stages. It is a 216kDa protein and was among the most enriched candidates in our BioID screen (logFC = 2.5).

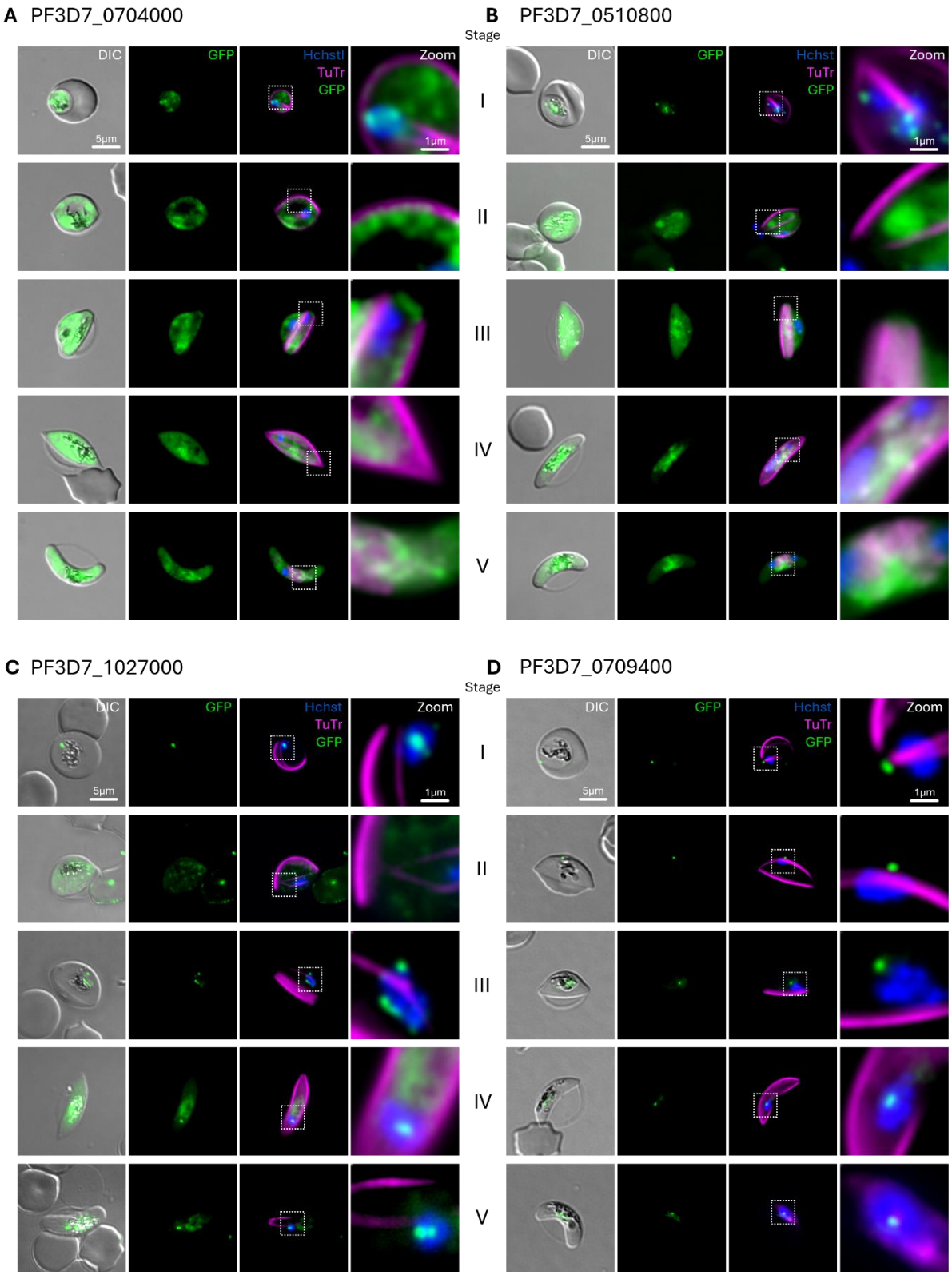

Figure 11: Four proteins show a cytoplasmatic or uncharacteristic localization in gametocytes.
Life cell fluorescence microscopy images of transgenic parasites. Each protein of interest was endogenously tagged with GFP (green). Microtubule were visualized with Tubulin Tracker-deep red (magenta) and the DNA was stained with Hoechst 33342 (blue). Pictures were taken every two days starting 72h after gametocytogenesis induction. Displayed are representative images of each Gametocyte stage. Zoom factor, 500%. DIC, differential interference contrast; GFP, green fluorescent protein; Hchst, Hoechst 33342; TuTr, Tubulin Tracker deep red.

Lastly, Pf3D7_0709400 (356) (Fig. 11 D), named Cg7, is a 153kDa protein. Throughout gametocytogenesis, Cg7 appeared as a single, distinct spot in close proximity to the DNA signal. In stage I gametocytes, it was observed near the tips of both nuclear and subpellicular microtubules, suggesting a possible role in microtubule organization. However, unlike other proteins that displayed a clear centriolar plaque-like localization (see paragraph 3.6), Cg7's distribution is more ambiguous. Therefore, we categorized it within this group of proteins that could not be definitively assigned to a specific cellular structure.

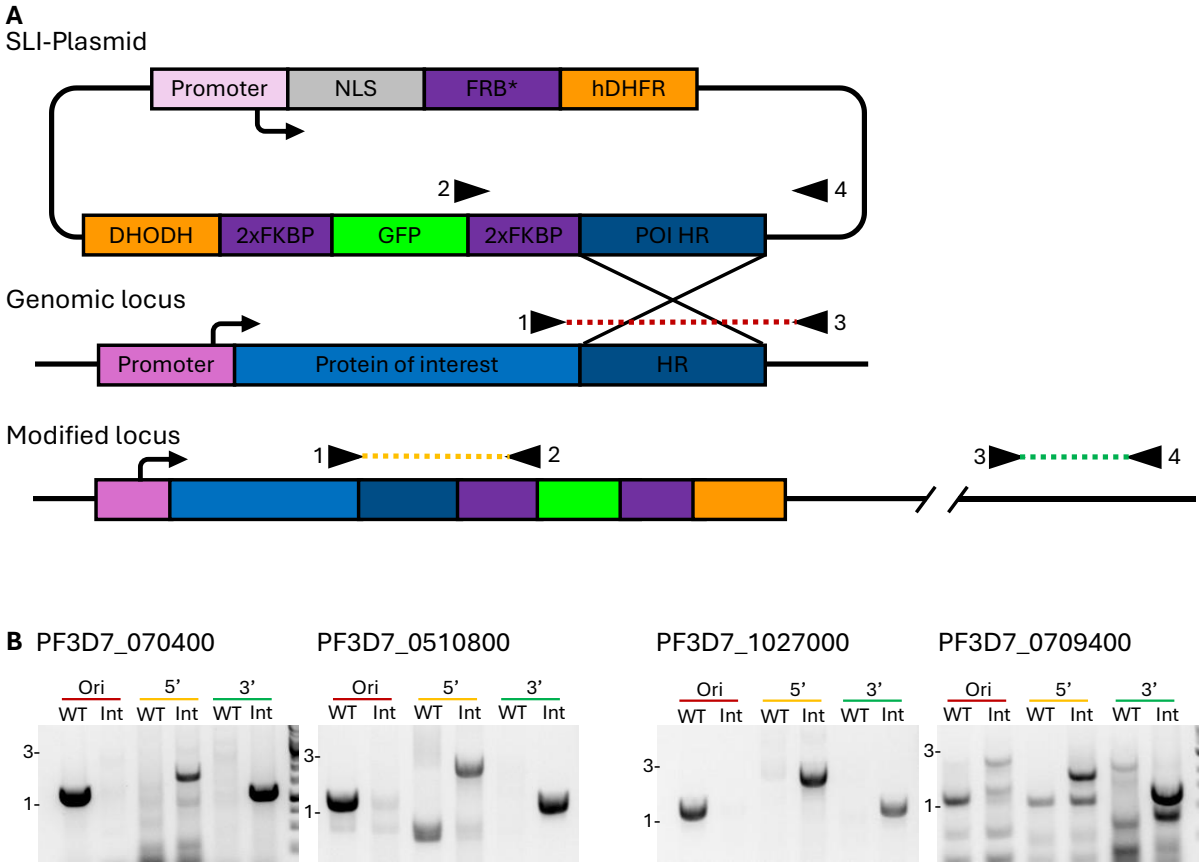

Figure 12: Integration check for tagged proteins
(A) Schematic depicting the SLI integration process and the binding sites for the primers used for the integration checks. The SLI plasmid is integrated into the genomic locus via a single homologous, crossover recombination event. The primer combinations 1+2 (yellow) and 3+4 (green) are used to verify the 5' and 3' integration sites, while the primer combination 1+3 (red) were used to confirm the right (ori) protein was modified. **(B)** Integration PCR for the cell lines showing an uncharacteristic localization, with genomic DNA from the integrant (Int) or parental NF54/iGP (WT) parasites. Primer combinations are shown in **A** and expected sizes are listed in Table12. DHFR, Dihydrofolate reductase; DHODH, Dihydroorotate dehydrogenase; FKBP, FK506-binding protein; FRB, FKBP-Rapamycin binding; GFP, Green fluorescent protein; HR, Homology region; NLS, nuclear localization signal; SLI, Selection linked integration; POI, Protein of interest.

2.7 Proteins predominantly colocalizing with the microtubule

2.7.1 Protein localization

This group includes PF3D7_0111400, PF3D7_0924600, PF3D7_0604500 and PF3D7_0522100. These four proteins predominantly colocalize with MTs within the gametocyte but exhibit distinct localization patterns relative to the SPMT network or nuclear microtubules (nucMTs) during gametocyte maturation. Their expression and localization suggest potential roles in MT organization, stability, or interactions with other cellular components.

Pf3D7_0522100 is a 90kDa protein. During gametocyte development, it exhibits strong colocalization with MTs, particularly at the two tips of the primary SPMT strands in stages I-IV. By stage V, it disappears alongside the disassembly of SPMTs (Fig. 13 A). In asexual parasites, it colocalizes with MT doubles in maturing merozoites (Fig. 14 A). This suggests Pf3D7_0522100 might be involved in MT organization and stabilization during both schizogony and gametocyte maturation.

The 334kDa Pf3D7_0604500 appears as thin patches along the MT strand in stage I gametocytes. By stages II and III, it predominantly labels specific subsets of MTs, sometimes only covering a specific part of the MT strand (Fig. 13 B). The disappearance of Pf3D7_0604500 in stage IV—long before SPMTs disassemble—hints towards a nucMT association. In asexual parasites, Pf3D7_0604500 shows a diffuse cytoplasmic signal across all stages (Fig. 14 B).

Pf3D7_0924600 is a 247kDa protein, partially colocalizing with MTs in stages II-IV but disappearing before the SPMT are disassembled. Interestingly, it appears to decorate segments of the SPMTs in a dotted pattern, but independently of both SPMTs and nucMTs (Fig. 13 C), suggesting it may associate with a distinct MT subpopulation or another cytoskeletal element. We were unable to detect a definitive signal in asexual parasites, only faint dots, barely above background levels in late stage asexual parasites (Fig. 14 C). This suggests that the protein might function exclusively in sexual-stage parasites.

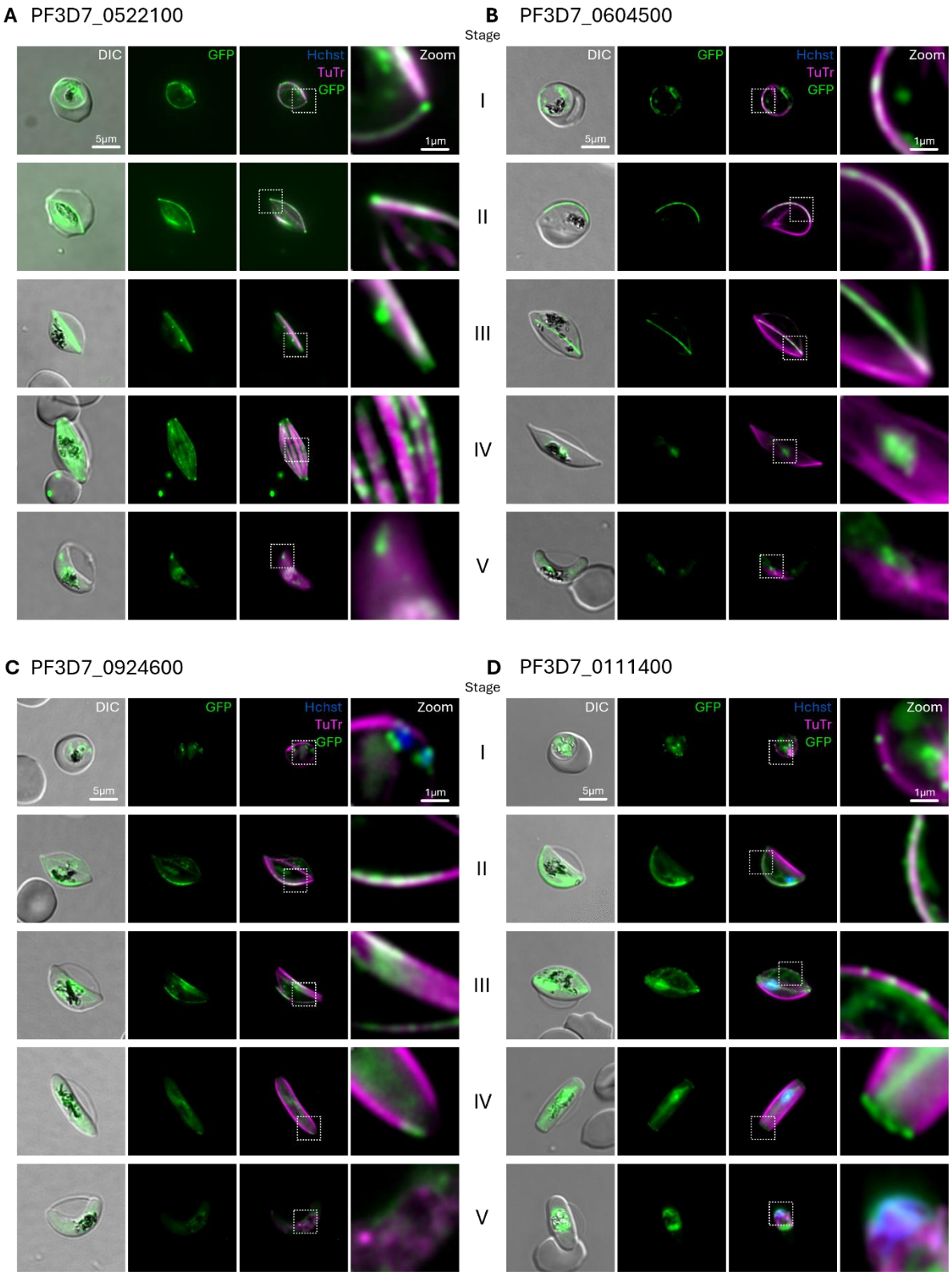

Figure 13: Four proteins predominantly colocalize with the microtubule strands in gametocytes.
Life cell fluorescence microscopy images of transgenic parasites. Each protein of interest was endogenously tagged with GFP (green). Microtubule were visualized with Tubulin Tracker-deep red (magenta) and the DNA was stained with Hoechst 33342 (blue). Pictures were taken every two days starting 72h after gametocytogenesis induction. Displayed are representative images of each Gametocyte stage. Zoom factor, 500%. DIC, differential interference contrast; GFP, green fluorescent protein; Hchst, Hoechst 33342; TuTr, Tubulin Tracker deep red.

Pf3D7_0111400, annotated as GEXP19 (258), is an 85kDa protein initially identified in a PEXEL-motif screen for gametocyte-enriched proteins (268). In gametocytes, it follows a dynamic localization pattern. In Stage I, GEXP19 appears as single dots on the initial SPMT strand. As the gametocyte transitions into Stage II, the protein colocalizes with nucMTs and forms additional punctate structures in close proximity to the SPMTs. In Stage III, it maintains its association with nucMTs while also appearing as discrete dots along the SPMT strand opposite the parasite's MT foot. By Stage IV, GEXP19 localizes as dots at the tips of the main SPMT sheet. Although it remains present in the nucleus, its signal becomes diffuse as nucMTs begin to disassemble in stage III. Finally, in Stage V, remnants of GEXP19 can still be detected in the nucleus and food vacuole (Fig. 13 D). In the asexual cycle, GEXP19 colocalizes with tubulin at the kinetochore in early and late trophozoites but disappears in late schizonts (Fig. 14 D), suggesting a role in MT organization that differs between gametocytes and asexual stages.

2.7.2 Functional analysis of PF3D7_0111400, PF3D7_0924600, PF3D7_0604500 and PF3D7_0522100 using targeted gene disruption

To investigate the significance of the MT-colocalizing proteins during gametocytogenesis, we generated transgenic targeted gene disruption (TGD) cell lines using the SLI system for gene truncation (255). Stable integrants were successfully obtained for all four target proteins (PF3D7_0111400, PF3D7_0924600, PF3D7_0604500 and PF3D7_0522100) (Fig. 15 D), indicating that none of them are essential for asexual proliferation.

To assess their role in gametocyte maturation, we induced gametocytogenesis and monitored parasite development through Giemsa smears and fluorescence microscopy every two days, beginning at day five (stage I). Additionally, we quantified parasitemia using flow cytometry to determine fold changes in parasite survival.

Among the tested proteins, Pf3D7_0522100 and Pf3D7_0111400 exhibited no apparent growth defects during gametocytogenesis (Fig. 15 E) when compared to the NF54-WT parasites. Giemsa smears and fluorescence images confirmed that these mutants completed gametocyte maturation without any obvious alteration in the SPMT cytoskeleton visualized by Tubulin Tracker (Fig. 15 A, C and F). However, a subset of parasites displayed an enlarged food vacuole from stage III onward, suggesting a potential, albeit subtle, impact on cellular homeostasis.

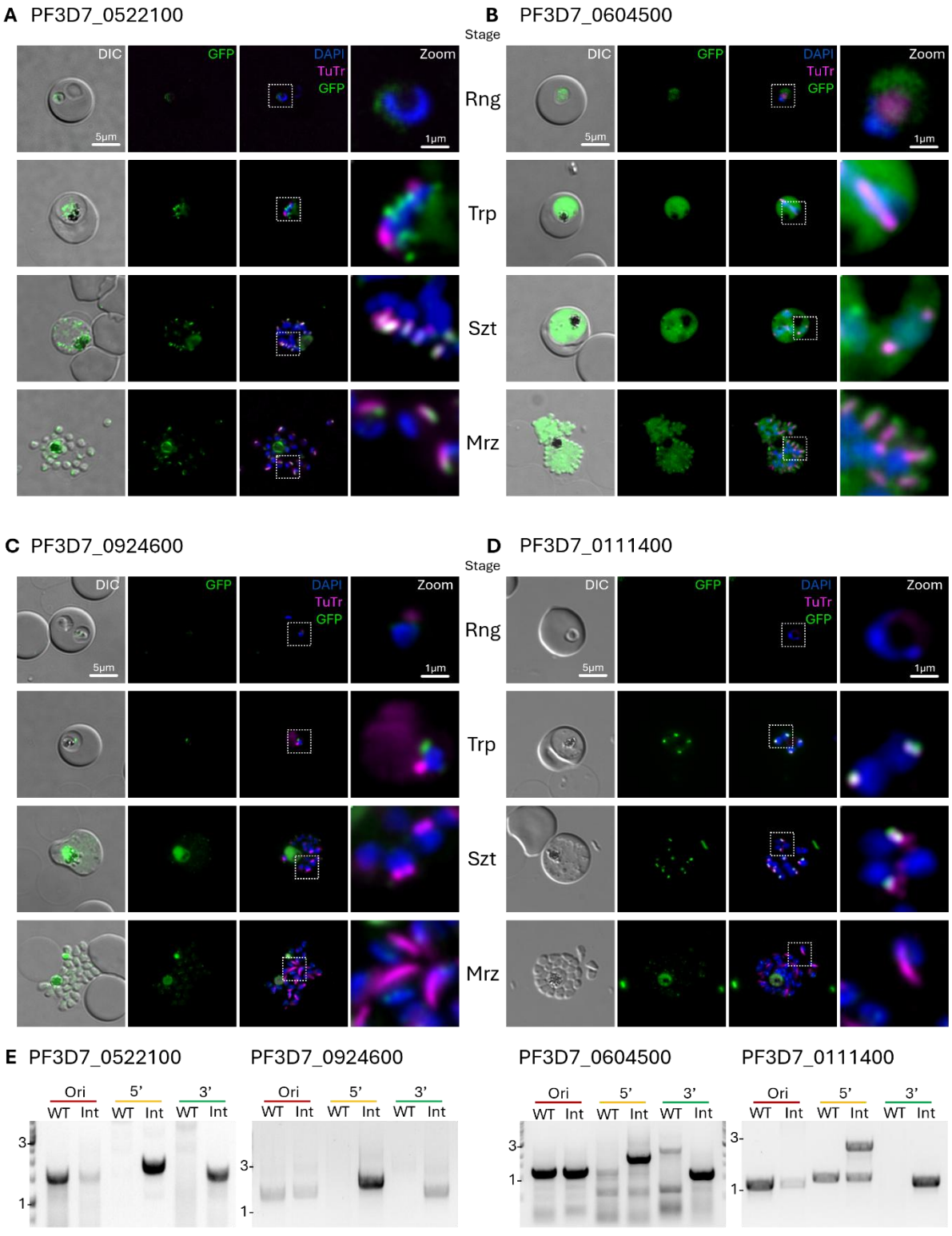

Figure 14: Localization of the MT-colocalizing proteins in asexual parasites.
(A-D) Life cell fluorescence microscopy images of transgenic parasites. Each protein of interest was endogenously tagged with GFP (green). Microtubule were visualized with Tubulin Tracker-deep red (magenta) and the DNA was stained with DAPI (blue). Pictures were taken 4h, 24h, 36h and 44h post invasion. Displayed are representative images of each lifecycle stage. Zoom factor, 500%. DIC, differential interference contrast; GFP, green fluorescent protein; TuTr, Tubulin Tracker deep red; Rng, ring stage; Trp, trophozoite; Szt, schizont; Mrz, merozoites. **(E)** Integration PCR for the cell lines showing a microtubule-like localization, with genomic DNA from the integrant (Int) or parental NF54/iGP (WT) parasites. Primer combinations are shown in Fig. 12 A and expected sizes are listed in Table12.

In contrast, the targeted gene disruption of PF3D7_0604500 led to a significant decline in parasite survival during the transition from stage II to stage III gametocytes (Fig. 15 E). Giemsa smears revealed that stage V parasites appeared to be smaller and with an abnormal phenotype in the Giemsa stain when compared to the controls (Fig. 15 F). Nonetheless, fluorescence microscopy revealed a normal assembly of the SPMT cytoskeleton, indicated by the Tubulin Tracker signal. Additionally, the PF3D7_0604500 deficient parasites seem to be able to complete gametocyte maturation (Fig. 15 B), suggesting that while PF3D7_0604500 is not essential for SPMT formation, it may play a role in gametocyte viability or structural integrity during development.

A more severe phenotype was observed in PF3D7_0924600-deficient parasites, which failed to progress beyond stage I gametocytes (Fig. 15 F), with a dramatic drop in parasite survival occurring at this early stage (Fig. 15 E). Given the MT localization of PF3D7_0924600, it is likely that this protein plays a crucial role in microtubule stability, potentially functioning as a stabilizer during early gametocytogenesis.

2.8 Proteins predominantly colocalizing with the MT tips

2.8.1 Protein localization

The third group of proteins is characterized by their predominant localization at the tips of the MTs during gametocyte development, along with an additional punctate nuclear localization near the DNA, reminiscent of centriolar plaque (CP) proteins (232; 238).

PF3D7_0529800, is a 225kDa protein. In early stage I gametocytes, it appears as a double-dotted structure near the DNA, always found in close association with nucMTs, which are easily visible at this stage. As gametocyte maturation progresses, from stage II onward, PF3D7_0529800 localizes to the tips of the main MT foot as well as the single MT on the opposite side of the foot, often appearing as one or two distinct dots. By stage IV, when the gametocyte reaches its maximum elongation, the protein adopts a ring-like structure at each end of the cell. In stage V, it disappears together with the SPMT corset and the only remaining fluorescence signal is a puncta in close proximity to the DNA signal. This DNA associated signal can be seen throughout gametocytogenesis, suggesting the protein mass that localizes to the nucleus is distinct to that at the SPMT (Fig. 16 A). Notably, in asexual parasites, PF3D7_0529800 localizes to the spindle MT tips during genomic replication, forming a "Mickey Mouse" structure when combined with the Tubulin Tracker signal—a pattern typical of centriolar plaque proteins (Fig. 17 C) (231).

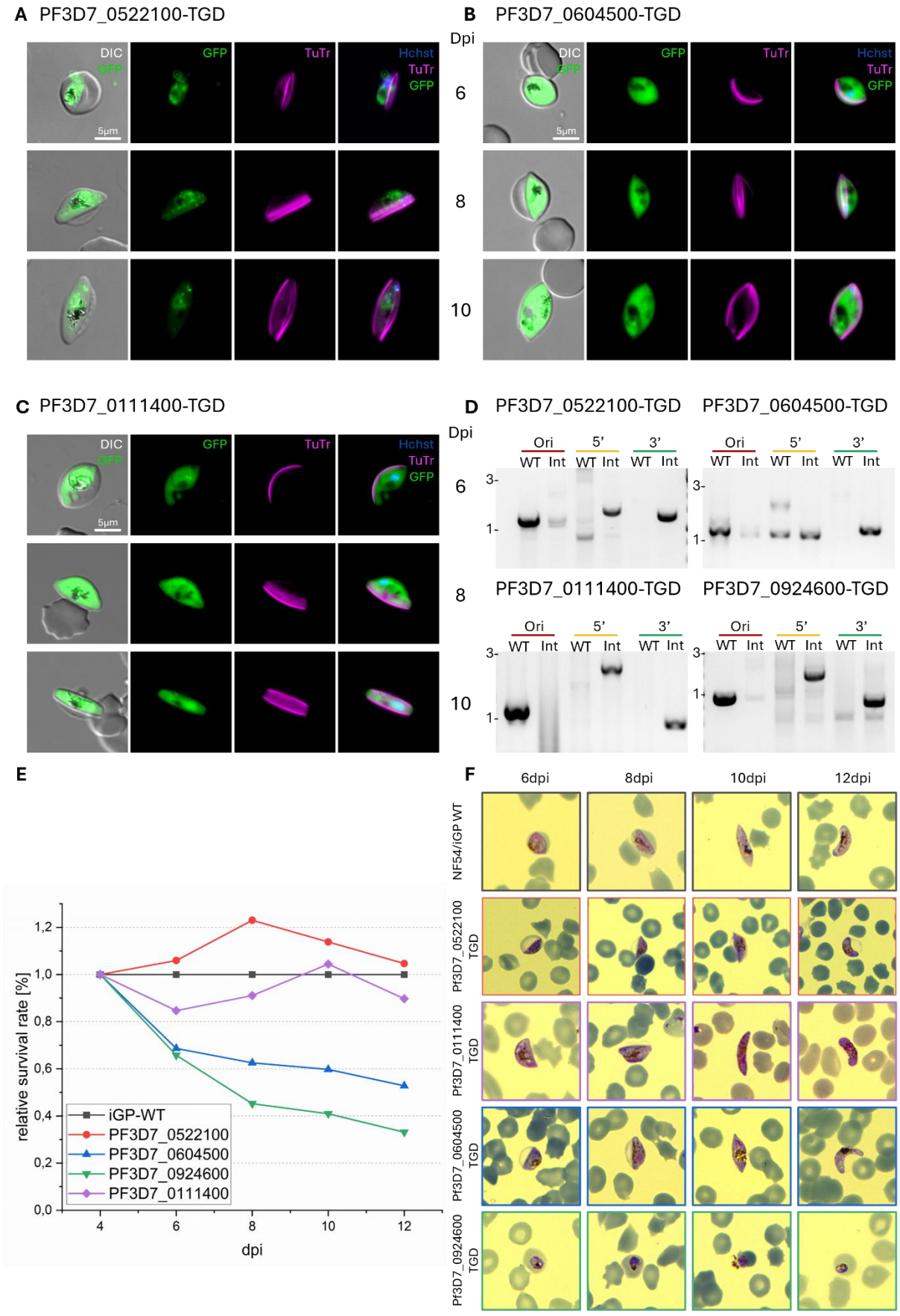

Figure 15: Functional knock out of the MT colocalizing proteins in gametocytes.

(A-C) Life cell fluorescence microscopy images of gene knock out parasites (6d, 8d and 10d post gametocyte induction). Microtubules were visualized with Tubulin Tracker-deep red (magenta) and the DNA was stained with Hoechst 33342 (blue). **(D)** Integration PCR for the TGD cell lines for proteins showing a microtubule-like localization, with genomic DNA from the integrant (Int) or parental NF54/iGP (WT) parasites. Primer combinations are shown in Fig. 12 A and expected sizes are listed in Table12. **(E)** Relative gametocyte survival of the knock out cell lines. Gametocytemia was determined by flow cytometry using SYBR green and DHE. The relative parasite survival rate was determined by first calculating the fold change between each gametocyte stage and stage I followed by dividing the respective fold change by the fold change of the NF54/iGP wildtype parasites. **(F)** Representative Giemsa smears of stage II to V gametocytes for NF54/iGP WT and each knock out cell line. DIC, differential interference contrast; GFP, green fluorescent protein; TuTr, Tubulin Tracker deep red.

The 118kDa PF3D7_0705100 is forming a double-dot structure in stage I gametocytes (Fig. 15 B) in close connection with both DNA and MTs and localizing to MT tips in later stages. Additionally, a punctate nuclear signal persists in later gametocyte stages (Fig. 16 B). However, its localization differs significantly in asexual parasites, where it forms a single dot near the spindle MTs in late asexual stages and appears at one tip of the double MT strand in merozoites (Fig.17 D). This polar localization suggests that PF3D7_0705100 binds to either the plus or minus end of MTs in asexual parasites.

PF3D7_0504800 is a 672kDa protein which is predicted to contain a trimeric LpxA-like domain and a 32kDa heat shock-like domain. PF3D7_0504800 shares a similar localization pattern with PF3D7_0529800, displaying a dotted pattern at MT tips in gametocytes (Fig.16 C) and a centriolar plaque-like localization in asexual parasites (Fig.17 E).

Lastly, PF3D7_1322200 is a 402kDa protein. Notably, it contains a TOG domain, a feature commonly found in microtubule-associated proteins (MAPs) like XMAP215. PF3D7_1322200 predominantly exhibits a nuclear localization, often colocalizing with nucMTs in a dotted pattern, until stage III, when these MTs depolymerize (Fig. 16 D). After this stage, it appears diffusely within the nucleus. Additionally, from stage I to IV, it is consistently found at MT tips until the SPMT network is depolymerized (Fig.17 A). This aligns well with the predicted function of its TOG domain, supporting its potential role as a MT plus-end binding protein. In asexual parasites, PF3D7_1322200 localizes to the spindle MTs of dividing nuclei but is absent in mature merozoites. In early asexual stages, it exhibits a diffuse cytoplasmic localization (Fig. 17 F).

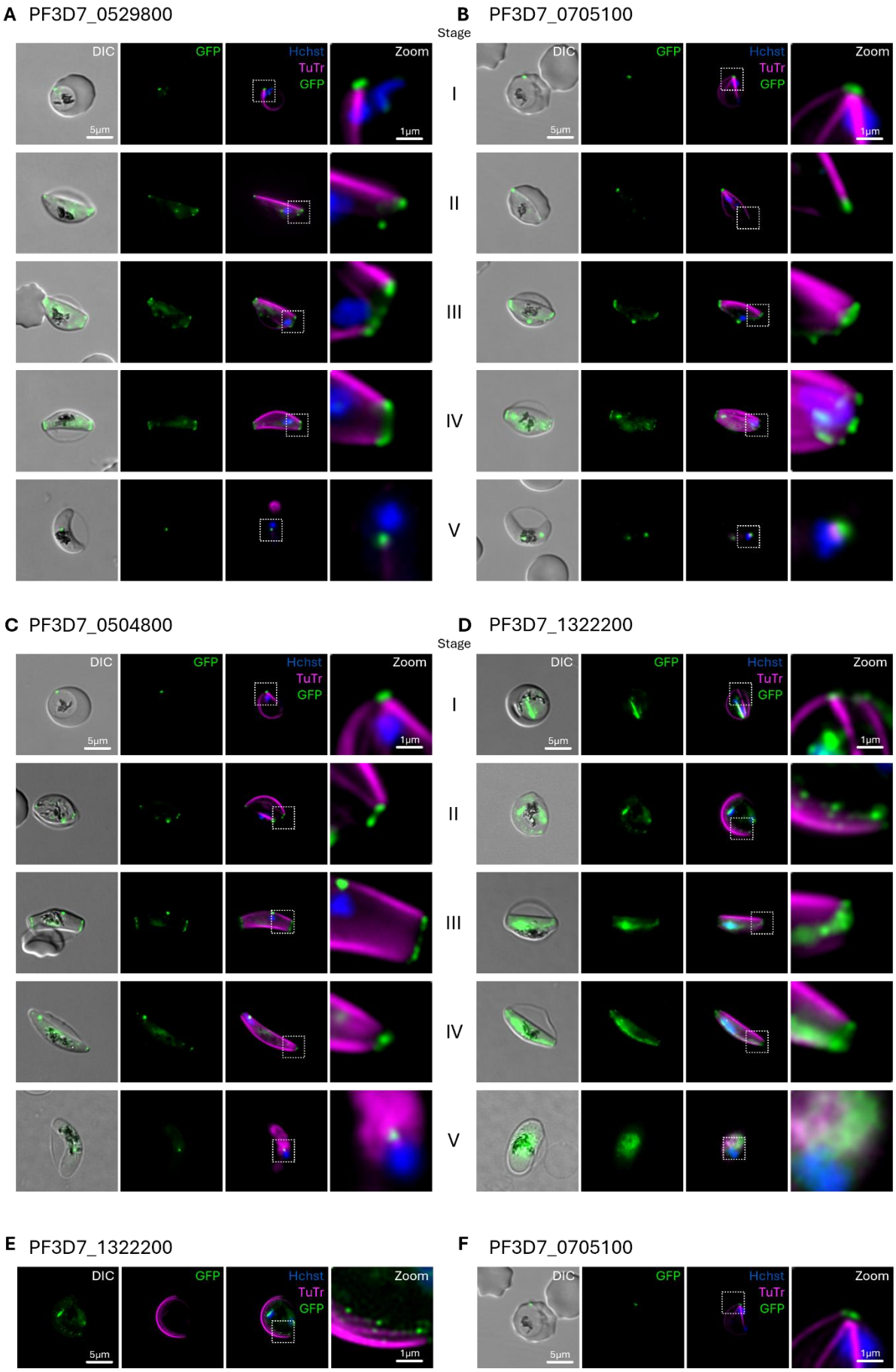

Figure 16: Four Proteins localize to the tip of the microtubule.

(A-D) Life cell fluorescence microscopy images of transgenic parasites. Each protein of interest was endogenously tagged with GFP (green). Microtubule were visualized with Tubulin Tracker-deep red (magenta) and the DNA was stained with Hoechst 33342 (blue). Pictures were taken every two days starting 72h after gametocytogenesis induction. Displayed are representative images of each Gametocyte stage. **(E, F)** Thunder improved images of PF3D7_1322200 and PF3D7_0705100 in Gametocytes. Zoom factor, 500%. DIC, differential interference contrast; GFP, green fluorescent protein; Hchst, Hoechst 33342; TuTr, Tubulin Tracker deep red.

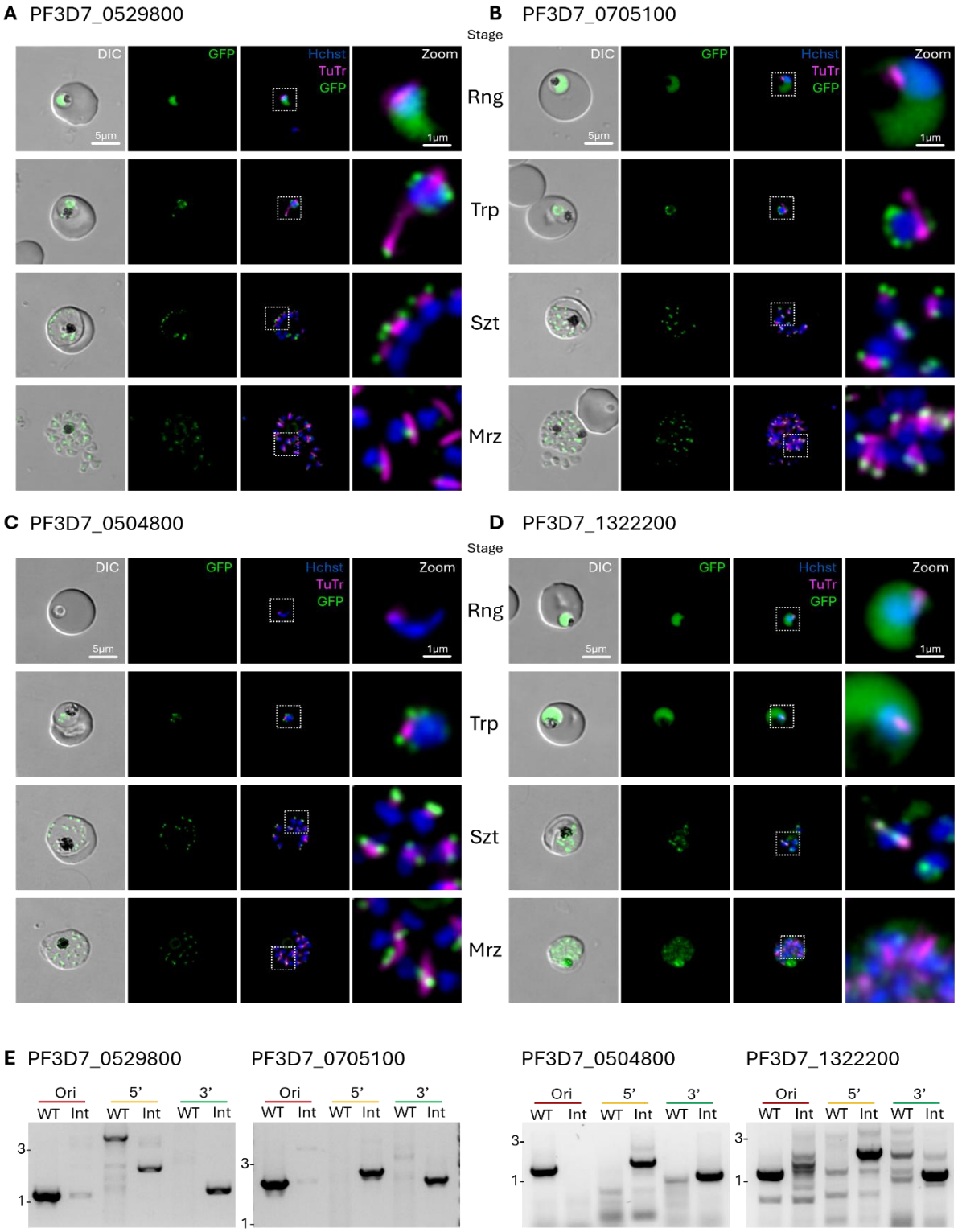

Figure 17: Localization of the microtubule tip-colocalizing proteins in asexual parasites.

(A-D) Life cell fluorescence microscopy images of transgenic parasites. Each protein of interest was endogenously tagged with GFP (green). Microtubule were visualized with Tubulin Tracker-deep red (magenta) and the DNA was stained with DAPI (blue). Pictures were taken 4h, 24h, 36h and 44h post invasion. Displayed are representative images of each lifecycle stage. Zoom factor, 500%. DIC, differential interference contrast; GFP, green fluorescent protein; TuTr, Tubulin Tracker deep red. **(E)** Integration PCR for the cell lines showing a microtubule-tip like localization, with genomic DNA from the integrant (Int) or parental NF54/iGP (WT) parasites. Primer combinations are shown in Fig. 12 A and expected sizes are listed in Table12.

These findings collectively highlight a group of proteins that share a common pattern of MT tip localization during gametocyte development, with additional CP-like properties in some cases. Their differential localizations in asexual parasites and gametocytes suggest specialized roles in MT organization, chromosome segregation, and structural integrity, making them intriguing candidates for further functional studies.

2.8.2 Knock sideways of MT tip proteins

To investigate the function of MT tip-binding proteins, we initially aimed to disrupt the respective genes using TGD. However, due to time constraints, we were unable to generate the necessary knockout cell lines. As an alternative, we utilized the NLS-based KS system (255), which was already integrated into the tagging plasmids. These constructs included multiple FKBP repeats, enabling inducible mislocalization. Upon addition of Rapalog, FKBP interacts with the FRB domain fused to a NLS, leading to rapid relocalization of the target protein into the nucleus and functional depletion from its native cytoplasmic site.

PF3D7_0529800, PF3D7_0705100 and PF3D7_0504800 did not show any apparent growth defects (Fig. 18 E) after the addition of Rapamycin and no morphological aberrations could be observed in the Giemsa smears (Fig. 18 F). Fluorescence microscopy revealed only a partial mislocalization of the proteins into the nucleus. Fractions of the proteins remained at the tip of the MTs (Fig. 18 A-D, white arrows).

Using the KS system, PF3D7_1322200 could be completely mislocalized into the nucleus (Fig.18 D). The mislocalization resulted in a moderate reduction in gametocyte survival compared to the NF54/iGP wild-type cell line, but did not cause any noticeable changes in gametocyte morphology (Fig. 18E, F).

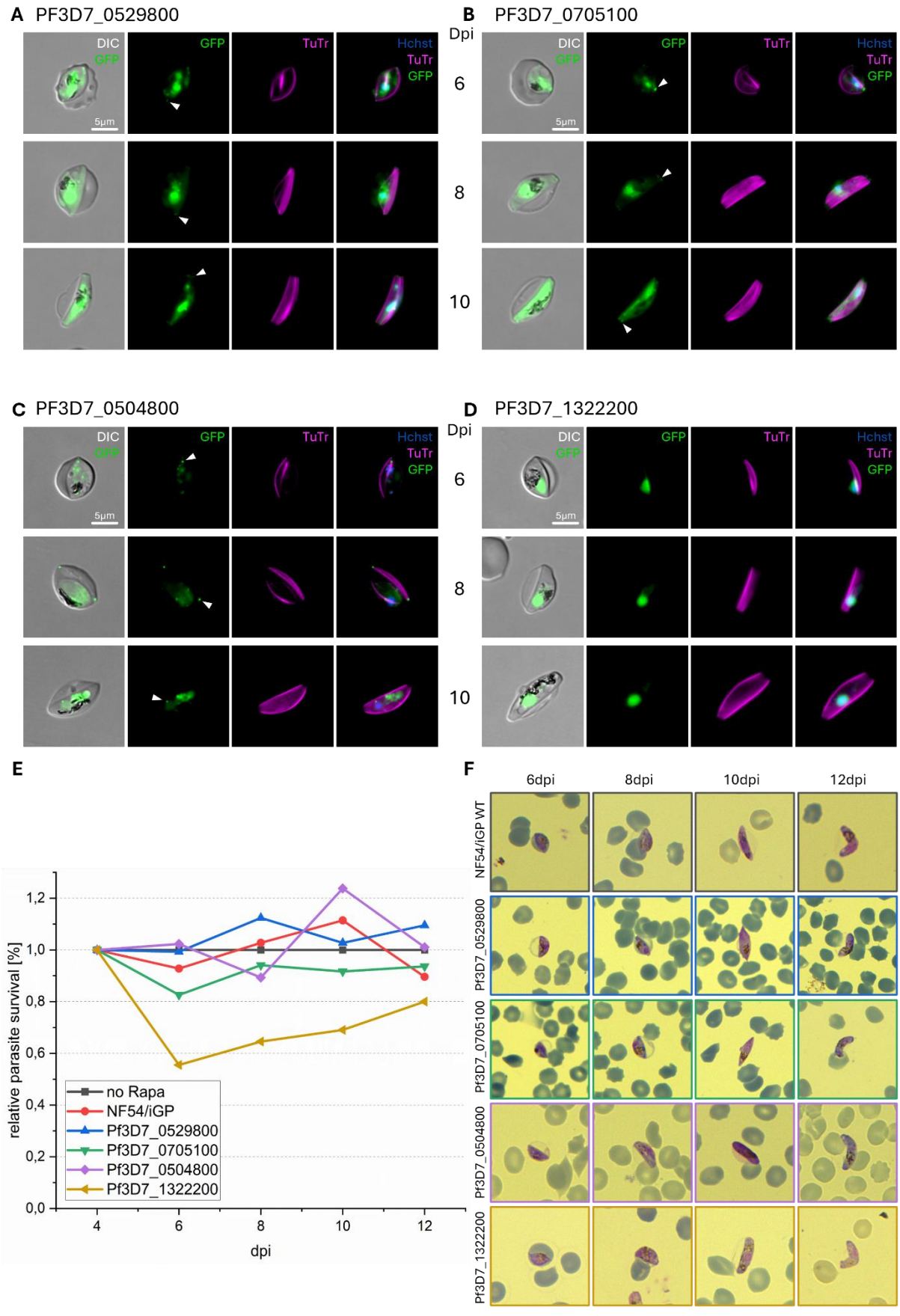

Figure 18: Functional knock sideways of the microtubule-tip localizing proteins in gametocytes.

(A-D) Life cell fluorescence microscopy images of gametocytes (day 7 to day 11 after gametocyte induction) cultured with (200nM) Rapamycin. Microtubule were visualized with Tubulin Tracker-deep red (magenta) and the DNA was stained with Hoechst 33342 (blue). **(E)** Relative survival of gametocytes cultured with (200nM) Rapamycin. Gametocytemia was determined by flow cytometry using SYBR green and DHE. The relative parasite survival rate was determined by first calculating the fold change between each gametocyte stage and stage I followed by dividing the respective fold change by the fold change of gametocytes cultured without Rapamycin. **(F)** Representative Giemsa smears of stage II to V gametocytes for each knock sideways cell line. DIC, differential interference contrast; GFP, green fluorescent protein; TuTr, Tubulin Tracker deep red.

2.9 Proteins with a suture like localization

2.9.1 Protein localization

This group of proteins exhibits a striped pattern perpendicular to the SPMT cytoskeleton in late-stage gametocytes, resembling the IMC sutures—proteinaceous fibers that connect IMC plates (166).

The proteins PF3D7_1203300, PF3D7_0805100, and PF3D7_1416600 share a highly similar localization pattern throughout gametocytogenesis. They first appear as evenly spaced dots along the main MT strand during the transition between Stage I and II gametocytes but do not interact with the nucMTs. As the gametocyte progresses to Stage III, these protein signals elongate into thin strips that extend with the growing MT sheet, covering the gametocyte's foot. By Stage IV, when the SPMT corset is fully assembled, the stripes span the parasite's width, running perpendicular to the SPMT cytoskeleton. Notably, these proteins disappear along with the SPMTs in Stage V (Fig. 19 A, B, C).

PF3D7_1203300 is a 117kDa protein, predicted to contain a TBCCD1-like domain, which in other organisms is involved in cellular organization, including mitochondrial, Golgi, and centrosome positioning (269; 270). PF3D7_0805100 is a 64kDa protein and PF3D7_1416600 is a 357kDa protein. Both proteins are annotated as putative, unknown proteins without any predicted function or domains. In asexual parasites, PF3D7_1203300 localizes to the spindle MT tips during genomic replication, similar to CP proteins (Fig. 20 A), while PF3D7_0805100, and PF3D7_1416600 seem not to be expressed in asexual parasites and only the GDV1-background signal near the DNA could be observed (Fig. 20 B, C).

PF3D7_0311400 or Protein Kinase related Protein (PKRP) is a 295kDa protein, which is predicted to contain a protein-kinase like domain. Previous work has shown that PKRP localizes as dots in close proximity to the nucleus in late stage asexual parasites (265). Preliminary data in gametocytes showed, that PKRP appears as a faint dots sitting on top of the initial SPMT strand and during gametocyte maturation, PKRP forms suture like stripes across the SPMT sheet (Fig. 19 D).

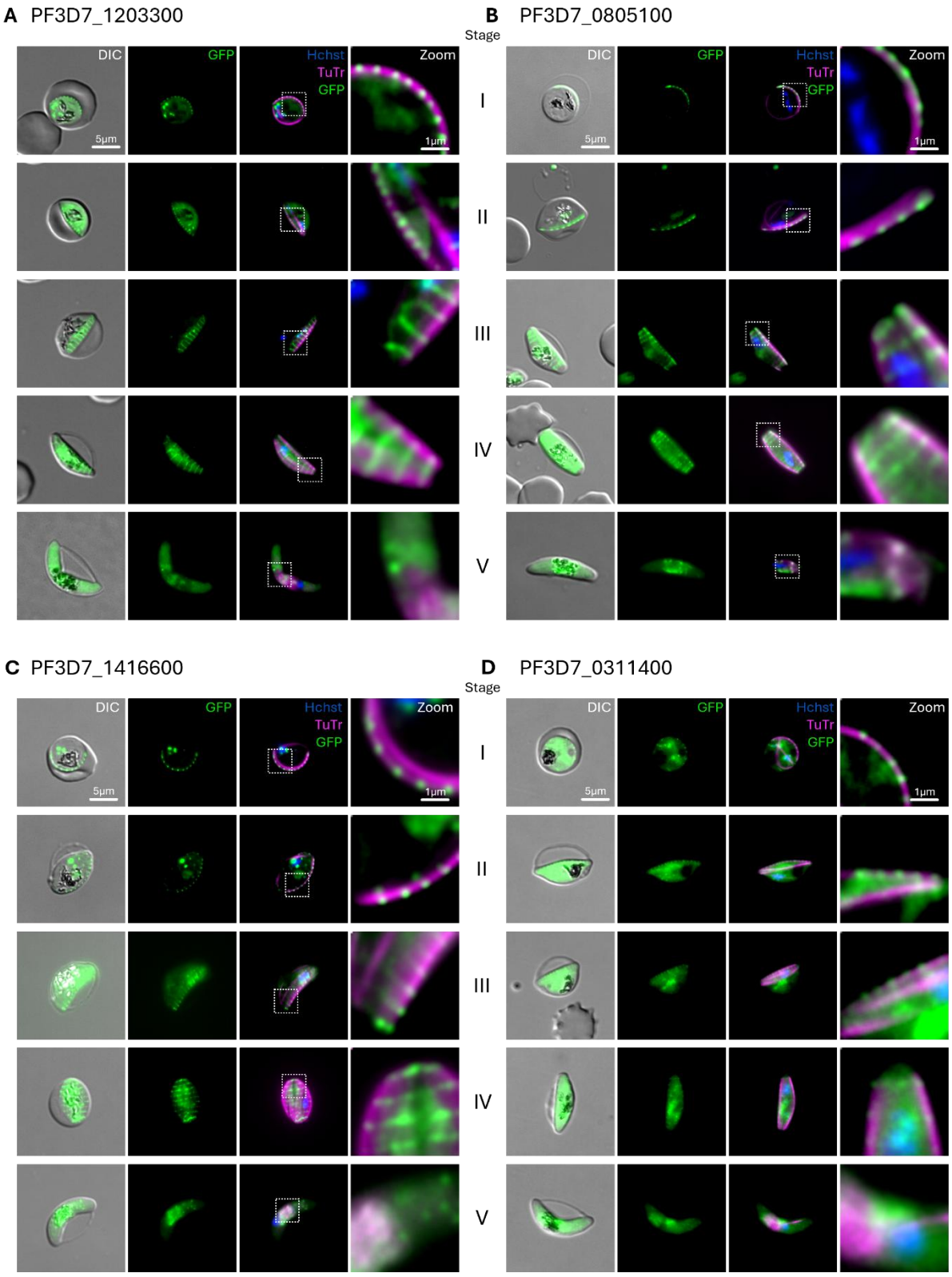

Figure 19: Suture-like localization of PF3D7_1203300, PF3D7_0805100, PF3D7_1416600 and PF3D7_0311400.

(A-D) Life cell fluorescence microscopy images of transgenic parasites. Each protein of interest was endogenously tagged with GFP (green). Microtubule were visualized with Tubulin Tracker-deep red (magenta) and the DNA was stained with Hoechst 33342 (blue). Pictures were taken every two days starting 72h after gametocytogenesis induction. Displayed are representative images of each Gametocyte stage.

Zoom factor, 500%. DIC, differential interference contrast; GFP, green fluorescent protein; Hchst, Hoechst 33342; TuTr, Tubulin Tracker deep red.

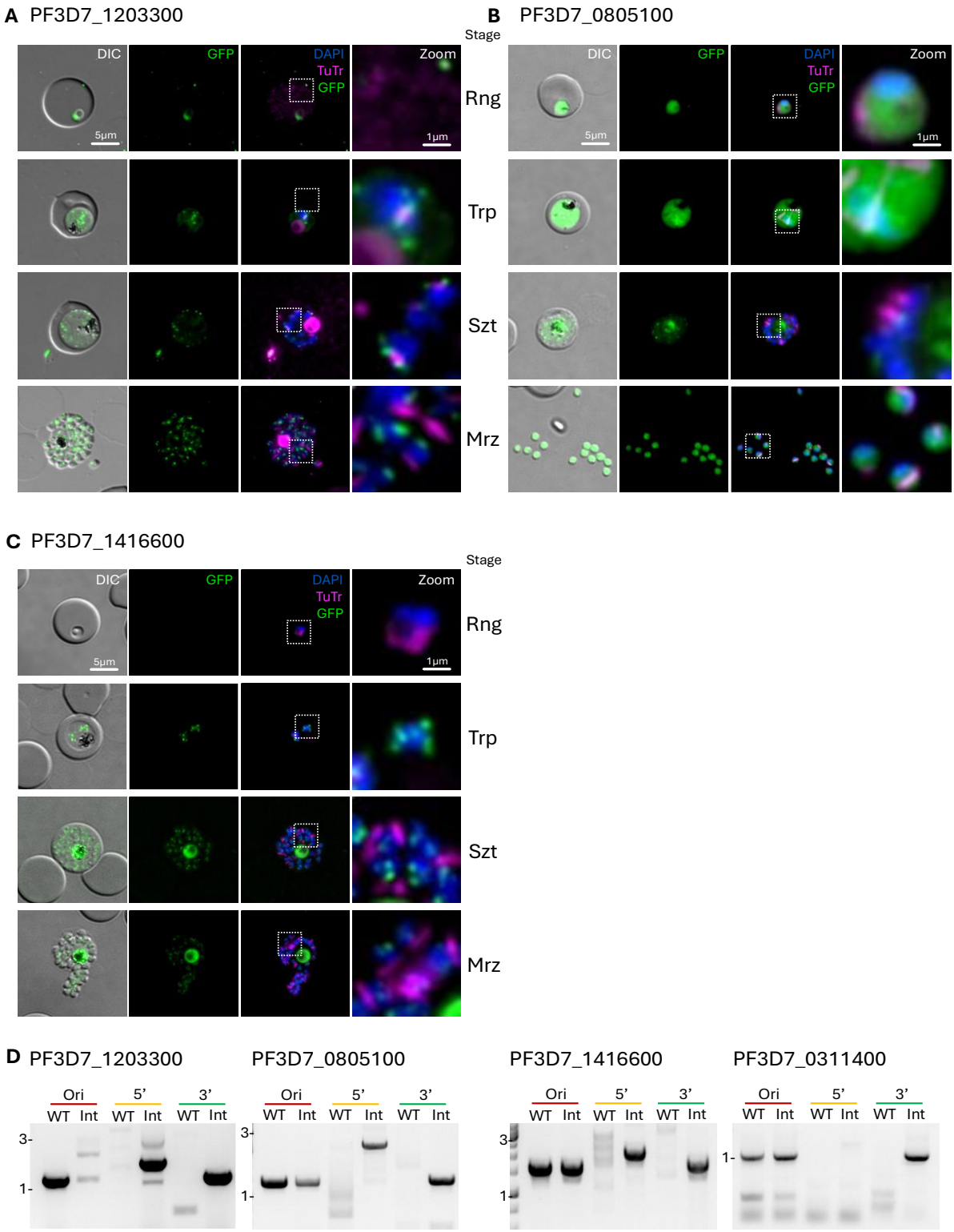

Figure 20: Localization of PF3D7_1203300, PF3D7_0805100 and PF3D7_1416600 in asexual parasites. **(A-C)** Life cell fluorescence microscopy images of transgenic parasites. Each protein of interest was endogenously tagged with GFP (green). Microtubule were visualized with Tubulin Tracker-deep red (magenta) and the DNA was stained with DAPI (blue). Pictures were taken 4h, 24h, 36h and 44h post

invasion. Displayed are representative images of each lifecycle stage. Zoom factor, 500%. DIC, differential interference contrast; GFP, green fluorescent protein; TuTr, Tubulin Tracker deep red. **(D)** Integration PCR for the cell lines showing a suture-like localization, with genomic DNA from the integrant (Int) or parental NF54/iGP (WT) parasites. Primer combinations are shown in Fig. 12 A and expected sizes are listed in Table12.

PF3D7_1449100 is a 121kDa protein, predicted to contain a C-terminal CLASP_N domain. In gametocytes, PF3D7_1449100 appears as evenly spaced dots along the main MT strand in Stage II, then transitions into a characteristic suture-like pattern with thin stripes across the parasite in Stages III and IV, before disappearing along with the SPMTs in Stage V (Fig. 21 A). Interestingly, in some Stage IV parasites, PF3D7_1449100 localizes at the tips of the SPMT cytoskeleton rather than forming a suture-like pattern (Fig. 21 C), while in others, both localizations coexist. In asexual parasites, it first appears as two kinetochore-associated dots during schizogony and later as a single dot at the tip of the MT double strand in merozoites (Fig. 22 D).

The 243kDa protein PF3D7_1003400 is predicted to contains a single transmembrane domain at the C-terminus, 12 amino acids from the stop codon. In gametocytes, the protein first appears as evenly spaced dots along the main MT strand in Stage II. By Stage III, these dots elongate into stripes perpendicular to the SPMT sheet. In Stage IV, the protein disappears, sometimes leaving small residual dots connected to a few MT strands before vanishing completely in Stage V (Fig. 21 B). Interestingly, in asexual parasites, it colocalizes with MTs in late schizonts and merozoites (Fig. 22 E). This makes PF3D7_1003400 the only known protein with a suture-like localization that contains a TMD, making it a prime candidate for linking the IMC to the SPMTs.

In gametocytes, the IMC has been reported to form 13 rectangular plates (271). To verify the suture like localization of our proteins, we counted the number of suture-like structures (SLS) (Fig. 21 D) for each suture-like candidate except PF3D7_0311400. Interestingly, while PF3D7_1003400, PF3D7_0805100 and 377 PF3D7_1416600 show a median number of 12 SLS, in PF3D7_1203300 most parasites showed 11 SLS. PF3D7_1449100 on the other hand, showed a median number of 14 SLS (Fig. 21 C). Given the fact that PF3D7_1449100 was also found to bind to the MT tips, there is the possibility that the two outer dots are not suture connected but the tip of the SPMTs.

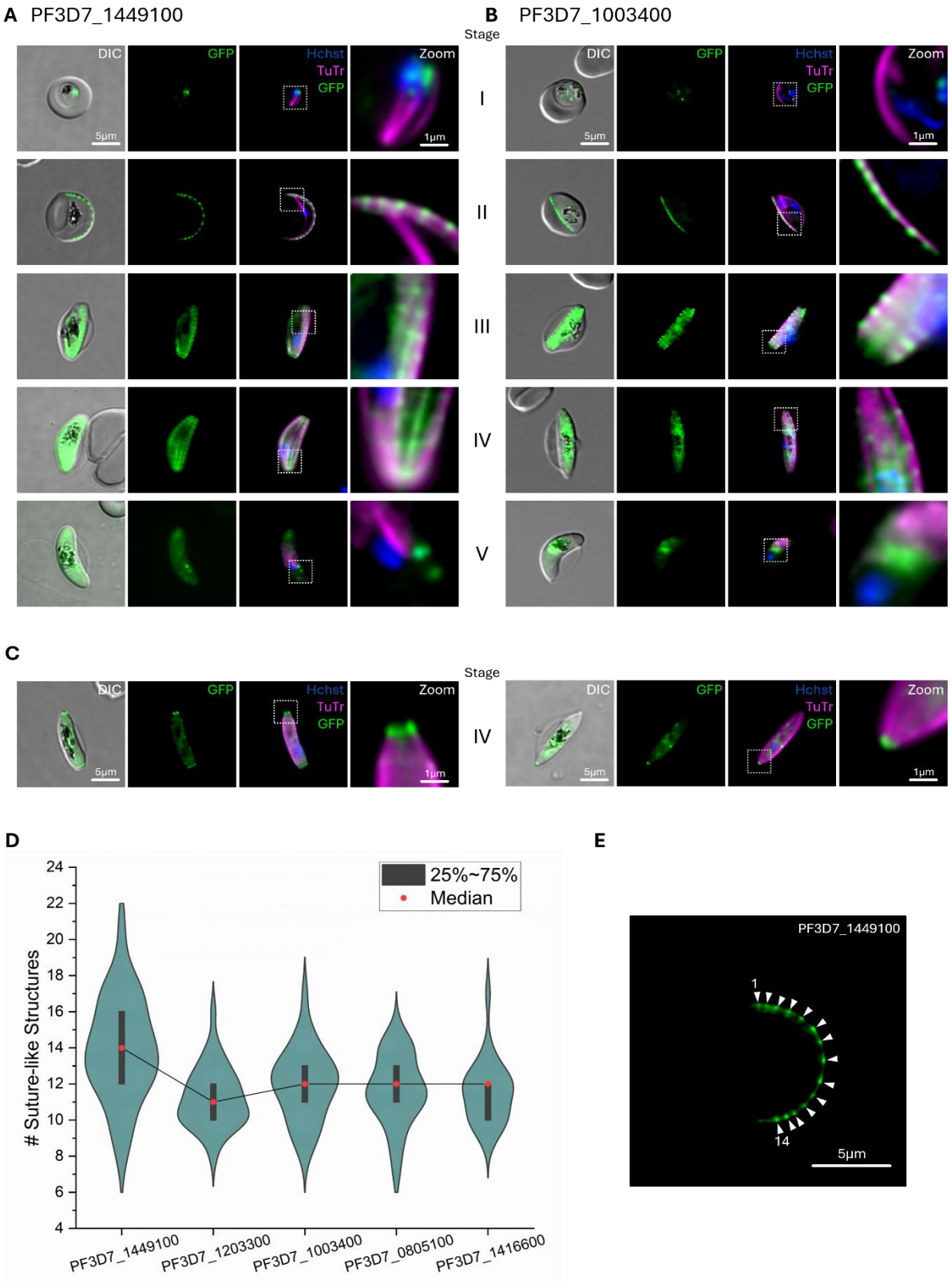

Figure 21: Suture like localization of PF3D7_1449100 and PF3D7_1003400.
(A, B) Life cell fluorescence microscopy images of transgenic parasites. Each protein of interest was endogenously tagged with GFP (green). Microtubule were visualized with Tubulin Tracker-deep red (magenta) and the DNA was stained with Hoechst 33342 (blue). Pictures were taken every two days starting 72h after gametocyte induction. Displayed are representative images of each Gametocyte stage. Zoom factor, 500%. DIC, differential interference contrast; GFP, green fluorescent protein; Hchst, Hoechst 33342; TuTr, Tubulin Tracker deep red. **(C)** Exemplary pictures of 357s additional microtubule tip localization.

Microtubule were visualized with Tubulin Tracker-deep red (magenta) and the DNA was stained with Hoechst 33342 (blue). Pictures were taken 11d after gametocyte induction. **(D)** Number of suture-like structures in a single gametocyte. The number of analyzed gametocytes is indicated with n. **(E)** Exemplary counting of suture-like structures in a stage II gametocyte of PF3D7_1449100. The arrows indicate the counted suture like structures.

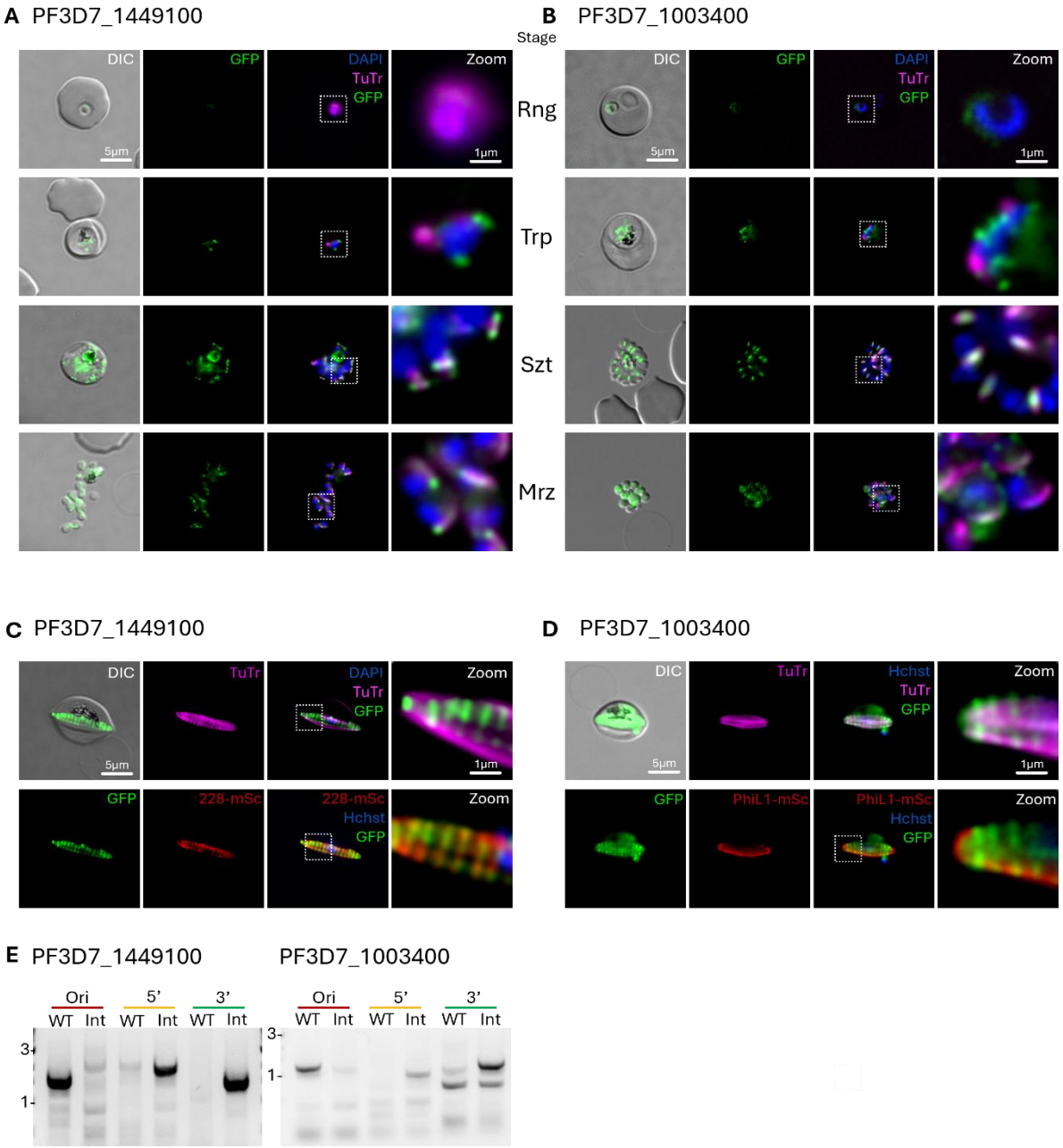

Figure 22: Localization of PF3D7_1449100 and PF3D7_1003400 in asexual parasites and their colocalization with suture or IMC marker.

(A, B) Life cell fluorescence microscopy images of transgenic parasites. Each protein of interest was endogenously tagged with GFP (green). Microtubule were visualized with Tubulin Tracker-deep red (magenta) and the DNA was stained with DAPI (blue). Pictures were taken 4h, 24h, 36h and 44h post invasion. Displayed are representative images of each lifecycle stage. **(C)** PF3D7_1449100 colocalizes with the suture protein 228-mCherry (yellow). **(D)** PF3D7_1003400 localizes between the IMC plates visualized with PhiL1-mCherry (red). Life cell fluorescence microscopy images of transgenic parasites co-transfected with episomal marker plasmids. Each protein of interest was endogenously tagged with GFP (green).

Microtubule were visualized with Tubulin Tracker-deep red (magenta) and the DNA was stained with Hoechst 33342 (blue). Pictures were taken every two days starting 72h after gametocyte induction. Displayed are representative images of different Gametocyte stages. Zoom factor, 500%. DIC, differential interference contrast; GFP, green fluorescent protein; Hchst, Hoechst 33342; TuTr, Tubulin Tracker deep red. **(E)** Integration PCR for the cell lines showing a suture-like localization, with genomic DNA from the integrant (Int) or parental NF54/iGP (WT) parasites. Primer combinations are shown in Fig. 12 A and expected sizes are listed in Table12.

To additionally verify the suture like localization, we representatively colocalized some of the suture-like candidates with known suture or IMC marker. To enable colocalization with the suture protein 228 (123), we endogenously cotransfected the pSLI- PF3D7_1449100-GFP-NLS cell line with mCherry tagged protein 228 facilitating the SLI system a second time. For the colocalization with the IMC marker PhiL1, we transfected the pSLI-PF3D7_1003400-GFP-NLS cell line with an episomale expressed PhiL1-mCherry construct.

Fluorescence microscopy in late-stage gametocytes showed, that PF3D7_1449100 colocalizes with the striped pattern of the suture marker protein 228 (Fig. 22 C). Additionally, we could show that PF3D7_1003400 localizes as strips between the PhiL1-mSc marked suture plates (Fig. 22 D). This observation further confirms the suture like localization of these candidates.

2.9.2 Super resolution images of suture like candidates

To gain a deeper understanding of the localization of these suture-like proteins, particularly in relation to the SPMT corset, we employed the THUNDER algorithm from Leica. This approach allowed us to enhance image resolution by reducing fluorescence background noise, providing clearer insights into protein distribution.

Our analysis revealed distinct localization patterns among the proteins. PF3D7_1203300 forms consistent stripes across the parasite, though it does not appear to be specifically associated with individual SPMT strands (Fig. 23 A). In contrast, PF3D7_1416600 creates concentric rings around the parasite, perpendicular to the SPMT cytoskeleton, with a distinct concentration on single MT strands (Fig. 23 C). PF3D7_1449100 exhibits a "beads on a string" pattern along the SPMT strands. Interestingly, colocalization studies with the suture marker 228 indicated only partial overlap—while the 228 signal forms continuous stripes across the parasite, PF3D7_1449100 appears as discrete dots positioned on top of the SPMTs (Fig. 23 E).

The localization pattern of PF3D7_1003400 proved to be more complex. By Stage IV, when the SPMT corset is fully formed, the protein appears to have disappeared. However, in Stage III, it forms stripes across the growing SPMT sheet without a specific association with individual SPMT strands (Fig. 23 D). These findings suggest that while all four proteins contribute to the structural organization of the gametocyte cytoskeleton, their precise roles and interactions with the SPMTs vary significantly throughout maturation.

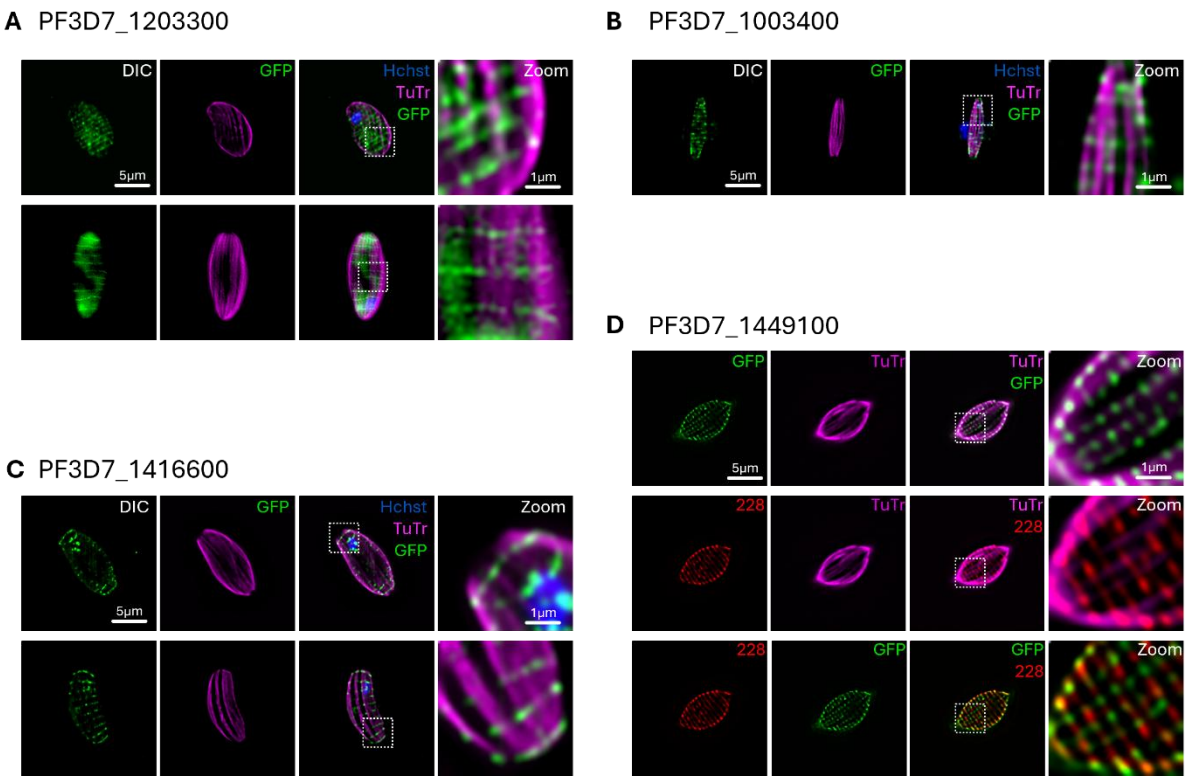

Figure 23: Super resolution images of suture-like proteins.
Life cell fluorescence microscopy images of transgenic parasites. Each protein of interest was endogenously tagged with GFP (green). Microtubules were visualized with Tubulin Tracker-deep red (magenta) and the DNA was stained with Hoechst 33342 (blue). Pictures were taken every two days starting 72h after gametocyte induction. Displayed are representative images stage IV gametocytes (stage III for PF3D7_1003400). Super resolution was achieved by using the Thunder SVCC algorithm from Leica. **(A)** Pf3D7_1203300 shows a stripe like pattern without specific microtubule interaction. **(B, C)** PF3D7_1003400 and PF3D7_1416600 show ring like structures around the SPMT corset with specific microtubule interaction. **(D)** PF3D7_1449100 shows a beads on a string pattern specifically interacting with the microtubules and partially colocalizing with the sutures. The sutures were visualized with protein-228-mCherry (red). Zoom factor, 500%. DIC, differential interference contrast; GFP, green fluorescent protein; Hchst, Hoechst 33342; TuTr, Tubulin Tracker deep red.

2.9.3 knock sideways of suture like proteins

To better understand the function of these suture-like proteins, we aimed to generate TGD lines for each candidate. However, despite multiple attempts, we were unable to establish stable TGD-integration lines for PF3D7_1203300, PF3D7_0805100, and PF3D7_1449100. This suggests that these proteins might be essential for asexual parasite survival. To further investigate their function, we utilized the NLS system, which was already integrated alongside the protein tags.

The addition of Rapalog to the culture of PF3D7_1203300 and PF3D7_0805100 led to the mislocalization of the proteins into the nucleus, where PF3D7_0805100 seem to interact with the nucMT (Fig. 24 A, B). The mislocalization did not lead to any observable growth defect or morphological alterations in both cell lines (Fig. 24 E, F).

For PF3D7_1449100, the addition of Rapalog did not result in a clear growth defect or observable phenotype throughout gametocytogenesis (Fig. 24 E, F). Fluorescence microscopy revealed that some of the protein was mislocalized into the nucleus, where it interacted with the nucMTs. However, portions of the proteins remained associated with the SPMTs, particularly at the tips. This residual localization was also observed in some untreated stage IV gametocytes. Notably, the classical suture-like stripes did not form in the late stages, indicating only partial functionality of the system (Fig. 24 C). It is possible that this protein is strongly bound to the MT tips, preventing their full mislocalization. Additionally, the lack of an apparent gametocytogenesis defect suggests that either these proteins are non-essential for this process or that their suture-like localization is not critical for function.

3.7.4 TGD of suture like proteins PF3D7_1416600 and PF3D7_1003400

We successfully generated TGD lines for the proteins PF3D7_1416600 and PF3D7_1449100, allowing us to investigate their roles in gametocyte development. In the PF3D7_1416600-TGD line, we observed a moderate reduction in gametocyte survival (Fig. 25 A). However, Giemsa smears did not reveal any morphological abnormalities (Fig. 25 B), and fluorescence microscopy confirmed that the SPMT cytoskeleton remained intact, enabling parasites to complete gametocyte maturation without apparent structural defects (Fig. 25 D).

In contrast, the PF3D7_1449100-deficient cell line exhibited a more pronounced phenotype. While gametocyte survival was only moderately reduced compared to the Nf54/iGP parental line (Fig. 25 A), a striking bloated morphology emerged in the parasites (Fig. 25 B). Quantification of abnormal gametocytes 13 dpi revealed that over 80% displayed this phenotype, which was absent in the PF3D7_1416600-TGD line (Fig. 25 C). Given its similarity to the SPM3-KO phenotype observed in previous studies, we employed fluorescence microscopy using the Tubulin Tracker to gain further insights into the ultrastructure of these abnormal cells.

Our analysis revealed that in PF3D7_1449100-deficient parasites, MTs clustered on one side of the cell, resembling a Stage III-like arrangement but with tapered ends (Fig. 25 E). Stage-specific quantification confirmed that the phenotype first appeared in Stage III (Fig. 26 A), aligning with the observed morphological defects. Additionally, in differential interference contrast (DIC) microscopy, we detected an accumulation of vesicular structures within some parasites. Previous studies have linked disruptions in IMC biogenesis to the accumulation of food vacuole-derived vesicles in the cytoplasm, prompting us to investigate further.

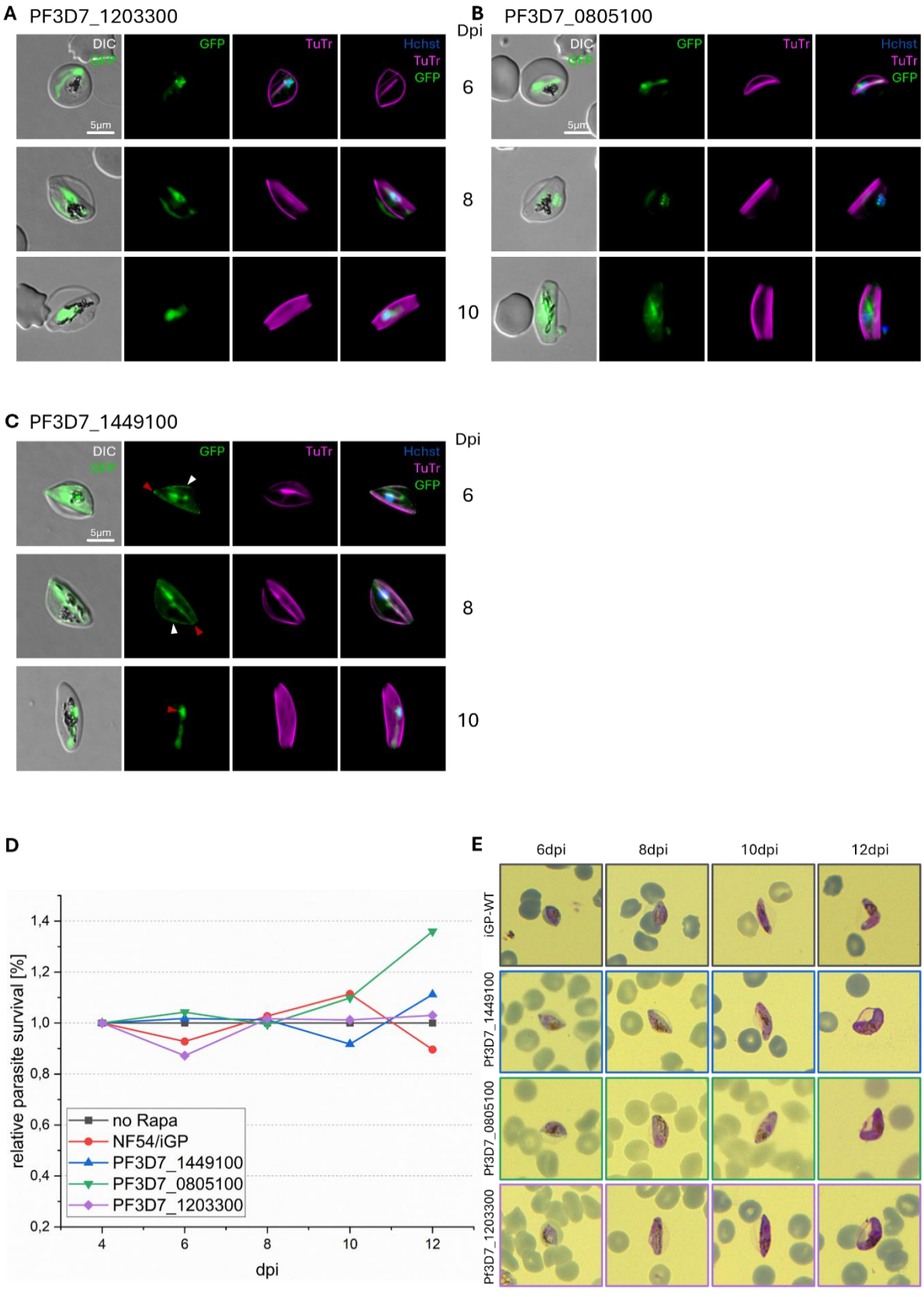

Figure 24: The suture like proteins lose their suture like localization after knock-sideway induction. **(A-C)** Life cell fluorescence microscopy images of gametocytes (day 7 to day 11 after gametocyte induction) cultured with (200nM) Rapamycin. Microtubules were visualized with Tubulin Tracker-deep red (magenta) and the DNA was stained with Hoechst 33342 (blue). **(D)** Relative survival of gametocytes cultured with (200nM) Rapamycin. Gametocytemia was determined by flow cytometry using SYBR green and DHE. The

relative parasite survival rate was determined by first calculating the fold change between each gametocyte stage and stage I followed by dividing the respective fold change by the fold change of gametocytes cultured without Rapamycin. **(E)** Representative Giemsa smears of stage II to V gametocytes for each knock sideways cell line. DIC, differential interference contrast; GFP, green fluorescent protein; TuTr, Tubulin Tracker deep red.

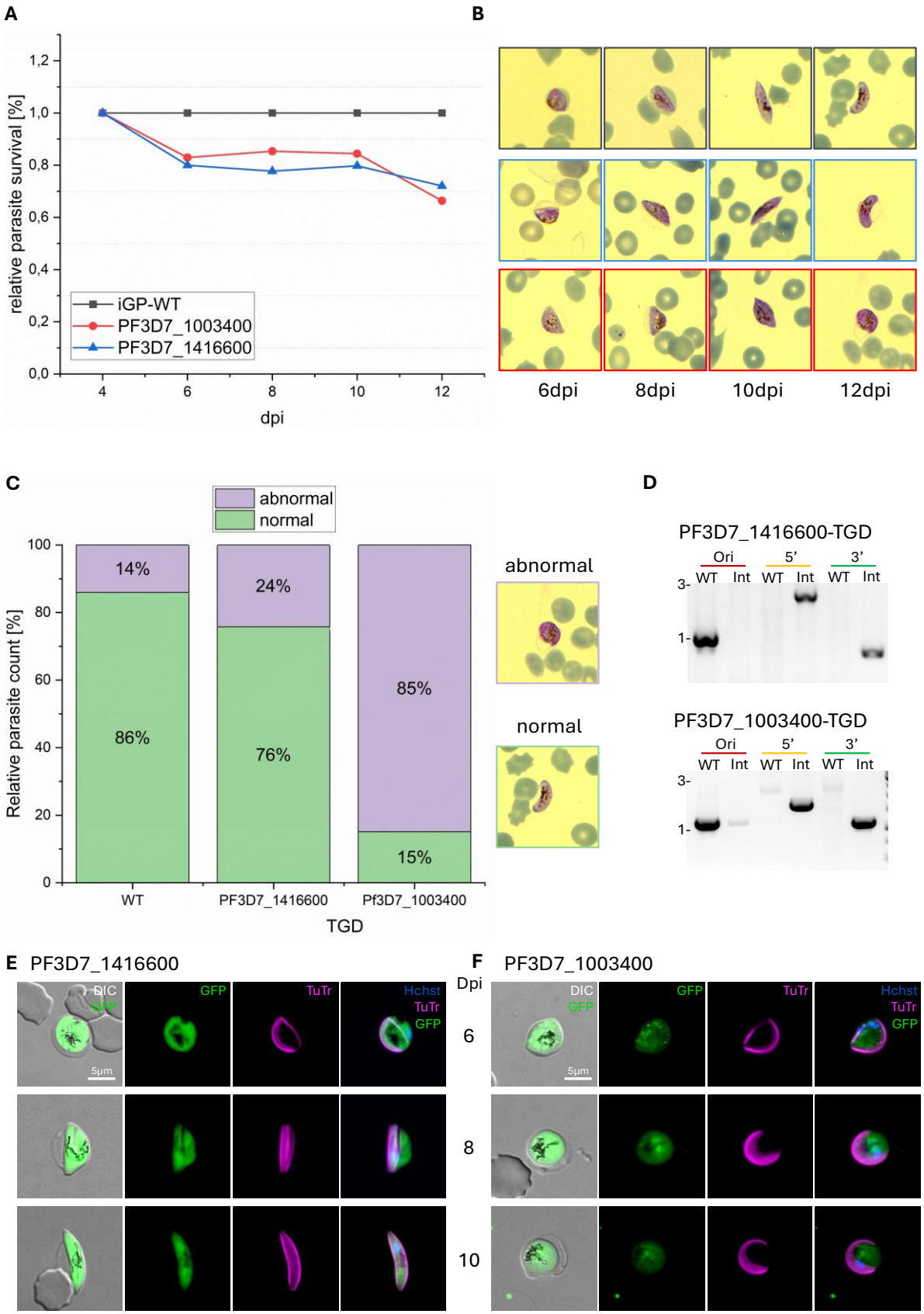

Figure 25: Depletion of PF3D7_1003400 leads to the formation of abnormal gametocytes.
(A) Relative gametocyte survival of the knock out cell lines. Gametocytemia was determined by flow cytometry using SYBR green and DHE. The relative parasite survival rate was determined by first calculating the fold change between each gametocyte stage and stage I followed by dividing the respective fold change

by the fold change of the NF54/iGP wildtype parasites. **(B)** Representative Giemsa smears of stage II to V gametocytes for NF54/iGP WT and each knock out cell line. **(C)** Quantification of gametocyte morphology (violet, abnormal; green, falciform) 13 days post gametocyte induction for NF54/iGP WT and each knock out cell line. For each condition, the relative parasite count was determined in 3 independent replicas. Representative images of the phenotype in Giemsa smears are depicted next to the graphs. **(D)** Integration PCR for the TGD cell lines, with genomic DNA from the integrant (Int) or parental NF54/iGP (WT) parasites. Primer combinations are shown in Fig. 12 A and expected sizes are listed in Table12. **(E,F)** Life cell fluorescence microscopy images of gene knock out parasites (7d, 9d and 11d post gametocyte induction). Microtubules were visualized with Tubulin Tracker-deep red (magenta) and the DNA was stained with Hoechst 33342 (blue). DIC, differential interference contrast; GFP, green fluorescent protein; TuTr, Tubulin Tracker deep red.

To explore this, we co-transfected the PF3D7_1449100-TGD line with episomally expressed PhiL1-mCherry, a known IMC protein (253), and P40X-mCherry, a marker for PI3P, which localizes predominantly to the food vacuole (272). In the PhiL1 cotransfectant lines, fluorescence microscopy revealed that IMC biogenesis was arrested in Stage III, mirroring the stalled development of the SPMTs. The IMC still formed its characteristic plates but remained confined to one side of the cell, closely associated with the mislocalized SPMTs, creating a "shrimp-like" appearance in fluorescence images (Fig. 26 B). Meanwhile, cotransfection with P40X-mCherry confirmed that the vesicular structures observed in the DIC channel were indeed food vacuole-derived (Fig. 26 D), aligning with previous reports on IMC biogenesis disruptions. Interestingly, PfSPM3 remains attached to the SPMTs (Fig. 26 C).

These findings suggest a critical role for PF3D7_1449100 in coordinating IMC and SPMT assembly during gametocytogenesis. Its absence results in structural disorganization, defective MT positioning, and impaired IMC biogenesis, ultimately leading to the characteristic bloated phenotype. Further investigations, such as inducible knockdowns or proteomic analyses, could provide deeper insights into the molecular mechanisms underlying these defects.

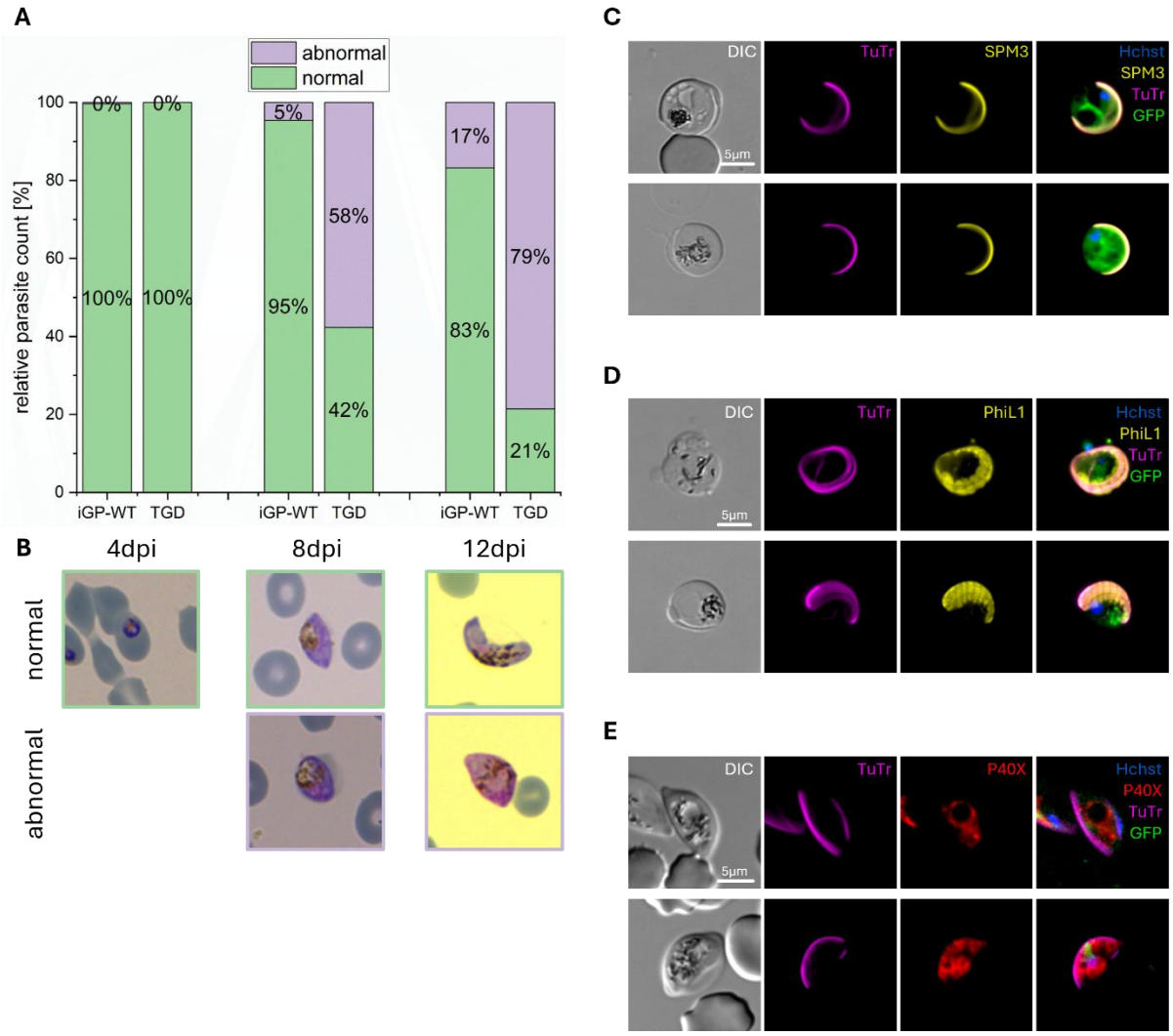

Figure 26: Depletion of PF3D7_1003400 leads to an arrest in stage III gametocytes and an accumulation of food vacuole derived vesicles.

(A) Stage specific (days 7, 9, 11 and 13 post gametocyte induction) quantification of gametocyte morphology (green, abnormal; yellow, normal; blue, pycnotic) for NF54/iGP WT and PF3D7_1003400 knock out parasites. Giemsa counts were performed in three independent experiments. **(B, C, D)** Life cell fluorescence microscopy images of abnormal parasites with additional markers. Microtubules were visualized with Tubulin Tracker-deep red (magenta) and the DNA was stained with Hoechst 33342 (blue). Additional colocalization with **(B)** SPM3-mCherry (yellow), **(C)** the IMC with PhiL1-mCherry (yellow) or **(D)** the food vacuole facilitating P40X-mCherry (red). DIC, differential interference contrast; GFP, green fluorescent protein; TuTr, Tubulin Tracker deep red.

Chapter 3: Discussion

Despite significant advances in malaria control and treatment over the past decades, malaria remains a persistent global health threat. With hundreds of thousands of deaths annually, most of which occur in sub-Saharan Africa, malaria continues to place a heavy burden on public health systems and vulnerable communities (3). A major challenge in controlling and ultimately eliminating malaria lies in two critical bottlenecks within the *P. falciparum* life cycle (273). The points of transition between the human host and the mosquito vector, and vice versa. These occur first when sporozoites are transmitted from the mosquito to the human host during a blood meal, and again when mature gametocytes are taken up by the mosquito, completing the cycle of infection.

While the sporozoite stage has been the focus of intensive research and vaccine development, leading to the approval of two sporozoite-targeting vaccines — RTS,S/AS01 and R21/Matrix-M (25; 26) — considerable work remains before similar interventions can be effectively deployed against the gametocyte stages responsible for transmission back to the mosquito. Gametocytes are the sexual precursors of *Plasmodium*, and in the case of *P. falciparum*, these cells undergo a tightly regulated and prolonged maturation process, progressing through five morphologically distinct stages (I–V) (60). The final, mature falciform Stage V gametocytes are the only forms found in the peripheral blood and the stage ingested by mosquitoes (61; 274), making them the exclusive agents of transmission to the vector.

The remarkable morphological transformations that occur during gametocyte development are driven by two key cellular structures: the inner membrane complex (IMC) and the underlying subpellicular microtubules (SPMTs). The IMC, a cisternal membranous network unique to apicomplexan parasites, provides structural support and shape to the gametocyte (164; 165), while the SPMTs form a corset-like scaffold beneath it, stabilizing the cell and enabling its characteristic elongation (164; 166; 167). Together, these structures orchestrate the dramatic cellular remodeling during gametocyte maturation. Targeting the processes that regulate the assembly and maintenance of the IMC and SPMTs represents a promising avenue for novel transmission-blocking strategies, although this remains an underexplored area of malaria research.

Beyond their role in establishing and maintaining cellular architecture, microtubules (MT) serve as a cornerstone of a wide range of essential cellular processes, underpinning both the parasite's proliferative and transmissive life cycle stages (223). As dynamic cytoskeletal filaments, MTs are indispensable for the assembly of mitotic and meiotic spindles (230), enabling the accurate segregation of chromosomes during the rapid rounds of nuclear division that characterize schizogony and gametogenesis.

A central player in microtubule organization within *Plasmodium* is the centriolar plaque (CP), a non-canonical microtubule organization center (MTOC) unique to apicomplexan parasites. Unlike classical centrosomes, the CP lacks centrioles and instead consists of an electron-dense bipartite structure that spans the nuclear envelope (231). It nucleates

nuclear microtubules (nucMT) necessary for spindle formation and controls their dynamics during both asexual and sexual stages (179; 163). Despite its fundamental importance, much about the CP's molecular composition and regulatory mechanisms remains to be elucidated. Emerging evidence suggests that specialized microtubule-associated proteins (MAP) and epigenetic cues coordinate MT nucleation and attachment at the CP, regulating not only mitosis but also the initiation of SPMT arrays during gametocytogenesis (243; 244; 163).

An ever-growing number of MAPs have been identified in *Plasmodium* and other apicomplexan parasites, progressively redefining our understanding of MT cytoskeleton organization in these organisms. Unlike many eukaryotic cells where well-characterized MAP families such as tau (275), MAP2, and MAP4 regulate MT stability and dynamics (276), apicomplexans appear to have evolved a unique repertoire of MAPs tailored to their specialized cell biology. These proteins serve diverse roles, from nucleating and stabilizing nucMTs during schizogony and gametogenesis to anchoring SPMTs beneath the IMC. Recent studies have identified key proteins like PfSPM1 (262), PfSPM3 (253), PfEB1 (261), and various kinesins as crucial regulators of these processes. Here we reveal novel, putative MAPs, that localize specifically to MT tips, others to spindle poles, and some bridging the cytoskeletal filaments to the IMC. This diversity highlights not only the structural but also the regulatory versatility of MAPs in orchestrating precise MT behavior during complex life cycle transitions. As proteomic and genetic screens continue to expand the catalogue of apicomplexan MAPs, it is becoming evident that these proteins represent a rich and largely untapped source of potential drug targets.

Given the indispensable roles of MTs in *Plasmodium* proliferation and transmission, the parasite's cytoskeletal network has long been recognized as a promising antimalarial drug target. Several compounds that destabilize or hyper-stabilize MTs have demonstrated antiplasmodial activity in vitro and in vivo. Agents such as colchicine and vinblastine (277; 278), though highly effective against mammalian MTs, have limited therapeutic windows due to their toxicity. However, newer compounds including dinitroaniline herbicides and trifluralin derivatives have shown selective activity against *Plasmodium* MTs without severely affecting human cells, exploiting subtle structural differences in tubulin isoforms and MAP-binding interfaces (279). Additionally, MT destabilizing agents have shown promise in blocking gametocyte development, preventing transmission stages from maturing and entering the mosquito (280). The continued discovery of *Plasmodium*-specific MAPs offers a unique opportunity to develop targeted inhibitors that disrupt essential MT functions while minimizing off-target effects on the human host. As resistance to frontline antimalarial drugs rises, targeting the MT cytoskeleton with novel MAP- or tubulin-directed compounds represents a highly attractive strategy to both treat malaria and curtail its transmission.

Previous studies have identified PfSPM3 as a critical MAP, playing a significant role in SPMT network organization (253; 254). The absence of PfSPM3 during gametocytogenesis results in a highly disordered SPMT network, underscoring its role in MT anchoring and stabilization. To further investigate the role of PfSPM3 in SPMT anchoring and to identify additional IMC- or SPMT-associated proteins, we performed a BioID analysis using PfSPM3 as a bait in both asexual parasites (SPM3-AS) and gametocytes (SPM3-Gam).

The BioID in gametocytes identified 181 proteins that were at least twofold enriched, implying a close proximity to the bait PfSPM3. This apparent spatial proximity might indicate a putative role in SPMT or IMC-associated functions. From this dataset, 26 candidate proteins were selected for further localization studies to better understand their roles during gametocyte development.

3.1 Context-related classification of the BioID data

Within the SPM3-Gam dataset, PfSPM3 itself was found to be the second most enriched protein, surpassed only by Ran-specific GTPase-activating protein 1 (PF3D7_0419600). Among the top 40 enriched candidates, eight proteins with known or predicted MT associations were identified, including MT-interacting proteins PfSPM1 (262; 281) and PfEB1 (261; 282), as well as the two kinesins 8 (259; 283) and 13 (284; 260). The strong enrichment of PfSPM3 and other MT-associated proteins reinforces the quality and specificity of the BioID dataset.

Interestingly, tubulin was not among the enriched proteins, an unexpected result given its fundamental role in microtubule formation. This absence could be due to spatial constraints, where the BirA* enzyme may be positioned too far away from the microtubules to efficiently biotinylate tubulin (BirA* was shown to biotinylate in a radius of ~10nm (285)). However, a more likely explanation is that SPMTs are heavily decorated with MAPs, such as PfSPM3, which may obscure accessible lysine residues and prevent efficient biotinylation.

Despite the strong enrichment of MT-associated proteins, the SPM3-Gam dataset did not include IMC-associated proteins such as GAPs (183; 286; 287), GAPMs (288; 289), or alveolins (184; 199). The absence of PfPhiL1, an important IMC-associated protein (271), was particularly surprising, as PfSPM3 was previously identified in a BioID experiment using PfPhiL1 as bait in asexual parasites (253). In contrast, the SPM3-AS dataset contained multiple IMC-associated proteins, including PfPhiL1, suggesting that PfSPM3 interacts with different protein networks in asexual parasites and gametocytes. Another possible explanation is that most IMC proteins were identified in asexual parasites and therefore might not be strongly expressed in gametocytes.

A comparison between the SPM3-AS and SPM3-Gam datasets revealed that 12 proteins were commonly enriched in both datasets (Fig. 27 A). Among them, PF3D7_1435600 and PF3D7_1121100 were only slightly enriched in gametocytes and displayed diffuse cytoplasmic localization in both asexual parasites and gametocytes (Fig. 11). This might indicate a less direct role in microtubule or IMC organization or a false-positive hit at least

in gametocytes. However, PF3D7_1003400 and PF3D7_1449100 were both highly enriched in both datasets. In asexual parasites, these two proteins colocalized with SPMTs in merozoites (Fig. 22) however in gametocytes these proteins displayed a suture-like localization (Fig. 21), an intriguing feature given that asexual parasites do not possess suture structures comparable to gametocytes. This could indicate that their function in MT organization may be conserved, but their spatial arrangement and regulatory interactions differ between life cycle stages.

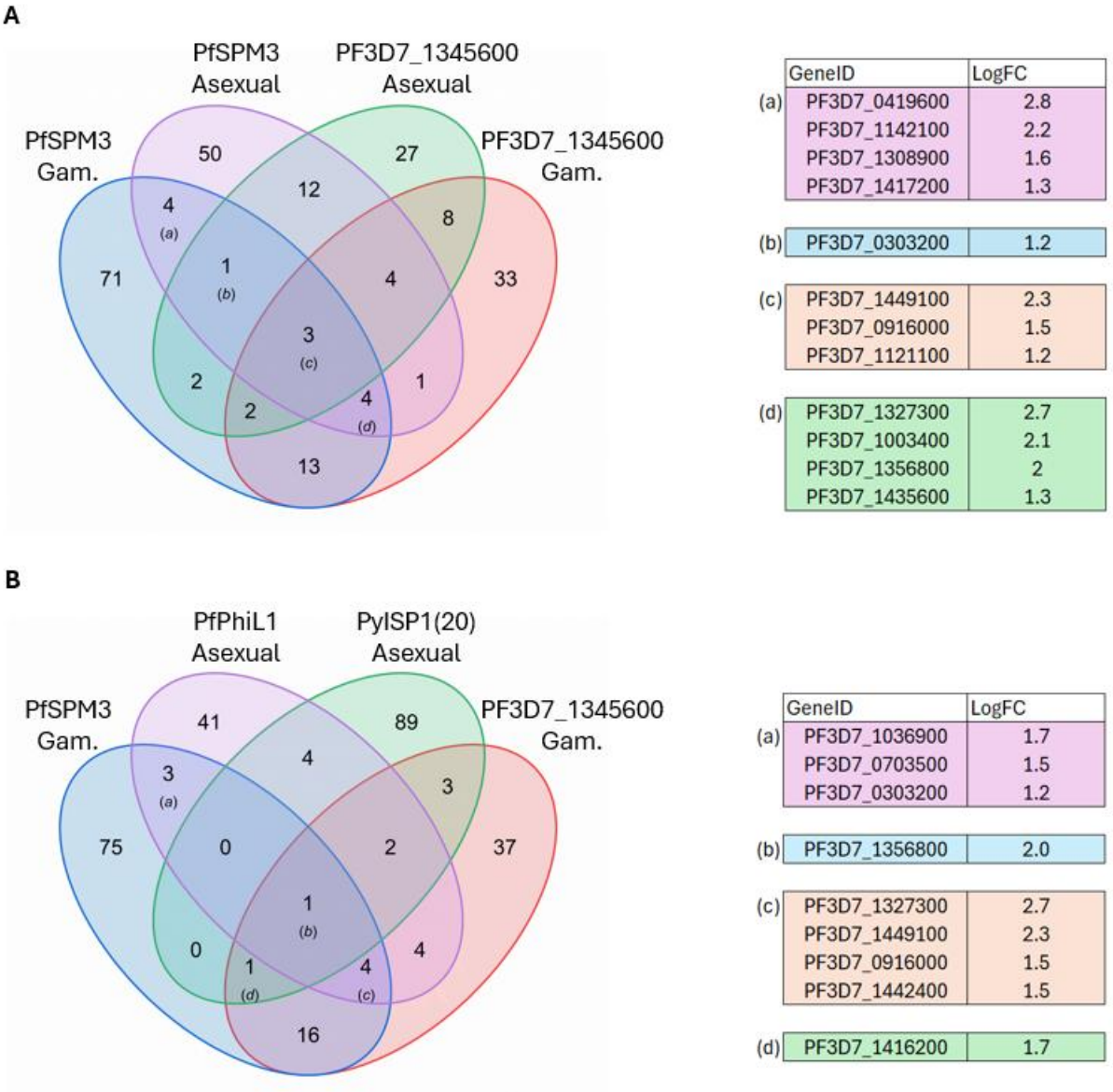

	GeneID	LogFC
(a)	PF3D7_0419600	2.8
	PF3D7_1142100	2.2
	PF3D7_1308900	1.6
	PF3D7_1417200	1.3
(b)	PF3D7_0303200	1.2
(c)	PF3D7_1449100	2.3
	PF3D7_0916000	1.5
	PF3D7_1121100	1.2
(d)	PF3D7_1327300	2.7
	PF3D7_1003400	2.1
	PF3D7_1356800	2
	PF3D7_1435600	1.3

	GeneID	LogFC
(a)	PF3D7_1036900	1.7
	PF3D7_0703500	1.5
	PF3D7_0303200	1.2
(b)	PF3D7_1356800	2.0
(c)	PF3D7_1327300	2.7
	PF3D7_1449100	2.3
	PF3D7_0916000	1.5
	PF3D7_1442400	1.5
(d)	PF3D7_1416200	1.7

Figure 27: Comparison of different BioID datasets.
Venn diagrams depicting the overlapping genes between different IMC or SPMT targeting BioID datasets.(A) Overlap between PfSPM3 and PF3D7_1345600 (228) BioID datasets in asexual and sexual parasites. (B) Overlap between the sexual PfSPM3 and PF3D7_1345600 dataset as well as with the asexual PfPhiL1 and PyISP1 BioID datasets. Proteins from relevant overlaps are listed on the right with the corresponding logFC value from the sexual PfSPM3 dataset.

Comparing our two datasets with previously published IMC-targeting BioID datasets (290; 253; 291) led to several key observations. Studies in asexual parasites showed a significant overlap in enriched proteins, particularly among IMC proteins including alveolins, which were absent in gametocyte-specific datasets. This suggests fundamental differences in IMC composition and function between asexual and sexual stages.

Expanding this analysis to include an additional gametocyte-specific BioID dataset using the suture protein 228 (PF3D7_1345600) as bait (228-Gam) (290), we identified 6 proteins that were commonly enriched across the SPM3-Gam, 228-Gam, and PhiL1-AS datasets (Fig. 27 B). Notably, the aurora related kinase PfARK3 (PF3D7_1356800) was present in all four datasets. While there are no publications directly connected with PfARK3, PfARK1, a related aurora kinase, was reported to be associated with the CP during schizogony (292). Additionally, PfSPM3 was present in all three datasets, further emphasizing its role in MT organization and its potential functional link between the IMC and SPMTs (Fig. 27 B, c).

Among these shared proteins, PF3D7_1003400 and PF3D7_1449100 were of particular interest due to their suture-like localization in gametocytes and their presence in both the SPM3-AS and SPM3-Gam dataset. Additionally, PF3D7_0705100 exhibited a CP-like localization during schizogony and was found to colocalize with SPMTs in merozoites (Fig. 17, B). In gametocytes, PF3D7_0705100 localized at both the SPMT tips and in a CP-like structure close to the nuclear DNA (Fig. 16. B), suggesting a potential role in MT anchoring or nucleation.

The overlap between the different IMC- or SPMT-associated datasets suggests the presence of a core set of proteins that function in both asexual and sexual stages, possibly involved in MT attachment, IMC organization, or MTOC activity. However, the presence of proteins with suture-like localization in gametocytes, which are absent in asexual stages, strongly supports the hypothesis that MT organization in gametocytes follows a fundamentally different pattern.

Overall, our findings provide strong evidence for a unique MT organization mechanism in gametocytes, distinct from that in asexual parasites. Understanding these differences could lead to new strategies for targeting gametocyte maturation, ultimately disrupting malaria transmission at a critical stage of the parasite's life cycle.

3.2 Insights into novel SPM3 associated proteins

From the initial 26 selected proteins, we successfully generated stable GFP fusion lines for 17 proteins, allowing us to investigate their subcellular localization and potential functional roles during *P. falciparum* development. Using fluorescence microscopy, we analyzed the localization of these fusion proteins in both asexual parasites and gametocytes, revealing a diverse range of subcellular distributions.

3.2.1 Centriolar plaque proteins

Among the localized candidate proteins, three (PF3D7_0529800, PF3D7_0705100 and PF3D7_0504800) displayed a CP-like localization in both late-stage schizonts and gametocytes.

The CP is a non-centrosomal MTOC in apicomplexans and is crucial for MT dynamics during cell division and parasite development (179). Structurally, the CP is described as an electron-dense bipartite structure, with one part located inside the nucleus and the other extending into the cytoplasm (232; 230; 171; 231; 238). Despite its fundamental role, little is known about the exact protein composition of the CP. Current knowledge is based primarily on microscopy studies that have identified a few CP-associated proteins, including γ-tubulin (239; 240), centrins (241; 242; 293), SAS6/4, and CPAP (243; 244; 294; 246), which localize to the CP structure and are thought to contribute to its MT nucleation function. Given the CP's involvement in cell division, gamete formation, and MT organization, there is significant interest in further characterizing its composition and function. However, the exact mechanism of SPMT nucleation and organization in gametocytes remains unresolved, especially given the absence of the apical ring, which serves as the MTOC in other *Plasmodium* life cycle stages (179; 295; 170).

Previous studies have shown that during early gametocyte development, the SPMTs initially nucleate from the centriolar plaque before detaching later in gametocytogenesis (238). Additional work has shown that some of the SPMTs might nucleate from the newly formed IMC starting in stage II gametocytes (163).

Interestingly, in life cycle stages where the apical polar ring (APR) is present, the SPMTs exhibit a uniform polarity, with their minus ends anchored at the APR. In contrast, gametocyte SPMTs appear to have a random polarity relative to each other, with both plus and minus ends distributed throughout the cytoplasm in an approximately 1:1 ratio (170). This unusual arrangement raises the intriguing possibility that gametocytes may possess MTOC-like structures at both ends of the cell, similar to the APR, but functionally distinct.

These hypothetical SPMT-organizing centers likely differ in composition from canonical CP-associated MTOCs. Previous studies showed that the CP proteins such as SAS4/6 localize to the basal body in *P. berghei* male gametocytes (246), but there are no current data on their localization during *P. falciparum* gametocytogenesis. On the other hand, PfCentrin-4 does not localize to the tip of the SPMT in late-stage gametocytes (163). This suggests that gametocytes may employ a unique form of MTOC to regulate SPMT nucleation and stability, which we will hereafter refer to as the subpellicular microtubule organization center (SPMTOC).

The proteins PF3D7_0529800, PF3D7_0705100 and PF3D7_0504800 exhibit a classical CP-like localization in late stage schizonts, where they sit on top of the spindle MTs during the last round of nuclear division (Fig. 17, A-C). During Stage I of gametocytogenesis, PF3D7_0529800, PF3D7_0705100 and PF3D7_0504800 initially localized as a single focus at the nucMTs and the first emerging SPMT strand. As gametocytes mature, they detach from the SPMTs and move with the nucleus towards the middle of the cell during

stage III, similar to PfCentrin-4 (163). As the SPMTs depolymerize in stage V, these three proteins are still connected to the nucleus(Fig. 16, A-C).

Remarkably, in addition to their CP-like localization, PF3D7_0529800, PF3D7_0705100 and PF3D7_0504800 also appeared to bind to the tips of the SPMTs in gametocytes (Fig. 16. A-C). While it remains unclear whether they interact with the plus or minus ends of the individual MTs, their initial appearance as a dot on top of nucMTs and the first SPMT strand suggests that they associate with the minus end of the SPMTs. By Stage V, the SPMT tip localization disappears together with the SPMT cytoskeleton (Fig. 16, A-C), suggesting a role in the structural maintenance or organization of the SPMTs throughout gametocyte maturation.

Consequently, these proteins (PF3D7_0529800, PF3D7_0705100, and PF3D7_0504800) could be tentatively designated as SPMTOC1, SPMTOC2, and SPMTOC3. To begin validating their roles as components of the SPMTOC, further experiments are needed. These should include co-localization studies both among these candidates and with established MTOC markers such as PfSAS4 (PF3D7_1458500), PfARK2 (PF3D7_0309200), and PfCentrin4 (PF3D7_1105500). In addition, co-immunoprecipitation assays, functional inactivation experiments, and high-resolution structural analyses would represent important next steps toward confirming their identity and function within the parasite's cytoskeletal architecture.

These findings open new avenues for studying SPMT organization in *P. falciparum* and highlight potential gametocyte-specific adaptations in MT organization. Understanding these unique MTOCs could provide crucial insights into parasite development and transmission, with potential implications for targeting gametocyte maturation as a strategy for malaria control.

3.2.2 PF3D7_1322200 - a new microtubule organizing protein?

We could localize PF3D7_1322200-GFP to the spindle MTs in asexual parasites and to nucMTs in early-stage gametocytes (Fig. 16, D; Fig. 17, D). PF3D7_1322200 possesses a predicted N-terminal TOG (Tumor Overexpressed Gene) domain, a hallmark of MAPs within the TOG/XMAP215 family (296; 297). Interestingly, PF3D7_1322200 is the only protein in the *P. falciparum* genome predicted to contain a TOG domain, suggesting that it may serve a specialized role in microtubule regulation within the parasite.

Members of the XMAP215 protein family are highly conserved and play key roles in MT dynamics, typically localizing to MT plus ends, MTOCs, and kinetochores (298). Despite being annotated as STU2 in PlasmoDB (258), a yeast MAP (299), PF3D7_1322200 shows a greater similarity to its human ortholog CKAP5, a MT regulator involved in spindle formation and MT growth during anaphase (300; 301). Notably, CKAP5 has also been shown to facilitate the formation of actin bundles templated by MTs (302), a particularly intriguing function given that *Plasmodium* encodes a very limited set of actin-nucleating proteins (303). This raises the possibility that PF3D7_1322200 might contribute to

cytoskeletal cross-talk between MTs and actin filaments, potentially influencing parasite motility or structural organization (252).

The localization pattern of PF3D7_1322200 strikingly similar to End-Binding Protein 1 (EB1) (304; 163; 282). EB1 is a well-characterized MT plus tip-binding protein, found across eukaryotic organisms, where it regulates MT growth and spindle dynamics during chromosome segregation (305; 306). Beyond its localization to the nucMTs, PF3D7_1322200 was also observed at the plus tips of growing SPMTs in stage II gametocytes, as well as at the stabilized SPMT tips in later stages (Fig. 17, B). This localization pattern is reminiscent of Formin1/2 (252), two other cytoskeletal regulators, and aligns with CKAP5's known function in guiding MT plus end growth and stability.

These observations suggest a potential functional association between PF3D7_1322200, PfEB1, and PfFormin1/2, raising the possibility that PF3D7_1322200 may contribute to MT plus-end tracking, actin-microtubule interactions, or cytoskeletal remodeling in gametocytes.

To confirm the proposed interactions between PF3D7_1322200 and PfEB1, further colocalization with PfEB1 could be performed to assess their spatial overlap at MT tips and during spindle formation. Additionally, co-immunoprecipitation assays could be used to determine whether PF3D7_1322200 directly interacts with PfEB1 or other MAPs. Given that *Plasmodium* lacks clear homologs of human CKAP5-interacting proteins such as CLIP, CLASP, SOGA, or GAS2L1 (307; 308; 309; 310), it remains to be determined whether PF3D7_1322200 functions independently or with novel parasite-specific interacting partners.

Further colocalization studies with actin and PfFormin2 could help clarify whether PF3D7_1322200 could facilitate the connection between actin and SPMTs, potentially contributing to the cytoskeletal organization of the developing gametocyte.

Given CKAP5's documented role in actin bundle formation (302), an important next step would be to assess whether PF3D7_1322200 is capable of initiating actin nucleation in *Plasmodium*. Actin polymerization assays could be conducted in the presence and absence of PF3D7_1322200 to evaluate its effect on actin filament growth. Additionally, experiments using pre-polymerized actin filaments could determine whether PF3D7_1322200 promotes actin bundle formation in vitro.

The discovery of Pf3D7_1322200’s unique localization at spindle MTs and nucMTs as well as at the SPMT tips, along with its similarity to CKAP5, raises important questions about its role in cytoskeletal organization and possible MT-actin interactions. Future functional studies will be crucial in determining whether Pf3D7_1322200 is involved in MT polymerization, stabilization, or actin nucleation, potentially revealing new mechanisms of cytoskeletal regulation in malaria parasites. Understanding these processes could open new avenues for targeting gametocyte maturation and, ultimately, disrupting parasite transmission.

3.2.3 Identification of novel suture-localizing proteins

In our study, we identified five previously uncharacterized proteins that exhibit a distinct stripe-like pattern across stage IV gametocytes. This pattern is reminiscent of the sutures observed in gametocytes, which are proteinaceous fibers connecting the suture plates during gametocytogenesis (168; 169; 123). Additionally, we confirmed the suspicion that the protein PKRP (PF3D7_0311400) localizes in a suture like pattern in gametocytes. Sutures were initially described as electron-dense stripes perpendicular to the SPMTs in early EM studies (166). They were hypothesized to play a role in stabilizing the IMC and the underlying SPMTs. While 12 suture proteins have been identified in *Toxoplasma gondii* (190; 191), only three have been characterized in *Plasmodium falciparum* so far:, PF3D7_1345600, PfDHHC1(PF3D7_0303400) and PfISC3 (PF3D7_1431900) (123; 189; 265).

By quantifying the suture-like structures (SLS), we observed a median of 12 SLS for proteins PF3D7_1003400, PF3D7_0805100 and PF3D7_1416600, while protein PF3D7_1203300 exhibited a median of 11 SLS, and protein PF3D7_1449100 displayed 14 (Fig. 21, E). The IMC in gametocytes was reported to form up to 13 distinct plates (271), and given the presence of two end plates, 12 connecting sutures would be expected. This prediction aligns with our findings for three of the newly identified suture-like proteins. Notably, PF3D7_1345600 showed a median of 13 SLS (123), while the slight deviation observed in PF3D7_1203300 (11 SLS) could be attributed to experimental variation. The 14 SLS observed for PF3D7_1449100 appears to be due to its additional association with the SPMT tips, a localization also observed in asexual parasites (Fig. 22, A).

PfDHHC1, a previously identified suture-associated protein, exhibits IMC-like localization, whereas protein 228 is more closely associated with the basal complex in schizonts (123; 189). Among our newly identified proteins, PF3D7_1203300 and PF3D7_1449100 localize in a CP-like structure during schizogony (Fig. 22, A, B). However, while PF3D7_1449100 remains associated with the tips of SPMTs, PF3D7_1203300 presents as an uncharacteristic signal near the nucleus. Meanwhile, PF3D7_1003400 appears only in late stage schizonts and colocalizes with the entire length of the SPMT doublet in merozoites (Fig. 22, B).

Interestingly, PF3D7_1003400 and PF3D7_1449100 were the only two suture-like proteins detected in both the SPM3-Gam and 228-Gam datasets, as well as in the SPM3-AS and PhiL1-AS BioID datasets (290; 253). This suggests a core subset of proteins involved in both gametocyte and asexual stages. Additionally, PF3D7_1003400 is the only other suture-associated protein, besides PfDHHC1, that contains a TMD. This raises the possibility that PF3D7_1003400 is anchored to the IMC membrane within the sutures, serving as a scaffold for additional protein interactions. Due to its TMD, PF3D7_1003400 has an internal and external domain, with the C-terminus predicted to reside inside the IMC. If this were the case, a C-terminal GFP tag would be expected to localize within the two IMC lobes, potentially producing an elongated or oval signal. However, our microscopy data do not show this, possibly due to resolution limitations.

3.2.4 PF3D7_1449100 – a suture like protein with a predicted CLASP-like domain

PF3D7_1449100 represents the only *Plasmodium* protein predicted to contain a CLASP domain. CLASP proteins are microtubule plus-end tracking proteins that either directly bind MTs or interact with MAPs like EB1 (308; 311). In eukaryotic cells, CLASP proteins contain TOG domains and are part of the TOG/XMAP215 family, which is essential for mitotic spindle formation and persistent cell motility (312; 313). However, despite being predicted to contain a CLASP-like domain, protein PF3D7_1449100 does not share any significant homology with human or yeast CLASP proteins.

Several studies have demonstrated that CLASP activity and localization during cell migration are regulated by phosphorylation via GSK3β (314; 315). Notably, the knockout of *Plasmodium* GSK3β leads to a block in gametocyte maturation and ultimately results in gametocyte death starting from stage III (316). It would be intriguing to investigate whether PfGSK3β truncation affects IMC or SPMT formation. In plants, CLASP proteins are known to play a crucial role in both cell division and MT reorganization (317; 318). They interact with katanin, a microtubule-severing enzyme, to stabilize MT plus ends after severing (319; 320).

The CP-like localization of PF3D7_1449100 in asexual parasites initially suggested an association with the nucMTs during early gametocytogenesis (Fig. 22, A). However, our findings indicate that, despite similar localization patterns in asexual parasites, PF3D7_1449100 likely interacts with MT plus ends, whereas SPMTOC2 (PF3D7_0705100) likely remains associated with MT minus ends (Fig. 17, D). Additionally, the inability to generate a TGD based knockout for PF3D7_1449100 suggests that it may be essential for asexual replication. To circumvent this issue, inducible knockout cell lines could provide further insights into its function. Attempts to knock down protein PF3D7_1449100 using the knock sideways system proved inefficient, with residual protein still associating with SPMT tips (Fig. 18).

Super-resolution microscopy with computational background signal clearing revealed that proteins PF3D7_1203300 and PF3D7_0805100 displayed continuous signals along the sutures (Fig. 23, A,B), whereas proteins PF3D7_1449100, PF3D7_1003400, and PF3D7_1416600 exhibited distinct signal dots directly overlying the SPMTs (Fig. 23, C-E). This suggests different subsets of suture proteins, where some facilitate IMC plate connections, while others anchor SPMTs to the sutures (Fig. 28).

Unexpectedly, PF3D7_1003400, despite containing a TMD, did not display a broad suture-wide localization but instead appeared as discrete dots. In merozoites, PF3D7_1003400 colocalizes with the entire SPMT strand, suggesting that it may serve as a direct bridge between the IMC and SPMTs in asexual parasites or act as an anchoring protein for additional interactions.

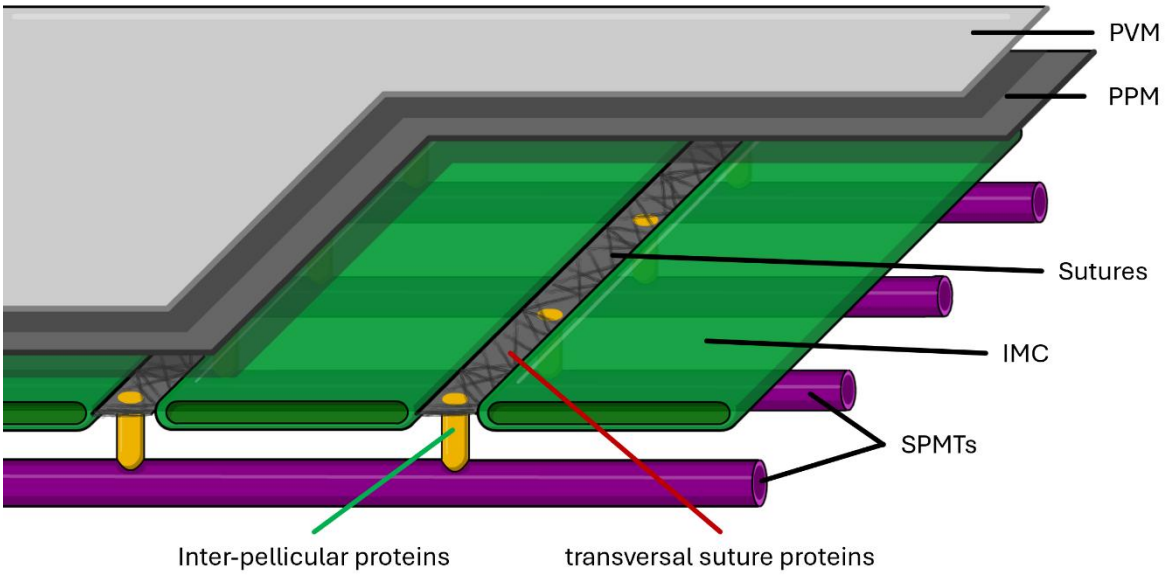

Figure 28: Model for suture-localizing proteins in gametocytes.
Schematic illustrating the two different localizations of the characterized suture-like proteins. IMC, inner membrane complex; PPM, parasite plasma membrane; PVM, parasitophorous vacuolar membrane; SPMTs, subpellicular microtubules.

Taken together, our findings suggest that during schizogony in asexual parasites, PF3D7_1449100 supports the nucleation of the two SPMTs, stabilizes their plus ends, and guides their growth along the IMC edge, potentially moving together with the basal complex (BC). Time-lapse microscopy during schizogony could provide further insights into this hypothesis. During late schizogony the IMC is formed, during the final round of nuclear division, and is subsequently pulled over the developing merozoite by the BC (321).

Although gametocytes do not possess sutures in the same manner as merozoites, some suture proteins from other life cycle stages may still be present at the growing IMC edge, possibly linking the IMC and BC. The idea that suture proteins might assist BC function is supported by the BC-like localization of protein 228 in asexual parasites (123; 265) and its interaction with PfCINCH in co-immunoprecipitation experiments (125). Future colocalization studies using BC markers such as PfCINCH or PfBPT1 (124) could determine whether PF3D7_1449100's microtubule tip localization overlaps with the BC. However, neither protein PF3D7_1003400 nor PF3D7_1449100 were identified in BC co-immunoprecipitation assays (125).

While we were unable to generate SLI based knockout parasites for protein PF3D7_1449100, a successful knockout of PF3D7_1003400 in asexual stages resulted in a developmental arrest at stage III gametocytogenesis (Fig. 26, A). This phenotype is characteristic of disruptions in IMC or SPMT morphogenesis, as seen with actin/tubulin depolymerization and knockouts of proteins like PfPhiL1, PfPIP, PfFormin1/2, and PfGAPs/PfGAPMs (167; 322; 252). The fact that these perturbations consistently result in a stage III arrest suggests the presence of a gametocytogenesis checkpoint at this stage (Dixon, M. W. A.; personal correspondence). This checkpoint may prevent dysfunctional gametocytes from re-entering the bloodstream, thereby reducing inflammation and increasing the likelihood of healthy stage V gametocytes being taken up by mosquitoes.

Interestingly, Pf*SPM3*-deficient gametocytes appear capable of forming and expanding the IMC normally, rather than arresting at stage III (Farias, G.; unpublished data). This suggests that IMC morphogenesis occurs independently of the SPMT scaffold, challenging the previously hypothesized interlocked relationship between these structures. Further localization studies could clarify whether PfSPM3 resides within the SPMTs like PfSPM1 or decorates their exterior as a stabilizing or anchoring factor for MAPs. Future colocalization experiments using 3D fluorescence microscopy techniques such as lattice light sheet or spinning disk microscopy could confirm whether PfSPM3 also associates with nuclear microtubules in gametocytes.

3.3 What we don’t know and speculate about gametocytogenesis

Despite its critical importance for malaria transmission, gametocytogenesis in *P. falciparum* remains one of the least understood aspects of the parasite’s biology. Much of our current knowledge is based on fragmented observations, with many processes surrounding gametocyte development remaining hypothetical. One of the major limitations in advancing this field stems from the fact that only *P. falciparum* and closely related *Laverania* species develop the characteristic falciform gametocyte morphology. As a result, established rodent malaria models like *P. berghei* cannot fully recapitulate the complexity of gametocyte biology seen in *P. falciparum*, the most lethal human malaria.

Compounding this issue is the technical challenge of producing reliable, high-density gametocyte cultures in vitro. Before the development of the inducible gametocyte producer (iGP) system (256), researchers had to rely on less efficient methods such as nutrient starvation, sub-lethal antimalarial treatment, or choline depletion to induce gametocytogenesis, which typically resulted in low gametocyte yields (323). Even with the iGP system, obtaining highly synchronized gametocyte populations remains difficult. Cultures often contain a mixture of developmental stages, making it hard to confidently attribute specific phenotypes to defined gametocyte stages, especially when investigating subtle morphological or molecular effects.

Another significant barrier is the inherent fragility and limited survival of gametocytes in culture. Even under optimized conditions, gametocyte numbers typically decline by around 30% over the 12-day maturation process. Coupled with a naturally low sexual commitment rate, this can result in insufficient parasitemia for reliable phenotype quantification or growth curve analysis. Moreover, gametocytes are highly sensitive to external stressors, often forming abnormally shaped, rounded cells in response to subtle changes in culture conditions. This issue is particularly problematic in genetic manipulation experiments like targeted gene disruption or knock-sideways systems, where morphological changes are frequently used as phenotypic readouts. Based on our observations, it appears that disruptions to the CO_2 atmosphere, such as leaving cultures too long in ambient air or using poorly sealed culture boxes, can trigger premature gametocyte death and morphological abnormalities resembling those seen when the IMC proteins are disrupted. Interestingly, nutrient depletion or high parasitemia, which are typically lethal to asexual parasites, seem to have a lesser effect on gametocyte viability.

Notably, this spontaneous gametocyte death tends to cluster around stage III and consistently produces morphological defects similar to those observed when gametocytogenesis is experimentally impaired (252). This lends further support to the hypothesis that a developmental checkpoint exists between stage III and IV, safeguarding against progression of structurally compromised gametocytes (Dixon, M. W. A.; personal correspondence). Adding to the complexity, male gametocytes can premature exflagellate if exposed to temperatures below 27°C from stage III onward, necessitating tight temperature control during handling and microscopy to prevent unintended activation (324).

3.3.1 What drives sexual commitment and conversion?

Before gametocytes can mature, *P. falciparum* undergoes two critical cell fate decisions. First, parasites must commit to gametocyte formation — a process termed *commitment* (138)— followed by a second decision determining whether they will become male or female gametocytes, known as *conversion* (139). While it is now well established that AP2-G, HP1, and GDV1 are key regulators of commitment (147), the upstream molecular signals governing GDV1 activation remain unknown. Similarly, although genetic screens have identified a number of male- or female-specific genes (158), how these factors interact to regulate sex differentiation is still poorly understood.

A particular challenge in deciphering sex ratio regulation in *P. falciparum* arises from its haploid genome and absence of sex chromosomes, eliminating classical chromosomal mechanisms of sex determination (325; 135). It remains uncertain whether sexual commitment is a stochastic event occurring randomly across the parasite population or whether a distinct, pre-disposed subpopulation exists with an inherent propensity for sexual development. Furthermore, the precise conversion ratio between male and female gametocytes, and whether it is influenced by environmental factors, is unresolved. Microscopy-based studies often report a female-biased ratio (326), and molecular marker-based approaches support this female bias, but also indicating possible

technical or stage-dependent biases in detection (327). Recent evidence suggests a parasite density-dependent sex ratio, where low parasitemia favors male-biased ratios and high parasite loads drive a female bias (328). Work in malaria species like *P. vivax* also point toward differential lifespans for male and female gametocytes (329; 330), introducing a potential time-dependent element to sex determination and further complicating the picture.

This conflicting and incomplete data landscape highlights a major grey area in malaria biology. If *Plasmodium* is indeed capable of modulating its sex ratio in response to environmental cues, it raises critical questions about how the parasite senses and processes these signals, particularly given that sexual conversion is decided early in the 12-day maturation process. Such anticipatory decision-making would require an unusually sophisticated sensing and regulatory network for a unicellular organism.

3.3.2 The nucleation of the SPMTs

Stage I gametocytes are traditionally indistinguishable from asexual parasites on standard Giemsa-stained blood films. However, molecular markers such as GEXP5 or fluorescently labeled Tubulin have greatly improved the ability to differentiate early gametocytes from asexual forms (331). These early stage gametocytes are roughly trophozoite-sized and display a unique cytoskeletal feature, a single MT strand encircling the parasite's periphery (Fig. 29 A,B). This initial SPMT strand can be detected within two days of induction, in parallel to the formation of the nucMTs (Fig. 29, A, B). Intriguingly, the initial MT strand consistently originates from a point adjacent to the nuclear DNA (as visualized by Hoechst staining) and the parasite plasma membrane (PPM), a positioning pattern reminiscent of SPMT formation in merozoites during schizogony.

This observation raises questions about how the CP and nucleus are positioned close to the PPM to facilitate this process. It remains unknown whether specific proteins actively guide the growing SPMT along the PPM, or if it passively follows the membrane curvature due to spatial constraints. Previous hypotheses propose that, in merozoites, the BC orchestrates SPMT positioning by migrating over the parasite body and coordinating IMC enclosure. However, no clear evidence for a basal complex in gametocytes has yet been observed, leaving the guidance mechanism for the initial SPMT strand an open question.

Parallel to the initial SPMT-strand formation, nucMTs begin to form, originating from the CP and radiating within the nucleus (163). Previous ultrastructural studies have shown that these nuclear microtubules differ from the mitotic spindle MTs typically found in dividing nuclei (170). The biological purpose of this extensive nuclear microtubule network is not entirely clear. One hypothesis is that they counterbalance the expanding SPMT strand, mechanically supporting nuclear elongation as the parasite remodels its cytoskeleton. Another intriguing possibility is that, as in merozoites (332), the nuclear microtubules function to separate duplicated CPs, which then establish new MTOCs at either end of the elongating gametocyte. This theory is supported by observations that in Stage II gametocytes, the nucleus is maximally elongated, extending from one apical end

of the parasite to the other (174), suggesting coordinated spatial remodeling of nuclear and cytoplasmic MTs.

3.3.3 Forming the IMC

Stage II gametocytes are characterized by their distinctive lemon-like shape, a morphological hallmark thought to arise from the deposition of the IMC and SPMTs predominantly on one side of the developing parasite. Notably, the IMC and SPMTs appear to assemble on the side opposite the elongated nucleus, as evidenced by DNA staining and the arrangement of nucMTs (Fig. 16). The mechanisms governing the formation and spatial organization of the IMC at this stage remain enigmatic. Earlier studies have suggested that the IMC initiates as a membranous structure connected to the CP in late Stage I or early Stage II gametocytes (167), a process intriguingly reminiscent of IMC formation during merozoite segmentation. However, the precise molecular players driving this membrane biogenesis, and whether the IMC initially forms as a single continuous plate or as discrete patches that subsequently fuse, is still unknown.

One open question is whether the plate-like appearance of the IMC arises later via integration of suture proteins, or whether sutures serve as organizational hubs from the start. Despite extensive microscopy work, including using suture-associated protein markers (124; 167; 252), no transitional, early gametocytes have been observed that display reduced numbers of suture-like structures — a finding that argues against a stepwise assembly model. Furthermore, a prior study reported that tubulin staining in gametocytes revealed discrete MT 'islands' which were interpreted as MTOCs located within the IMC (167). Yet this interpretation remains debatable, as it does not readily explain the apparent lack of uniform SPMT polarity in gametocytes — a striking difference from the uniformly oriented SPMTs seen in merozoites and ookinetes. An alternative explanation might be that these islands represent tubulin-based structures (and perhaps suture-associated assembly points) that subsequently recruit IMC membranes, rather than the other way around.

3.3.4 How are the SPMTs connected to the IMC?

Stage III gametocytes progress to a D-shaped morphology, driven by the expansion of the SPMT sheet on one side of the cell, protruding against the host red blood cell membrane. By this stage, it seems likely that the SPMTs have already been organized around two apical ends, and intriguingly, they display relatively uniform lengths (Fig. 16). Whether this precise arrangement is maintained by specific MT end-binding proteins or by physical constraints imposed by the IMC plates and their associated end plates remains unknown. In Stage III, individual IMC plates and the sutures separating them become clearly distinguishable. Both our observations and those of other groups indicate that the IMC consistently overlays the expanding SPMT network, extending only minimally beyond it (124; 167). This suggests that the IMC could act as the leading structure, guiding the direction of MT polymerization and organizing the cytoskeletal array beneath it.

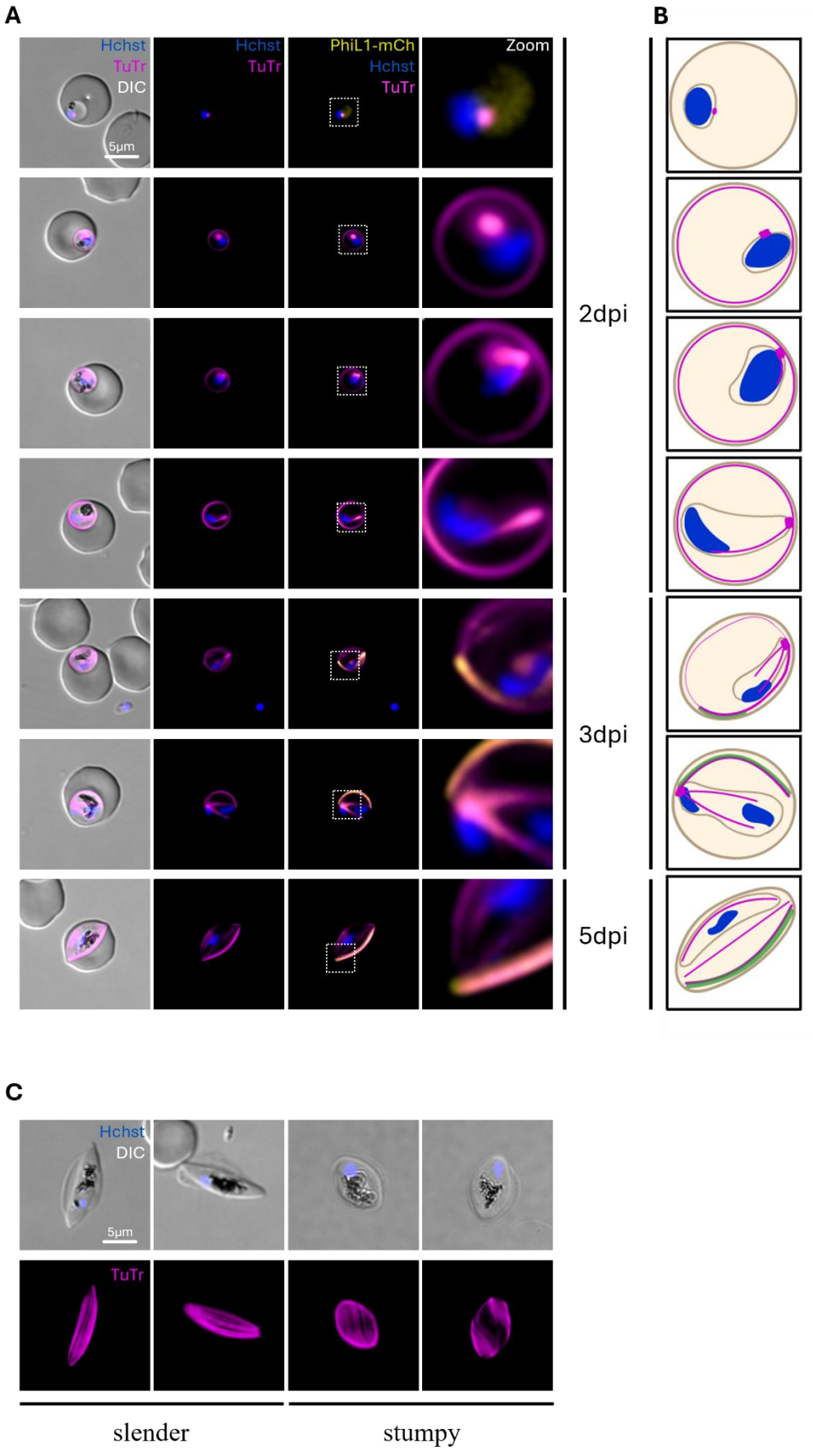

Figure 29: The nuclear microtubule and IMC nucleation in gametocytes.

A) Life cell fluorescence microscopy images of early-stage gametocytes (2d, 3d and 5d post gametocyte induction). Microtubules were visualized with Tubulin Tracker-deep red (magenta) and the DNA was stained with Hoechst 33342 (blue). The IMC was visualized with episomale expressed PhiL1-mCherry fusion construct (yellow). **B)** Schematic illustrating the composition of DNA, microtubule and the IMC during early gametocytogenesis. **C)** Life cell fluorescence microscopy images of stage IV gametocytes, depicting the different forms observed throughout stage IV. Microtubules were visualized with Tubulin Tracker-deep red (magenta) and the DNA was stained with Hoechst 33342 (blue). DIC, differential interference contrast; GFP, green fluorescent protein; PhiL1, PfPhiL1-mCherry fusion construct; TuTr, Tubulin Tracker deep red.

A remaining puzzle is whether all SPMTs are generated during Stage II/III and subsequently redistributed along the elongating IMC during Stage IV, or whether new SPMTs continue to be nucleated and integrated into the growing corset. EM studies have shown that SPMT spacing becomes increasingly regular from Stage II to IV (171; 333; 170), supporting the idea of progressive addition and organization during gametocytogenesis. This raises further questions: are new SPMTs incorporated preferentially at the growing edge of the corset, or randomly within gaps where existing filaments are pushed aside to maintain a regular pattern? And crucially — which proteins regulate this spacing and alignment, and why does uniformity not exist from the outset?

During Stage III, the nucMTs are dismantled, and the nucleus condenses (163; 174). The rationale for the dramatic nuclear elongation seen in earlier stages is still speculative, though it appears to be associated with preparatory cytoskeletal rearrangements completed by this point.

3.3.5 The SPMT zoo

Stage IV gametocytes are maximally elongated, with pronounced pointed ends protruding through the host red blood cell. At this stage, the gametocyte is entirely encapsulated by both the IMC and the SPMT corset. In early Stage IV gametocytes, it is still possible to observe openings in the SPMT array, suggesting incomplete fusion of IMC plates. Whether this final closure involves plate fusion along horizontal sutures, as seen in sporozoites, or through a different mechanism remains unresolved. Notably, we have observed two distinct morphological subtypes within Stage IV gametocytes: one featuring blunted, stumpy ends and another displaying sharp, bundled apices (Fig. 29, C). It remains unclear which appears first. One hypothesis posits that the SPMT sheet initially wraps around the parasite, forming a tubular corset, and only later do MT-binding proteins aggregate the filament ends into points. Alternatively, the filaments might initially grow into bundled tips, which then relax and fan out once tip-associated regulatory proteins are disassembled.

This also ties into another fundamental question: whether specialized structures exist at the apical ends of gametocytes, akin to the APR in other stages, or whether distinct sets of MT-associated proteins manage the terminal organization and anchorage of the SPMTs.

Adding further complexity to the gametocyte cytoskeleton is the remarkable structural variability of the SPMTs. In most *Plasmodium* life cycle stages SPMTs are composed of the classical 13 protofilaments. This conserved architecture is typical of eukaryotic MTs and is considered optimal for balancing tensile strength and flexibility (334). However, EM studies have revealed that in gametocytes, there is a surprising diversity in the number of protofilaments per MT, with some filaments deviating from the canonical 13-protofilament arrangement (170).

The biological significance of this protofilament heterogeneity remains speculative, but several hypotheses can be proposed. One possibility is that varying protofilament numbers confer differential mechanical properties to individual MTs within the gametocyte, contributing to the overall flexibility and resilience of the subpellicular corset as the parasite elongates and navigates mechanical constraints within host tissues. MTs with fewer protofilaments are known to exhibit increased curvature and reduced rigidity, while those with additional protofilaments are stiffer (335; 336). This variation could allow localized tuning of stiffness within different regions of the gametocyte.

Another intriguing idea is that non-standard protofilament counts might influence the binding dynamics of MAPs, many of which recognize specific lattice geometries (337). Atypical MT architectures could thus regulate the spatial recruitment of MAPs involved in SPMT anchoring, bundling, or capping and potentially explaining the unique SPMT polarity and organization patterns observed in gametocytes compared to other *Plasmodium* stages.

It is also conceivable that this protofilament diversity reflects a form of developmental plasticity, allowing gametocytes to rapidly adapt their cytoskeletal architecture in response to subtle environmental changes, such as fluctuations in mechanical pressure, temperature, or host tissue composition. Since SPMT remodeling is a key prerequisite for transitioning from the sequestered, rigid falciform shape of Stage IV to the deformable, circulation-competent Stage V, the ability to fine-tune MT properties through protofilament number variation could be a biologically advantageous trait.

Interestingly, the molecular determinants controlling protofilament number selection in *Plasmodium* remain entirely unknown. In other systems, tubulin isotypes, post-translational modifications, and specific MAPs can influence protofilament assembly geometry — whether similar mechanisms exist in gametocytes is an open and promising field of investigation. Moreover, the lack of uniformity from the beginning of SPMT formation raises further questions about the timing and regulation of MT nucleation and elongation in this unique life cycle stage.

3.3.6 Back to the bloodstream

Stage V gametocytes undergo dramatic cytoskeletal remodeling as the SPMT network is progressively dismantled, allowing the once-rigid, falciform gametocyte to assume a more flexible, sausage-like form suitable for circulation in the peripheral bloodstream. This transformation appears to occur in a stepwise manner. Initially, the inter-filament

rigidity of the SPMT corset is lost, enabling individual MTs to slide relative to one another. Combined with external pressure from the enclosing red blood cell, this results in the gametocyte adopting a pill-shaped form as the corset begins to twist and constrict (Fig. 29, C). Subsequently, the SPMTs are disassembled from their apical ends inward, further softening the cell and producing the characteristic stumpy, deformable shape of mature Stage V gametocytes.

Once gametocytes return to circulation, how they evade immune clearance remains an open question. Unlike asexual stages, which express variant surface antigens for immune evasion, mature gametocytes downregulate these molecules. It is hypothesized that sequestration within the immune-privileged bone marrow shields immature gametocytes from splenic clearance and immune detection (61). However, how young gametocytes adhere to the bone marrow niche until rigid enough for passive retention remains unclear. Furthermore, it is unknown how they avoid detection within the bone marrow environment, which paradoxically serves as a major immune cell reservoir, rich in both B- and T-cells.

3.4 Conclusion

Using fluorescence microscopy, we were able to gain valuable insights into the subcellular localization of specific subpellicular microtubule (SPMT)-associated proteins during *P. falciparum* gametocytogenesis. These findings contribute to our understanding of the cellular architecture and dynamics underlying this essential developmental process. Notably, we identified six previously uncharacterized proteins associated with the inner membrane complex (IMC)-sutures, effectively tripling the number of known suture proteins in *P. falciparum*.

Interestingly, our data revealed that these proteins are not uniformly distributed across the entire suture network. Instead, they appear in discrete, punctate patterns precisely located at the intersections between the sutures and the underlying SPMTs. This highly specific localization strongly suggests that these proteins may serve a structural or regulatory role in anchoring or bridging the IMC to the microtubule (MT) cytoskeleton, offering a new perspective on how parasite shape and stability are maintained during gametocyte maturation.

In addition to suture-associated proteins, we also identified three proteins that localize to the centriolar plaque (CP) in asexual stages, which are then relocated to the tips of the SPMTs in gametocytes. This intriguing observation opens the possibility that these proteins may mark or form a novel microtubule organization center (MTOC) in gametocytes. The presence of a specialized MTOC could help explain the unique, non-polar arrangement of SPMTs seen in *P. falciparum* gametocytes.

Furthermore, we identified the protein PF3D7_1322200, which shows a plus-end MT localization consistent with that of EB1-family proteins and Formin2. This dual localization pattern suggests that PF3D7_1322200 may function as a molecular link

between the MT and actin cytoskeleton, potentially coordinating cytoskeletal remodeling during the later stages of gametocyte development.

Taken together, the localization data presented here represents an important step forward in unraveling the molecular framework of gametocyte morphogenesis in *P. falciparum*. By defining the spatial dynamics of proteins involved in microtubule organization, IMC anchoring, and cytoskeletal interaction, this study provides a solid foundation for future investigations into the mechanistic underpinnings of gametocytogenesis. Ultimately, a deeper understanding of these biological processes is essential for developing novel interventions targeting parasite transmission, thereby advancing global efforts in the fight against malaria.

Chapter 4: Material and Methodes

4.1 Microbiological methods

Preparation of XL10 Gold Competent Cells

XL10 Gold bacteria were made chemically competent following the protocol described by Hanahan (338). A glycerol stock of XL10 Gold bacteria was inoculated into 10 mL of SOB medium containing 34µg/mL chloramphenicol and incubated overnight at 37°C with shaking. The overnight culture was then diluted into 200mL of fresh SOB medium and further incubated overnight at 18°C until the optical density at 600nm (OD_{600}) reached 0.5–0.6. The bacterial cells were harvested by centrifugation at 4000×g for 20min at 4°C, and the supernatant was removed. The pellet was resuspended in 80mL of ice-cold transformation buffer and incubated on ice for 10min. After centrifugation at 2400×g for 5min at 4°C, the supernatant was discarded, and the pellet was resuspended in 16mL of ice-cold transformation buffer supplemented with 1.2mL DMSO. The prepared cells were aliquoted in 100µL volumes into pre-cooled microcentrifuge tubes and immediately frozen in liquid nitrogen. The aliquots were stored at -70°C until further use.

Bacterial Transformation

For transformation, 100µL of ultracompetent XL10 Gold bacteria were thawed on ice for 5 minutes. The appropriate plasmid DNA was added to the bacterial suspension, followed by incubation on ice for 3min. The cells were subjected to a heat shock at 42°C for 30 seconds and then immediately cooled on ice for 3min. To allow for recovery, 1mL of LB medium was added to the bacteria, and the culture was incubated at 37°C for 1 hour with shaking (338). The transformed bacteria were then spread onto LB-agar plates containing 50µg/mL ampicillin and incubated overnight at 37°C (339).

On the following day, up to eight individual colonies were selected and transferred into 1.8mL of LB medium supplemented with ampicillin. The cultures were incubated overnight at 37°C with shaking. The next day, bacteria were harvested by centrifugation, and plasmid DNA was extracted using the QIAGEN Plasmid Mini Kit (QIAmp® DNA Mini Kit), with elution in 200µL of ddH_2O.

Correct plasmid integration was confirmed using restriction hydrolysis (see section below, 4.2 DNA Hydrolysis).

Successfully transformed bacteria were then expanded in 100mL of LB medium supplemented with ampicillin and incubated overnight at 37°C with shaking. Bacterial cells were harvested by centrifugation, and plasmid DNA was extracted using the PureYield Plasmid Midiprep System (Promega) following the manufacturer's protocol, with final elution in 500µL of ddH_2O.

Bacterial Freezing for Long-Term Storage

For long-term storage, bacterial cultures were frozen after plasmid verification by sequencing. To prepare glycerol stocks, 0.5mL of bacterial culture was mixed with 1mL of 50% glycerol containing ampicillin. The mixture was transferred to cryogenic vials and stored at -70°C for future use.

4.2 Molecular biological methods

Plasmid Generation

For endogenous tagging of the protein of interest (POI), approximately 1000 base pairs (bp) of the homologous recombination (HR) C-terminal region were amplified from NF54/iGP genomic DNA (gDNA) using specific primer pairs. The resulting PCR fragments were cloned into pSLI-VPS11-2xFKBP-GFP-2xFKBP_1xNLS-FRB-T2A-hDHFR (340) or pSLI-mNeonGreen-glmS (267) plasmid vectors using *NotI* and *AvrIII* or *NotI* and *MluI* restriction sites.

For targeted gene disruption, approximately 500bp of the HR N-terminal region were amplified from NF54/iGP gDNA using the corresponding primer pairs. These PCR fragments were subsequently cloned into *pSLI-TGD* plasmid vectors using *NotI* and *MluI* restriction sites. The correct integration of the insert was verified by restriction hydrolysis and DNA sequencing (see section below, 4.2, DNA Hydrolysis).

Genomic DNA Extraction

Genomic DNA was extracted from a 5mL culture containing 3–5% late-stage parasites. The culture was centrifuged at 4000×g for 1min, and the supernatant was discarded. The pellet was then processed using the Qiagen DNeasy Blood & Tissue Kit according to the manufacturer's protocol. The extracted DNA was eluted in 200µL of ddH_2O and stored at 4°C.

Amplification PCR (ampPCR)

DNA fragments for cloning were amplified by PCR using Phusion High-Fidelity DNA Polymerase in GC buffer supplemented with DMSO, following the designated protocol. The DNA template was NF54/iGP gDNA, and amplification was performed with the appropriate primer pairs (see section 4.11.1).

Phusion ampPCR reaction mix	Phusion ampPCR program		
-10ul Phusion GC buffer (5x)	-Initial denaturation:	94°C	2min
-5ul dNTPs (10mM)	-Denaturation: 94°C	30sec	
-1ul forward primer (10uM)	-Annealing:	42°C	30sec
-1ul reverse primer (10uM)	-Elongation:	68°C	3min
-1ul NF54/iGP gDNA	-> 35 cycles		
-2.5 ul Phusion DNA polymerase	-final Elongation:	68°C	3min
-0.6ul DMSO (100%)	-Storage:	10°C	=
-> fill up to 50ul ddH2O			

Following PCR, the amplification products were analyzed by agarose gel electrophoresis. A total of 5µL of the PCR reaction was mixed with 1µL of 6× DNA loading dye and loaded onto a 1% agarose gel supplemented with ethidium bromide (EtBr). The gel was run in TAE buffer at 100 V for 30min and was imaged under UV light. If the correct product size was obtained, the PCR reaction was purified using the QIAquick PCR Purification Kit, following the manufacturer's protocol, and the DNA was eluted in 30µL of ddH_2O.

Integration PCR (intPCR)

To confirm the correct genomic integration of the plasmid after selection via SLI, PCR was performed using gDNA from transfectants as a template. Phusion High-Fidelity DNA Polymerase in GC buffer supplemented with DMSO was used according to the designated protocol. Three primer combinations were employed to check for the original locus, the 5' integration site, and the 3' integration site (see Fig. 12 and section 4.11.2). Control reactions were conducted using parental NF54/iGP gDNA.

Phusion intPCR reaction mix	Phusion intPCR program		
-2ul Phusion GC buffer (5x)	-Initial denaturation:	94°C	2min
-1ul dNTPs (10mM)	-Denaturation: 94°C	30sec	
-1ul forward primer (10uM)	-Annealing:	50°C	30sec
-1ul reverse primer (10uM)	-Elongation:	68°C	3min
-1ul transfectant gDNA	-> 35 cycles		
-0.2ul Phusion DNA polymerase	-final Elongation:	68°C	3min
-0.4ul DMSO (100%)	-Storage:	10°C	=
-> fill up to 10ul ddH2O			

PCR products were analyzed by agarose gel electrophoresis. A total of 5µL of the PCR reaction was mixed with 1µL of 6× DNA loading dye and loaded onto a 1% agarose gel supplemented with EtBr. The gel was run in TAE buffer at 100 V for 30 min and visualized under UV light to verify the expected product sizes.

DNA Hydrolysis

Prior to cloning, plasmid vectors and PCR fragments were digested with restriction enzymes (endonucleases, NEB) to generate sticky ends. Additionally, DNA hydrolysis was used to analyze the correct integration of PCR products into plasmid vectors.

Vector restriction digest	PCR restriction digest	Analytic restriction digest
-100ng Plasmid DNA	-30ul PCR product	-2ul Plasmid DNA
-5ul CutSmart buffer (10x)	-5ul CutSmart buffer (10x)	-2ul CutSmart buffer (10x)
-0.5ul NotI	-0.5ul NotI	-0.1ul NotI
-0.5ul AvrIII or MluI	-0.5ul AvrIII or MluI	-0.1ul AvrIII or MluI
->fill up to 50ul with ddH2O	->fill up to 50ul with ddH2O	->fill up to 20ul with ddH2O

Digestion was performed using the corresponding restriction enzyme combinations: NLS-Tag*: NotI + AvrII* or *GlmS-Tag/TGD: NotI + MluI*, following the designated protocol (341). To prevent self-ligation, hydrolyzed vector DNA was treated with QuickCIP (NEB) to remove phosphates from sticky ends. The digested DNA was purified using the QIAquick

Purification Kit, with vector DNA eluted in 30µL of ddH_2O and PCR product DNA eluted in 20µL of ddH_2O.

To verify successful hydrolysis, digested plasmid DNA was stained with 6× DNA loading dye and analyzed by agarose gel electrophoresis. Samples were loaded onto a 1% agarose gel supplemented with EtBr, run at 100 V for 30 min in TAE buffer, and visualized under UV light to confirm the expected fragment sizes.

Molecular Cloning

For molecular cloning, digested PCR fragments were ligated into the corresponding vector at a 3:1 molecular ratio based on 50ng of vector DNA. Ligation was performed using T4 DNA ligase according to the designated protocol, with incubation at 16°C for 1 hour. The ligation product was subsequently transformed into competent XL10 Gold bacteria for propagation.

T4-DNA ligase mixture

-50ng DNA Vector

-Xng PCR product

-T4-DNA ligase buffer (10x)

-T4-DNA ligase

->fill up to 20ul with ddH2O

DNA Precipitation

Plasmid DNA was precipitated before transfection into parasites. For precipitation, 50µg of DNA in 100µL of ddH_2O was supplemented with 35µL of 3M NaOAc (pH 5.2) and 250 µL of ice-cold 100% ethanol.

DNA precipitation mixture

-50ug DNA (in 100ul ddH2O)

-35ul NaOAc (3M)

-250ul EtOH (100%, ice cold)

The mixture was incubated overnight at -8°C, followed by centrifugation at 20,000×g for 15min at 4°C. The supernatant was removed, and the DNA pellet was washed with 1 mL of 70% ethanol, followed by another centrifugation at 20,000×g for 15min at 4°C. After removing the supernatant, the pellet was dried under a laminar flow bench and resuspended in 10µL of TE buffer. The DNA was stored at 4°C until further use.

DNA Sequencing

To verify successful plasmid integration, sequencing was performed using plasmid DNA. A total of 12µL of plasmid DNA at a concentration of 100ng/µL was sent to Seqlab (Göttingen) for sequencing. The standard Seqlab primer *M13 reverse* was used for sequencing analysis.

4.3 Cell biological methods

Parasite maintenance:

Asexual blood stage *P. falciparum* (NF54 and NF54/iGP) were cultured in human B+ erythrocytes (obtained from the university clinic Eppendorf, Hamburg) at 5% hematocrit in RPMI-1640 complete medium supplemented with 0.5% Albumax II, 25mMHepes, and 500µm choline. Cultures were incubated at 37°C in a mixed gas environment (5% CO2, 5%O2, 90% N2). Culture medium was changed every other day but at least every third day by removing the old medium and adding prewarmed, fresh medium to the culture. Parasites were maintained at around 1-2% parasitemia by diluting the culture in fresh blood. Transgenic parasites were cultured in the presence of 400µg/ml G418 (342; 255).

Transfection of p. falciparum parasites:

The Plasmid DNA was transfected in P. falciparum NF54/iGP schizonts via electroporation (343).

Prior to transfection, the precipitated DNA was resuspended in 10µl TE buffer and mixed with 100µl transfection buffer.

Late stage Schizont parasites were layered on 60% Percoll and centrifuged for 5min at 2,000xg with low acceleration and break. The schizont interphase was transferred in a fresh 15ml tube and washed once with 5ml RPMI-medium.

The schizont pallet was then resuspended in the DNA/TE/TF mixture and transferred into a electroporation cuvette followed by electroporation using the AMAXA Nucleofactor II (Lonza) as previously described (344). After electroporation, the parasites were immediately transferred into 250µl prewarmed blood mixed with 500µl RPMI medium and incubated at 37°C for 1h under rigorous shaking. Following incubation, the parasites were transferred in a newly prepared culture dish. The next day 4nM WR99210 was added to the culture for positive selection.

To generate double transfectants, parasite lines with an already confirmed first transfection were transfected a second time with either an episomal overexpression

plasmid (e.g. PhiL1-mCherry-hDHODH (254)) or a second SLI based plasmid (255). The transfection was carried out as described above.

For the selection of transgenic parasites, carrying the episomal overexpression plasmid, parasites were cultured in RMPI medium supplemented with 1.5µM of the Dihydroorotate Dehydrogenase inhibitor DSM1 (345).

SLI based selection of transgenic parasites:

For selection of transgenic parasites, two rounds of drug selection were carried out (255). In the first round, the culture was supplemented with 4nM WR99210 to select for the episomal presence of the plasmid. After the reappearance of transfectants, a second round of selection with 400µg/ml G418 was carried out to select for genomic integration.

For selection of double transfected parasites, two rounds of drug selection were carried out in the presence of 400µg/ml G418. In the first round, the culture was supplemented with 2.5µg/mL blasticidin S (BSD) to select for the episomal presence of the second plasmid. After the reappearance of transfectants, a second round of selection with 1.5µM DSM1 was carried out to select for genomic integration.

Parasite Freezing:

For long term storage, parasites were cultured to 5% ring stages and harvested at 4000xg for 1min. The pellet was resuspended in 1mL malaria freezing solution (MFS, (346)) and stored at -70°C in cryo-conservation tubes.

Parasite Thawing:

Frozen parasites were thawed with 1ml prewarmed malaria thawing solution (MTS, (346)), transferred into 15ml tube and washed twice with pre-heated 5ml RPMI medium at 2000xg for 3min. After the washing steps, the parasites were transferred to a freshly prepared 5ml culture dish. Drug selection was applied the next day.

Parasite synchronization:

Parasites were synchronized at the ring stage by sorbitol treatment (347). Asynchronous cultures, predominantly in the ring stage, were transferred into a 15mL Falcon tube and centrifuged at 4000xg for 1min. The supernatant was discarded, and the pellet was resuspended in 5mL of pre-warmed 5% sorbitol in RPMI medium. The suspension was incubated at 37°C in a water bath for 15min. Following incubation, parasites were pelleted by centrifugation at 4000xg for 1min, and the supernatant was removed. The pellet was then washed with 5mL of pre-warmed RPMI medium and transferred into a fresh cell culture dish for further cultivation.

Induction of Gametocytogenesis:

Gametocytogenesis in NF54/iGP parasites was induced by supplementing a 5% ring stage culture with 2µM Shield-1 (Vector Laboratories) to stabilize the overexpression of GDVI-GFP-DD for three consecutive days (256). To prevent overgrowth, the parasite culture was expanded from 5ml to 10ml. Non-committed asexual parasites were selectively eliminated by treatment with 50mM N-acetyl-D-glucosamine for five days, starting 72 hours post-induction. Gametocyte cultures were maintained at 5% hematocrit in RPMI-1640 medium supplemented with 0.25% Albumax II and 0.25% sterile-filtered human serum. The medium was replaced daily, and cultures were incubated at 37°C in a controlled gas environment consisting of 5% CO_2, 5% O_2, and 90% N_2. Gametocyte stages were confirmed by Giemsa smears.

Induction of KS:

Knock-sideways was induced at 48 hours post-induction by splitting the gametocyte culture into two separate dishes. One dish was supplemented with 250nM Rapalog (AP21967), while the other remained untreated as a control. Gametocyte cultivation continued as previously described (255), with daily medium changes and the addition of Rapalog to the treated culture.

Flow cytometry survival assay:

Gametocyte survival was assessed by measuring parasitemia every 48 hours using flow cytometry (348). For each measurement, 20µL of gametocyte culture was diluted 1:5 in RPMI medium and stained with 1µM dihydroethidium (DHE) and a 1× SYBR Green solution (Sigma-Aldrich) for 30min at 37°C. Parasitemia was quantified using an NovoCyte 1000 (ACEA) flow cytometer, acquiring 100,000 events with CellQuest software. Single cells were gated along the diagonal in an SSC-A vs. SSC-H plot to exclude doublets and debris. Parasitemia was then determined from the SYBR Green fluorescence histogram of the singlet events.

Biotin labeling in gametocytes:

Stage III/IV gametocytes (day 8 post-gametogenesis induction) were exposed to 150µM biotin (Sigma) in complete culture medium and incubated for 8 hours at 37°C. After incubation, cultures were lysed with 0.03% saponin on ice, washed twice with ice-cold PBS, and pelted. The pellets were resuspended in lysis buffer (50mM Tris-HCl, pH 7.5, 500mM NaCl, 1% Triton X-100, 1mM DTT, 1mM PMSF, and protease inhibitor cocktail) and stored at -80°C.

Affinity purification of biotinylated proteins:

Lysates underwent three freeze-thaw cycles before centrifugation at 21,000xg for 1 hour at 4°C. Supernatants were incubated overnight with 50µL of streptavidin-conjugated Sepharose beads (GE Healthcare) at 4°C with rotation. Beads were washed sequentially with lysis buffer, dH_2O, 50mM ammonium bicarbonate (pH 8.3), and 80% acetonitrile/0.1% trifluoroacetic acid. Proteins bound to beads were eluted and digested on-bead with trypsin (1µg, Roche) at 37°C for 16 hours, followed by a second digestion for 2 hours with 0.5µg trypsin. Peptides were desalted, dried, and stored at -20°C.

Subsequent MS analysis:

The eluted proteins were subjected to trypsin digestion using the filter-aided sample preparation (FASP) method (349). Resulting peptides were desalted with C18 StageTips (Thermo Fisher Scientific) and labeled with tandem mass tag (TMT6plex) reagents according to the manufacturer's instructions. Peptides from different samples were pooled for simultaneous analysis. Liquid chromatography tandem mass spectrometry (LC-MS/MS) was performed using an UltiMate 3000 RSLCnano system connected to a Q Exactive Plus Orbitrap mass spectrometer (Thermo Fisher Scientific). Peptides were separated over a 90-minute linear gradient of acetonitrile in 0.1% formic acid. Full MS spectra were acquired at a resolution of 70,000, with the top 15 most abundant ions subjected to high-energy collision dissociation (HCD) fragmentation for MS/MS analysis.

Data Analysis:

Raw mass spectrometry data were processed using MaxQuant software (version 1.6.0.16). Peptide and protein identification was performed by searching the data against the UniProt *P. falciparum* 3D7 reference proteome. Carbamidomethylation of cysteine residues and TMT6plex labeling of lysine residues and peptide N-termini were set as fixed modifications, while methionine oxidation and N-terminal acetylation were set as variable modifications. A false discovery rate (FDR) of 1% was applied at both the peptide and protein levels. Label-free quantification (LFQ) was performed to assess relative protein abundance across samples.

4.4 Microscopy

Light microscopy:

Parasites were routinely inspected using Giemsa-stained thin blood smears. For smear preparation, 0.4µL of blood was collected from the bottom of the culture dish, smeared onto a microscope slide, air-dried, and fixed in 100% methanol. Fixed cells were stained in a 10% Giemsa solution for at least 10min, followed by rinsing with water and air drying

(350). Parasites were examined under a cell culture light microscope (Leica DM2000 LED) at 630x magnification using an oil immersion objective.

For stage quantification, images were captured at 400x magnification (oil immersion) using a Leica DMC2900 camera and analyzed with LAS software.

Live cell fluorescence microscopy:

Live fluorescence microscopy was performed on asexual parasites and gametocytes endogenously expressing GFP and/or episomally expressed mScarlet using a Leica DMi8 inverted microscope. For imaging, 250µL of resuspended parasite culture was transferred into an Eppendorf tube and stained with 50ng/mL Hoechst 33342 and 1µM Tubulin Tracker Deep Red for 45 minutes at 37°C. Following incubation, 100 µL of supernatant was removed, and the pellet was resuspended. A 7.5µL aliquot of the resuspended culture was placed on a microscope slide, covered with a coverslip, and gentle pressure was applied to ensure even cell distribution. Parasites were imaged at 10,000× magnification using a Leica DFC9000GT sCMOS fluorescence microscope camera and analyzed with LAS X software.

4.5 Computational Analysis

Phylogenetic analysis:

For the phylogenetic analysis of the 27 selected candidate proteins, orthologous sequences in non-falciparum species were identified using a position-specific iterated BLAST (PSI-BLAST) approach. The search was carried out in two rounds to ensure comprehensive coverage. In the first round, the candidate proteins were blasted against the NCBI non-redundant (nr) protein database restricted to *Plasmodium* species. In the second round, the search was performed against the NCBI-nr database with *Plasmodium* species excluded, allowing the identification of more distantly related homologues.

For each candidate, sequence coverage and e-values were extracted, and significant hits were selected for further analysis. Representative species were chosen to visualize the phylogenetic distribution. For the Laverania clade, *P. falciparum*, *P. reichenowi*, and *P. gaboni* were selected. To cover the major human-pathogenic *Plasmodium* species, *P. vivax*, *P. berghei*, *P. ovale*, and *P. malariae* were included. *Hepatocystis sp.* was added as a representative of the *Haemosporida* order, and *Theileria parva* was selected to represent the *Aconoidasida* class.

To assess conservation among related Apicomplexan species, sequences from *Toxoplasma gondii* and *Cryptosporidium parvum* were included. Furthermore, orthologues from *Saccharomyces cerevisiae* (yeast) and *Homo sapiens* were incorporated to serve as outgroup references for evolutionary comparison.

The resulting data were analyzed and visualized using R. A bubble plot was generated, in which bubble size was determined by sequence coverage, and color intensity was based on the negative logarithm of the e-value ($-\log_{10}$(E-value)). For e-values equal to zero, the maximum color intensity was applied to reflect strong homology.

Image analysis:

Microscope images were analyzed using FIJI (version 1.54p, 17.02.2025). Lif image files were imported into FIJI using the Bio-Formats plugin. Suitable parasites were selected and cropped using a 300 x 300 px square. The intensity of individual fluorescence channels was then adjusted separately. Images of individual or merged channels were converted into RGB format and saved as TIFF files using a custom FIJI macro.

For zoomed-in views, images were cropped a second time using a 60 x 60 pixel square, generating a 5x zoom. These zoomed-in images underwent background subtraction, intensity adjustment, and conversion to RGB before being saved as TIFF files. The final processed images were organized using Adobe Illustrator (version 29.5.1).

THUNDER SVCC:

To improve image quality and resolution, selected images underwent computational clearing using the LEICA THUNDER software. The Structured Variation Contrast Clearing (SVCC) method was applied with an adaptive strategy, using water as the mounting medium (refractive index: 1.33000). Computational clearing parameters were set to a 2000 nm feature scale and 60% strength. The processed SVCC images were subsequently prepared as described above.

4.5 Laboratory equipment

Table 2: Equipment

Equipment	Name/ Catalog #	Manufacturer
-70°C (-80C°) freezer	CryoCube FC660h	Eppendorf (Hamburg)
Agarose Gel Chamber	PeqLab PerfectBlue	PeqLab/VWR (Radnor)
Analytic balance	Atilon	Satorius (Göttingen)
Analytic balance	Kern 572	Kern&Sohn (Balingen)
Centrifuge	5412 D (F45-24-11)	Eppendorf (Hamburg)
Centrifuge	5424 R (FA-45-24-11)	Eppendorf (Hamburg)
Centrifuge	5810 R (A-4-62)	Eppendorf (Hamburg)
CO2-Incubator (for bacteria)	CO 150	Eppendorf (Hamburg)
Electroporator	Lonza Nucleofactor II	Lonza (basel)
Flow cytometer	NovoCyte 1000	ACEA, Agilent (Santa Clara)

Fume hood	/	Köttermann Labortechnik (Uetze)
Gel Documentation Chamber	Molecular Imager® Gel Doc™ XR - System	Bio-Rad (Hercules)
Heating Plate (cell culture)	CultureTemp	SP Industries (Warnister)
Ice machine	EF 156 easy fit	Scotsman (Vernon Hills)
Incubator	Hera Therm	ThermoScientific (Waltham)
Magnetic stirer	RSM-01HS	Phoenix Instruments (Garbsen)
Microwave	Micromaxx MM41568	Medion (Mühlheim)
PCR-cycler	ThermalCycler C1000 Touch	Bio-Rad (Hercules)
pH Meter	766 Calimatic	Knick International (Berlin)
Pipette	Pipetman L P2L/P20L/P200L/P1000L	Gilson (Middleton)
Pipette	Eppendorf Research® plus 2uL/20uL/200uL/1000uL	Eppendorf (Hamburg)
Pipettor	Pipetboy/Pipetgirl acu 2	Integra (Zizers)
Power supply (Bio-Rad)	PowerPac™ Basic Power/ HC High Current Supply	Bio-Rad (Hercules)
Shaking Incubator	Innova 40	Eppendorf (Hamburg)
Shaking Incubator	May Q 4000	ThermoScientific (Waltham)
Spectrophotometer	DS-11+ Spectrophotometer	DeNovix (Willington)
Sterile lamina flow bench	Maxisafe 2020	ThermoScientific (Waltham)
Thermoblock	Thermomixer Compact/F1.5	Eppendorf (Hamburg)
Ultrpure water purification system	Mil-i-Q Q-Pod CDUFBI001	Merck (Darmstadt)
Vacuum pump (cell culture)	BVC control	Vacuubrand (Wertheim)
Vacuum pump (Benchtop)	2522Z-02 Vac Dry Pump	Gardner Denver (Davidson)
Vortexer	VV3	VWR (Radnor)
Waterbath	GFL 1083	Gesellschaft der Labortechnick (Wedel)

Microscope	Camera	Manufacturer
Leica DM2000 LED	Leica DMC2900	Leica (Wetzlar)
Leica DMi8	DFC9000GT sCMOS	Leica (Wetzlar)

4.6 Consumables

Table 3: Consumables

Consumable	Specification	Manufacturer
Autoclave bags	200x300mm	neoLab Migge (Heidelberg)
Cell culture plates	6-/12-/24-wells	Greiner (Frickenhausen)
Centrifuge tube	15ml/50ml	Sarstedt (Nümbrecht)
Cryotubes	2.5mL	Nunc (Roskilde)
Culture flask T75	250mL	Sarstedt (Nümbrecht)
electroporation cuvette	20mm	Bio-Rad (Hercules)
Eppendorf reactin tubes	1.5ml/2ml	Eppendorf (Hamburg)

Erlenmeyer flask	500ml/1L/2L	Kimble Chase Life Science (Meiningen)
Filter tips	10ul/20ul/200ul/1000ul	Sarstedt (Nümbrecht)
Glas beaker	100ml/250ml/500ml/1L	Kimble Chase Life Science (Meiningen)
Glas Coverslips	24x65mm	Roth (Karlsruhe)
Glas Coverslips	10x10mm	Roth (Karlsruhe)
Glas Pearls	1.7-2-1mm	Roth (Karlsruhe)
Glas slides	/	Engelbrecht (Edermünde)
Gloves (Nitrile)	/	Kimberly-Clark (Koblenz)
Measuring cylinder	100ml/250ml/500ml/1L	Kavalierglas (Sazava)
Parafilm	Bemis	neoLab Migge (Heidelberg)
Pasteur pipettes	glas	ThermoScientific (Waltham)
Pasteur pipettes	plastic	Brand (Wertheim)
Petri dishes	10x35mm/15x60mm/16x92mm	Sarstedt (Nümbrecht)
Plastic pipettes	5mL/10mL/25mL	Sarstedt (Nümbrecht)
Scalpel	/	Braun (Darmstadt)
Sterile filter	0.22um Stericup Quick Release	Merck (Darmstadt)
Syringes	5ml/10ml	Braun (Darmstadt)
Whatman™ paper	/	Sigma-Aldrich (Steinheim)
Wipes	Incidin Premium Wet Wipes	Ecolab (Monheim a. R.)

4.7 Chemicals

Table 4: Chemicals

Chemical	Company
1,4-Dithiothreitol (DTT)	Roth (Karlsruhe)
4',6-Diamidino-2-Phenylindole (DAPI)	Roche (Mannheim)
Acetic acid	Roth (Karlsruhe)
Acetone	Roth (Karlsruhe)
Acrylamide/Bisacrylamide (40%)	Roth (Karlsruhe)
Agar LB (Lennox)	Roth (Karlsruhe)
Agarose	Invitrogen (Karlsruhe)
AlbumaxII	Invitrogen (Karlsruhe)
Albumin Fraction V (BSA)	Biomol (Hamburg)
Ammonium persulfate (APS)	Roth (Karlsruhe)
Bacto™ Peptone	Becton Dickinson (Heidelberg)
Bacto™ Yeast Extract	Becton Dickinson (Heidelberg)
Bromphenol Blue	Merck (Darmstadt)
Calcium chloride ($CaCl_2$)	Roth (Karlsruhe)
Choline	Sigma-Aldrich (Steinheim)
Coomassie Brilliantblau R250	Merck (Darmstadt)
D-(+)-Glucosamine hydrochloride	Sigma-Aldrich (Steinheim)
Deoxyribonucleotides (dNTPs)	Fermentas (St. Leon-Rot)
Descosept	Dr. Schumacher GmbH (Malsfeld)
D-Glucose	Sigma-Aldrich (Steinheim), Roth (Karlsruhe)
Dihydroethidium (DHE)	Biomol (Hamburg)
Dimethyl sulfoxide (DMSO)	Sigma-Aldrich (Steinheim)
Disodium hydrogen phosphate (NaH_2PO_4)	Roth (Karlsruhe)

Disodium phosphate (Na_2HPO_4)	Roth (Karlsruhe)
Dulbecco's Phosphate Buffered Saline (DPBS)	PAN Biotech (Aidenbach)
Ethanol, 70% (denatured)	Roth (Karlsruhe)
Ethanol, absolute	Roth (Karlsruhe)
Ethidium bromide (EtBr)	Sigma-Aldrich (Steinheim)
Ethylene glycol-tetraacetic acid (EGTA)	Roth (Karlsruhe)
Ethylenediaminetetraacetic acid (EDTA)	Roth (Karlsruhe)
FCCP	Biomol (Hamburg)
GeneRuler 1kb DNA ladder	Fermentas (St. Leon-Rot)
Giemsa azur eosin methylene blue solution	Merck (Darmstadt)
Glutaraldehyde (25%)	Roth (Karlsruhe)
Glycerol	Roth (Karlsruhe)
Glycine	Merck (Darmstadt)
HEPES (4-(2-hydroxyethyl)-1-piperazineethanesulfonic acid)	Roth (Karlsruhe)
Hoechst333842	Biomol (Hamburg)
Hydrochloric acid (HCl)	Roth (Karlsruhe)
Hypoxanthine	Sigma-Aldrich (Steinheim)
Immersion Oil TypF Ne23=1,5180/ve=46	Leica (Wetzlar)
Isopropanol	Roth (Karlsruhe)
Isopropyl-beta-D-thiogalactopyranosid (IPTG)	Roth (Karlsruhe)
Magnesium chloride ($MgCl_2$)	Sigma-Aldrich (Steinheim)
Manganese(II) chloride ($MnCl_2$)	Merck (Darmstadt)
Mannitol	Sigma-Aldrich (Steinheim)
Methanol (MeOH)	Roth (Karlsruhe)
Milk powder	Roth (Karlsruhe)
Mounting medium	Dako (Carpinteria)
N-Acetyl-glucosamine	Roth (Karlsruhe)
Percoll	GE Healthcare (Freiburg)
PIPES [1,4-Piperazinediethanesulfonic acid]	Sigma-Aldrich (Steinheim)
Poly-D-Lysine	ThermoFisher (Waltham)
Potassium chloride (KCl)	Sigma (Karlsruhe)
Potassium dihydrogen phosphate (KH_2PO_4)	Merck (Darmstadt)
Potassium hydroxide (KOH)	Roth (Karlsruhe)
Protease inhibitor cocktail	Roche (Mannheim)
RPMI (Roswell Park Memorial Institute) medium	Invitrogen (Waltham)
Saponin	Applichem (Darmstadt)
Sekusept Plus	BDH Bioscience/VWR (Darmstadt)
Sodium acetate ($NaCH_3COO$)	Ecolab GmbH (Monheim am Rhein)
Sodium cacodylate buffer	Sigma-Aldrich (Steinheim)
Sodium dihydrogen phosphate (NaH_2PO_4)	Roth (Karlsruhe)
Sodium dodecyl sulfate (SDS)	Roth (Karlsruhe)
Sodium hydroxide	Roth (Karlsruhe)
Sorbitol	Merck (Darmstadt)
Sucrose	Roth (Karlsruhe)
SYBR Green I	ThermoFisher (Waltham)
Tetramethylethylenediamine (TEMED)	Roth (Karlsruhe), Merck (Darmstadt)
Tris	Roth (Karlsruhe)
Tris-Base	Roth (Karlsruhe)
Triton X-100	United States Biological (Salem)

Tubulin Tracker Deep Red	ThermoScientific (Waltham)
Tween 20	Roth (Karlsruhe)

Table 5: Selection drugs

Drug	Stock	Company
Ampicillin	100mg/mL in ddH2O	Roche (Mannheim)
Blasticidine S (BSD)	10.9mg/mL in RPMI	Invitrogen (Karlsruhe)
DSM1	3.75mM in DMSO	Biomol (Hamburg)
Neomycine (G418)	50mg/mL in RPMI	Sigma-Aldrich (Steinheim)
WR99210	20mM in DMSO	Jacobus Pham. (USA)

4.8 Solutions

Table 6: Composition of used solutions

Solution	Components
SOB-Medium	0.05% (w/v) NaCl; 2% (w/v) tryptone; 0.5% (w/v) yeast extract; 1% (v/v) 250mM KCl; 0.5% (v/v) 2M MgCl2 in ddH2O
Transformation Buffer	10mM PIPES; 15mM CaCl2; 250mM KCl; 55mM MgCl2 in ddH20; pH=6.7
LB-Medium	20g/L LB-medium in ddH2O; autoclaved
LB-Agar plate solution	35g/L LB-Agar in ddH2O; autoclaved, 100ug/ml Ampiciline
Ampicillin Stock solution	100mg/mL in ddH2O
Tris-EDTA (TE) buffer	10mM Tris/hCl; 1mM EDTA; pH=8.0
Tris-Acetat-EDTA (TAE) buffer	2M Tris; 2M Acetic acid; 50mM EDTA in ddH2O; pH=8.5
Sodium Acetate solution	3M NaOAc in ddH2O; pH=5.2
RPMI-1640 medium	1.578% (w/v) RPMI-1640; 12mM NaHCO3; 6mM D-Glucose; 0.5% (w/v) Albumax II; 0.2mM Hypoxanthine; 0.4mM Gentamycin in ddH2O; pH=7.4
Blasticidine S (BSD) solution	5mg/ml BSD in RPMI medium
DSM1 solution	3,75mM DSM1 in DMSO
G418 (Neo) solution	50mg/ml G418 in RPMI medium
WR99210 (WR) solution	20uM WR in DMSO
Malaria Freezing Solution (MFS)	28% (w/v) glycerol; 4.2 (w/v) D-sorbitol; 0.9% (w/v) NaCl in ddH2O
Malaria Thawing Solution (MTS)	3.5% (w/v) NaCl in ddH2O
5% Sorbitol Solution	5% (w/v) D-Sorbitol in ddH2O
Parasite Transfection buffer	90mM NaPO4; 5mM KCl; 0.15mM CaCl2; 50mM HEPES in ddH2O; pH=7.3
Rapalog (AP21967) solution	50mM AP21967 in ethanol
Hoechst 33342 solution	0.45mg/mL Hoechst 33342 in DMSO
DHE solution	0.5mg/mL DHE in DMSO
Giemsa Staining solution	10% (v/v) Giemsa's Azure, Eosin, Methylen blue solution in H2O
Tubulin Tracker deep red (1000x)	content of the vial was dissolved in 60ul DMSO (according to manufacturer's instructions)

4.9 Molecular biological Kits

Table 7: Ready to use kits

Molecular Kits	Purpose	Manufacturer
NucleoSpin® Plasid Kit	Plasmid purification	Macherey-Nagel (Düren)
NucleoSpin® Gel and PRC clean-up	PCR purification and DNA gel extraction	Macherey-Nagel (Düren)
QIAmp® DNA Mini Kit	Extration of parasite genomic DNA	Qiagen (Hilden)
PureYield™ Plasmid Midiprep System	Plasmid purification	Promega (madison)

4.10 Enzymes and Buffers

All restriction enzymes and their corresponding buffers were purchased from New England Biolabs (NEB, Ipswich).

The phosphates quick-CIP (5U/uL), the polymerases Phusion High fidelity DNA Polymerase (2U/uL) and FirePol DNA Polymerase (10U/uL) and the T4 DNA Ligase (400U/uL) as well as their corresponding buffers were purchased from NEB (Ipswich).

The PKG inhibitor Compound 2 (C2) was kindly provided by Michael Blackman, Francis Crick Institute, London.

4.11 Oligonucleotides

Oligonucleotides (primers) were ordered from Sigma-Aldrich (Steinheim) as 100uM stock solutions in ddH2O and were stored at -20°C. Before use, primers were diluted 1:10 in ddH2O for a final concentration of 10uM.

4.11.1 Primer for cloning

Table 8: Primer for molecular cloning

Primer	DNA sequence
0111400 Tag fwd	atactcgcggccgcTAAATGAATCCATATCATCATAGTAGTCGTAGCG
0111400 Tag rev	ccatacgcgtcctaggATTGCAAAATGCTTGGTCATAAAACTTTTGACC
0205100 Tag fwd	ccaagctatttaggtgacactatagaatactcgcggccgctaaTCTTCTAAAAGGAAGAAGG ATAAAAGAAACTTGGACC
0205100 Tag rev	CCACCAGCACCAGCAGCAGCAGATCTTGATCTCAATCCTGAcctaggTTGCTC ATCTATATTATCCATTTTCGCATTGTC
0311400 Tag fwd	atactcgcggccgctaaCAGCCCACTAATGATCAGGATGGG

0311400 Tag rev	TCAATCCTGAcctaggTTTTATTTTTTTAAAAAAATAAGGATCTAGTATGAAGTTTATAGAATTAG
0504800 Tag fwd	ccaagctatttaggtgacactatagaatactcgcggccgctaaCCATATATTAACAATTCAGAAATATTAAAATTACCGG
0504800 Tag rev	CCACCAGCACCAGCAGCAGCAGATCTTGATCTCAATCCTGAcctaggAGATATGGGTGGAGGAATTTTAGGTAATGTTAATAAAGG
0510800 Tag fwd	ccaagctatttaggtgacactatagaatactcgcggccgctaaGCTTCTGCTTCAATGGATCAAACAATAAG
0510800 Tag rev	CCACCAGCACCAGCAGCAGCAGATCTTGATCTCAATCCTGAcctaggGTTTGTTTTTTCCCCCCAAATATATATATTTCCAC
0522100 Tag fwd	ccaagctatttaggtgacactatagaatactcgcggccgctaaCTTACACCTAAAGAAATTCATTATAATTCTTTATGTGG
0522100 Tag rev	CCACCAGCACCAGCAGCAGCAGATCTTGATCTCAATCCTGAcctaggTATTATATGAACTTTAATATCCACTTGTTCGAACATA
0529800 Tag fwd	atactcgcggccgctaaGTGCAAGAGGAATATGATGAAGATATGATAGCA
0529800 Tag rev	CAATCCTGAcctaggTTCAAAATAATCACGGTTCGATTCCTC
0604500 Tag fwd	ccaagctatttaggtgacactatagaatactcgcggccgctaaGATGTTGCAGACTTTCCATATTTAACAACAGGTG
0604500 Tag rev	CCACCAGCACCAGCAGCAGCAGATCTTGATCTCAATCCTGAcctaggTTTTTTTTTTTTTTCATTATTATTTGTATTATTTTTATTGTTTATTCTG
0704000 Taf rev	gccatgttgtcttcttctcccttacttaccatacgcgtcctaggATTTTTGTGCATATACTTATGTTGGTAATGTTGG
0704000 Tag fwd	cgccaagctatttaggtgacactatagaatactcgcggccgctaaGAACATGAGACATTTTCTAAATACCTTAGTGTTCC
0705100 Tag fwd	atactcgcggccgctaaCATAGTTGCCCAGGTACTTTTAGTCTG
0705100 Tag rev	CAATCCTGAcctaggTATATATGCCCCAATTTTTGCCAATTTATTCTTCC
0709400 Tag fwd	ccaagctatttaggtgacactatagaatactcgcggccgctaaGAAATAATGGAAAAGGAAAGAAAAAGCGAATTTG
0709400 Tag rev	CCACCAGCACCAGCAGCAGCAGATCTTGATCTCAATCCTGAcctaggATTTAATAAGGCGTTTAACTTTTTTTTCATACTTTTAATTATTTCG
0805100 Tag fwd	ccaagctatttaggtgacactatagaatactcgcggccgctaaAGTAGCACATTTATTCCCTTACCACATGC
0805100 Tag rev	CCAGCACCAGCAGCAGCAGATCTTGATCTCAATCCTGAcctaggAAAATTAAAGAATTTAACTCCCCTTTTTTTTAACATATTATCATTTTCTTCC
0825900 Tag fwd	atactcgcggccgctaaGAACTTGAACTATCGTATGAAAGAGAACTTGAT
0825900 Tag rev	ATCCTGAcctaggACTTGTACATTTCAACTTGTTTAATTTTTTATCACCTAACTTTGC
0924600 Tag fwd	ccaagctatttaggtgacactatagaatactcgcggccgctaaACTTTGGATGAGCGTTATACTCCTTTTCG
0924600 Tag rev	CCACCAGCACCAGCAGCAGCAGATCTTGATCTCAATCCTGAcctaggGATGAGTAGATGCTCATCCATTTTTTTTTTTATCTTATCG
0928100 Tag fwd	atactcgcggccgctaaGAAGGTGTAAGCGAGAATGTAAGAAGA
0928100 Tag rev	ATCCTGAcctaggGAAATTTTCATCCACGAGGACATATGG
1003400 Tag fwd	cgccaagctatttaggtgacactatagaatactcgcggccgctaaGGAATGTATACTCCATTGGTTCCTATGC
1003400 Tag rev	gccatgttgtcttcttctcccttacttaccatacgcgtcctaggTTTTTTTGTTGGTTTGTTTTTAAATAAGGTTGATCG
1019100 Tag fwd	atactcgcggccgctaaGACTTGAAGGATAATATATCCCCTTCTTACC
1019100 Tag rev	ATCCTGAcctaggTTTAGCACTAATTTTTTCATATTTTTCAAGAAGATCAATTG
1027000 Tag fwd	ccaagctatttaggtgacactatagaatactcgcggccgctaaGTGGTGTCCCCAGAATTTAAGACACATAC
1027000 Tag rev	CCACCAGCACCAGCAGCAGCAGATCTTGATCTCAATCCTGAcctaggATTTTCCCTTTTAATTTTACATTCTAAAGTATTATATCCATAGAGG

1036900 Tag fwd	atactcgcggccgctaaGGTGTGTGTGTAGATAATACTACCAATAGTGGA
1036900 Tag rev	TCAATCCTGAcctaggTTCTTCTCTATCTATAAAATTGAA
1114900 Tag fwd	ccaagctatttaggtgacactatagaatactcgcggccgctaaCATCCCTCAAGATTGTCTTC TTTTCATC
1114900 Tag rev	CCACCAGCACCAGCAGCAGCAGATCTTGATCTCAATCCTGAcctaggTTCTTTT TGTATGTTTATTTTGGACTTGACTATGTG
1203300 Tag fwd	ccaagctatttaggtgacactatagaatactcgcggccgctaaGCATTACCAATGGGTATGG AGAAAG
1203300 Tag rev	CCACCAGCACCAGCAGCAGCAGATCTTGATCTCAATCCTGAcctaggTAACAT ACTTCCTTCGTGTTCCCTCTG
1322200 Tag fwd	ccaagctatttaggtgacactatagaatactcgcggccgctaaCGTAGAGAATCTCCCAACG TTTCTCAC
1322200 Tag rev	CCACCAGCACCAGCAGCAGCAGATCTTGATCTCAATCCTGAcctaggCTTATTT GTATTTTCTATACAGAAAAAAGAAAAATGAAC
1416600 Tag fwd	ccaagctatttaggtgacactatagaatactcgcggccgctaaCCAAAAATGATTGGTGAAG ACAATTCCTATGTC
1416600 Tag rev	CCACCAGCACCAGCAGCAGCAGATCTTGATCTCAATCCTGAcctaggTAAAAAT TCTGTAATACTTATGTACCATTTCACTATACC
1417100 Tag fwd	atactcgcggccgctaaGATAAGAGTATAAAATACAAGTGTCCGTCT
1417100 Tag rev	ccatacgcgtcctaggATTATATTTATCCTGATAACTAGAATGAAAAACTTTTAAAATTT CATATCC
1423700 Tag fwd	ccaagctatttaggtgacactatagaatactcgcggccgctaaGTGGACCAAGATAGTTGGG TCTC
1423700 Tag rev	CCACCAGCACCAGCAGCAGCAGATCTTGATCTCAATCCTGAcctaggTTTTACA AATACATTATTTTTTTTGTTTTTAATGAGGAGGATG
1449100 Tag fwd	ccaagctatttaggtgacactatagaatactcgcggccgctaaTGGATGATGTAATATTACCAT GTTTGAAAAAGGC
1449100 Tag rev	CCACCAGCACCAGCAGCAGCAGATCTTGATCTCAATCCTGAcctaggATTAAAT TTAATTTTCCCCAAAACAAGGTCG
Primers for TGD	
1449100 TGD fwd	gaatactcgcggccgcTAACCTACAATAGGACAGAATAAATATAGAGCTAACAC
1449100 TGD rev	cacctctagcacgcgtACCCATAGCACTAGTACGTGTTAATCC
0706500 TGD fwd	gaatactcgcggccgcTAAAGTAACAATAAAGATAGCAGCAGTAATAAAAATATG
0706500 TGD rev	cacctctagcacgcgtTCCTACCATTTCTTCCTCATCTTGATC
1423700 TGD fwd	gaatactcgcggccgcTAAAATAAACAATCGGATTCAAAGCCTTATACTAAAAG
1423700 TGD rev	cacctctagcacgcgtCTTGTCATTACTATTACAATTCTGTGGGAACAC
1203300 TGD fwd	gaatactcgcggccgcTAAGAGAAAAAGAAAAAGAAAACAAAAAACGATCATGTAC
1203300 TGD rev	cacctctagcacgcgtTCGCACACTCTGTATAGTTATACTTAATAATATCCA
1003400 TGD fwd	gaatactcgcggccgcTAATTATATTCGAAGAGTAATTTGAATGTAGGTAACATTCC
1003400 TGD rev	cacctctagcacgcgtTACATCCCATATTAACTCATATTTAACAAATGGATG
0510800 TGD fwd	gaatactcgcggccgcTAAGTCAATGTTAATGAGAAAAACATTTCAGAAAAGAAG
0510800 TGD rev	cacctctagcacgcgtGAAAGATAAAGCCATAGGCAAATGTTTTCC
0604500 TGD fwd	gaatactcgcggccgcTAAGAAAAATATAATTTGAAAGAAGATAATATCATGGATCCA GATAAC
0604500 TGD rev	cacctctagcacgcgtGTGCTCATCATTTAATCTCCTATTATCAAAGTC

0805100 TGD fwd	gaatactcgcggccgcTAAAAATCTCTATATCAAATGAATCACATTGGACATCCC
0805100 TGD rev	cacctctagcacgcgtATCTAAGGATGGTTTCATTGGTTTTGG
0924600 TGD fwd	gaatactcgcggccgcTAAAACTCAACTAACGAATCCTATCCAATG
0924600 TGD rev	cacctctagcacgcgtGTTTATTATATGATCGTTAGCACTGATATGGTG
1027000 TGD fwd	gaatactcgcggccgcTAATATAGGAATTACACGGGTAAAGACTCAAATG
1027000 TGD rev	cacctctagcacgcgtCGTGTGTTCATGTTCATTTATATATGTGTC
1416600 TGD fwd	gaatactcgcggccgcTAAGAAAAGAGTTCAAAATTATACCTTCTACAAGAATATATG AAGG
1416600 TGd rev	cacctctagcacgcgtGTATGATGATGATTTATTCATAGTTCTATTCTTTTCTGTTTC

4.11.2 Primer for integration checks

Table 9: Primer for integration checks

Primer Name	DNA sequence
0111400 int fwd	CATGTACAAATGATAAGTTTGTAGGTG
0111400 int rev	CATACGTTTGGTTGTATAACGAATG
0205100 Tag fwd	CAAGATATATTGAACGATAACAAACTACTAAATCTAC
0205100 Tag rev	CCTTTCTAGTTCTCTTGAAATGTGTC
0311400 int fwd	CACGAAAGGATATGTACC
0311400 int rev	CACAAGGGCACACATATACC
0504800 Tag fwd	GACATCTATTTATCAATACAACACATTGAAAG
0504800 Tag rev	GTGAATTCAAAAGTGCCTTATGGG
0510800 int fwd	GGAGCTTATCGTTTCATCATCAAGG
0510800 int rev	CACAATGTTGTCAAATTATATTTGTATGAG
0522100 Tag fwd	GAATACATTTGTTCCCAAATATAATAACC
0522100 Tag rev	GAAAAAGAGCATAATTAAAGGGAGGAGG
0529800 Tag fwd	GGATATGAAAAAGGGAAGGGATGTG
0529800 Tag rev	GATAAGAGATTATATACACGCGGC
0604500 int fwd	CGAAAAAATGAAATGGACTATATTAAGTGAGAG
0604500 int rev	GTAAATAAAAGGACGAAGGATAGAG
0704000 Tag rev	GACTCCAATCTAGCTACGACAAC
0704000 Tag fwd	GAAAACAGCTGTTCTATGTCGAAAG
0705100 Tag fwd	GTCCTATTTTGTATCCAATCGTAAG
0705100 Tag rev	GCAGAAATGTTGCTGAGG
0709400 int fwd	GGAAAGAAAAAGAAGAAGATGTTATGAGAAG
0709400 int rev	CCTAAATATGGTATTATTGAAATGGCTTTAAC
0805100 int fwd	GTTTCCTTTACTACCTTCTTCGCC
0805100 int rev	CAATTACAATGTATGAACCAACACATAAATATAGAATC
0825900 int fwd	CGAAATTACCAATGATAACAATCCTC
0825900 int rev	CTCACAAGGTGTTTTACACC
0924600 int fwd	GGAGATGATGGGAAATTGATAAGTAGTTG
0924600 int rev	CCGTAACAGTATTTTGTCGTTTTG
0928100 int fwd	GTGTAAGTATGCCTATTCGATC
0928100 int rev	CTTCGTCAAGACAAGTCAC
1003400 int fwd	CCATGGAATTTTGGTGTAGACAC
1003400 int rev	CTATTTTGGAATGTTGTGGTTTTTTGGTG
1027000 int fwd	CATGCTCCTAAAAATAATAACGCGCAG
1027000 int rev	GCATTTATGTATGTGCTTGTGCG

1114900 int fwd	GACCATATGGATTATTAAGAATAATGCC
1114900 int rev	CCTCATTAGTGTGTTCACGAATATAATG
1203300 int fwd	CAATGAAAGCTCCTGCTTATTTTTCTGC
1203300 int rev	CGTATAAAATAAATGAATATACAGGGGCATACTC
1322200 int fwd	GTAACGAATCAGCCAGTTCTGTTC
1322200 int rev	GGGTCACCCGTCAACACAATATTC
1416600 int fwd	GAAAGTATCTACACCTTTAAGTGATGTACC
1416600 int rev	GAGACACACAACATGTCGATTTAGAAG
1423700 int fwd	GAACATGAACAGAAGAGTACTGAAGTG
1423700 int rev	CCATTGGATGACAAAAAGTTAAAATGAAGAC
1449100 int fwd	GCTATTACAAAAGATCATGAATGGACAAAAC
1449100 int rev	CAGCCAAACATGAGCATATTTCATGC
3' Int fwd	GCGGATAACAATTTCACACAGG
GFP-seq rev	GAATTGGGACAACTCCAGTG
Primer for TGD integration check	
1449100 TGD int fwd	CCACTGTTAAGGTGTTATAAGAAG
1449100 TGD int rev	GCTGGTTTAGGACATGACGG
1203300 TGD int fwd	GCTTAGAACTTGCAGAGTTTACAC
1203300 TGD int rev	GGCCAATGGTCCTCACTC
1003400 TGD int fwd	GGATCTACTTATAAGAACTATTCAGTAGTACC
1003400 TGD int rev	GAGGTATTGTTCTTTTCTGAAGACTG
0924600 TGD int fwd	CGCGTGTCCTACACTAACTTG
0924600 TGD int rev	GAATTCAGTTCATCGGTTTCTTTATC
0604500 TGD int fwd	CGACATAAACGGACCAGCAAG
0604500 TGD int rev	CCACGTTAATCTCATGAGATGTAC
0805100 TGD int fwd	GTGTTGTTTCTAGTTACAAGAGTGC
0805100 TGD int rev	GTACCTATAATTTGAGGTGTTCCCATTTC
1416600 TGD int fwd	GTGTGTGTGTGTGTTTACCTTC
1416600 TGd int rev	CATTTCCGTGACATATGTTATCCGTTAC
0111400 TGD int fwd	GTAGGTATGAAACGAAAAGGTGG
0111400 TGD int rev	GATCCGCTTTGTGCTCTTCC
Neo-seq rev	GAGAACCTGCGTGCAATCC

4.12 DNA vectors

Table 10: Plasmid vectors

Plasmid Name	Plasmid #	HR length [bp]
Tagging plasmids		
pSLI_0111400-GFP_GlmS_hDHFR	421	942
pSLI_0205100-GFP_NLS_hDHFR	378	1056
pSLI_0311400-GFP_NLS_hDHFR	437	993
pSLI_0504800-GFP_NLS_hDHFR	358	897
pSLI_0510800-GFP_NLS_hDHFR	373	1149
pSLI_0522100-GFP_NLS_hDHFR	359	1026
pSLI_0529800-GFP_NLS_hDHRF	434	1140
pSLI_0604500-GFP_NLS_hDHFR	374	943
pSLI_0704000-GFP_GlmS-hDHFR	368	780
pSLI_0705100-GFP_NLS_hDHFR	435	1803
pSLI_0709400-GFP_NLS_hDHFR	356	1200

pSLI_0805100-GFP_NLS_hDHFR	375	1086
pSLI_0825900-GFP_NLS_hDHFR	436	873
pSLI_0924600-GFP_NLS_hDHFR	376	1143
pSLI_0928100-GFP_NLS_hDHFR	431	1206
pSLI_1003400-GFP_GlmS-hDHFR	369	927
pSLI_1019100-GFP-NLS_hDHFR	443	924
pSLI_1027000-GFP_NLS_hDHFR	372	1134
pSLI_1036900-GFP_NLS_hDHFR	432	1256
pSLI_1114900-GFP_NLS_hDHFR	365	864
pSLI_1203300-GFP_NLS_hDHFR	367	900
pSLI_1322200-GFP_NLS_hDHFR	366	969
pSLI_1416600-GFP_NLS_hDHFR	377	1254
pSLI_1417100-GFP_NLS_hDHFR	442	702
pSLI_1423500-GFP_NLS-hDHFR	433	1431
pSLI_1449100-GFP_NLS-hDHFR	357	1002
TGD plasmids		
pSLI-0111400-TGD	422	597
pSLI-0504800-TGD	380	522
pSLI-0522100-TGD	381	447
pSLI-0604500-TGD	396	540
pSLI-0805100-TGD	397	306
pSLI-0924600-TGD	398	438
pSLI-1003400-TGD	385	633
pSLI-1203300-TGD	388	435
pSLI-1359700-TGD	424	1458
pSLI-1416600-TGD	400	537
pSLI-1449100-TGD	393	554
Plasmids for co-localization		
pSLI2-228-mCherry-yDHODH	409	819
pSLI2-PhiL1-mCherry-yDHODH	419	672
pSLI2-SPM3-mCherry-yDHODH	407	1065
pNMD3-Phil1-mCherry-yDHODH	438	x
pAMA1_P40X-mCherry-yDHODH	445	x

Table 11: Sizes for integration checks

Plasmid Name	PCR fragment size [bp]		
	Ori	5'	3'
Tagging plasmids			
pSLI_0111400-GFP_GlmS_hDHFR	1123	1884	1160
pSLI_0205100-GFP_NLS_hDHFR	1559	2016	1132
pSLI_0311400-GFP_NLS_hDHFR	1076	1908	1044
pSLI_0504800-GFP_NLS_hDHFR	1673	2191	1016
pSLI_0510800-GFP_NLS_hDHFR	1358	2110	832
pSLI_0522100-GFP_NLS_hDHFR	1627	1921	1464
pSLI_0529800-GFP_NLS_hDHRF	1327	2038	1244
pSLI_0604500-GFP_NLS_hDHFR	1264	2012	960
pSLI_0704000-GFP_GlmS-hDHFR	1309	1861	996
pSLI_0705100-GFP_NLS_hDHFR	2357	2827	1120
pSLI_0709400-GFP_NLS_hDHFR	1431	2150	1216
pSLI_0805100-GFP_NLS_hDHFR	1426	2020	856
pSLI_0825900-GFP_NLS_hDHFR	1634	1831	1668

pSLI_0924600-GFP_NLS_hDHFR	1733	2184	1150
pSLI_0928100-GFP_NLS_hDHFR	2078	2580	1060
pSLI_1003400-GFP_GlmS-hDHFR	1252	1818	1180
pSLI_1027000-GFP_NLS_hDHFR	1398	2160	942
pSLI_1036900-GFP_NLS_hDHFR	1470	2007	808
pSLI_1114900-GFP_NLS_hDHFR	1169	1874	644
pSLI_1203300-GFP_NLS_hDHFR	1113	1793	1108
pSLI_1322200-GFP_NLS_hDHFR	1141	1976	1264
pSLI_1416600-GFP_NLS_hDHFR	1607	2149	1748
pSLI_1423500-GFP_NLS-hDHFR	1599	2407	1162
pSLI_1449100-GFP_NLS-hDHFR	1632	2101	1108
TGD plasmids			
pSLI-0111400-TGD	1230	1971	606
pSLI-0522100-TGD	1208	1419	1134
pSLI-0604500-TGD	1307	1483	1734
pSLI-0924600-TGD	907	1490	872
pSLI-0805100-TGD	872	1608	614
pSLI-1003400-TGD	1209	1657	1168
pSLI-1203300-TGD	1115	1435	1438
pSLI-1359700-TGD	2043	2719	740
pSLI-1416600-TGD	865	1490	522
pSLI-1449100-TGD	743	1508	548

4.13 Software and Databases

Table 12: Used software

Software	Provider	Version
Adobe Animate	Adobe	24.0 (10.2023)
Adobe Illustrator	Adobe	29.5.1 (04.2025)
FIJI (ImageJ)	https://imagej.net/software/fiji/	1.54p (17.02.2025)
Leica Application Suite X	Leica	
Microsoft Office (Excel, Word)	Microsoft	2503 (04.2025)
Origin Pro	OriginLab Corporation	10.2 SR1 (01.2025)
R	R Core Team	R-4.5.0 (04.2025)
SnapGene Viewer	GSL Biotech LLC	8.0 (11.2024)
ChatGPT	OpenAI	GPT-4o

Database	URL
AlphaFold-DB	https://alphafold.ebi.ac.uk/
BioRender	https://app.biorender.com/
Clustal Omega	https://www.ebi.ac.uk/jdispatcher/msa/clustalo
PlasmoDB	https://plasmodb.org/plasmo/app

Chapter 5: References

1. **White, N. J., et al.** Malaria. *Lancet.* 2014.

2. **Sachs, J. and Malaney, P.** The Economic and Social Burden of Malaria. *Nature.* 2002.

3. **WHO.** World Malarie Report. 2024.

4. —. Global technical strategy for malaria 2016-2030, 2021 update. 2021.

5. **Trampuz, A., et al.** Clinical review: Severe malaria. *Crit. Care.* 2003.

6. **Wassmer, S. C., et al.** Investigating the Pathogenesis of Severe Malaria: A Multidisciplinary and Cross-Geographical Approach. *Am. J. Trop. Med. Hyg.* 2015.

7. **Deutsche Gesellschaft für Tropenmedizin, Reisemedizin und Globale Gesundheit e.V. (DTG).** Leitlinie: Diagnostik und Therapie der Malaria. *AWMF online.* 2021.

8. **Menkin-Smith, L. and Winders, W. T.** *Plasmodium vivax Malaria*. Treasure Island (FL) : StatPearls Publishing, 2023.

9. **Okafor, C. N. and Finnigan, N. A.** *Plasmodium ovale Malaria*. Treasure Island (FL) : StatPearls Publishing, 2023.

10. **Flannery, E., et al.** Plasmodium vivax latent liver infection is characterized by persistent hypnozoites, hypnozoite-derived schizonts, and time-dependent efficacy of primaquine. *Mol. Ther. Methods Clin. Dev.* 2022.

11. **Sutherland, C. J.** Persistent Parasitism: The Adaptive Biology of Malariae and Ovale Malaria. *Trends Parasitol.* 2016.

12. **Cowman, A. F., et al.** Malaria: Biology and Disease. *Cell.* 2016.

13. **MacPherson, G. G., et al.** Human cerebral malaria. A quantitative ultrastructural analysis of parasitized erythrocyte sequestration. *Am. J. Pathol.* 1985.

14. **Fried, M. and Duffy, P. E.** Adherence of Plasmodium falciparum to chondroitin sulfate A in the human placenta. *Science.* 1996.

15. **Helbok, R., et al.** The use of the multi-organ-dysfunction score to discriminate different levels of severity in severe and complicated Plasmodium falciparum malaria. *Am. J. Trop. Med. Hyg.* 2005.

16. **Newbold, C., et al.** Cytoadherence, pathogenesis and the infected red cell surface in Plasmodium falciparum. *Int. J. Parasitol.* 1999.

17. **Carvalho, B. O., et al.** On the cytoadhesion of Plasmodium vivax-infected erythrocytes. *J. Infect. Dis.* 2010.

18. **Fatih, F. A., et al.** Cytoadherence and virulence - The case of Plasmodium knowlesi malaria. *Malar. J.* 2012.

19. **WHO.** Global Malaria Programme operational strategy 2024-2030. 2024.

20. **Nissan, H., Ukawuba, I. and Thomson, M.** Climate-proofing a malaria eradication strategy. *Mal. J.* 2021.

21. **Angelo, K. M., et al.** Malaria after international travel: a GeoSentinel analysis, 2003–2016. *Mal. J.* 2017.

22. **Huan, J., et al.** Global burden of malaria before and after the COVID-19 pandemic based on the global burden of disease study 2021. *Sci. Rep.* 2025.

23. **Ippolito, M. M., et al.** Antimalarial Drug Resistance and Implications for the WHO Global Technical Strategy. *Curr. Epidemiol. Rep.* 2021.

24. **Riveron, J. M., et al.** Insecticide resistance in malaria vectors: an update at a global scale. In Towards malaria elimination-a leap forward. *IntechOpen*. 2018.

25. **Cohen, J., et al.** From the circumsporozoite protein to the RTS,S/AS candidate vaccine. *Hum. Vaccin*. 2010.

26. **Venkatraman, N., et al.** Phase I assessments of first-in-human administration of a novel malaria anti-sporozoite vaccine candidate, R21 in matrix-M adjuvant, in UK and Burkinabe volunteers. *medRxiv.* 2019.

27. **White, M. T., et al.** Immunogenicity of the RTS,S/AS01 malaria vaccine and implications for duration of vaccine efficacy: secondary analysis of data from a phase 3 randomised controlled trial. *Lancet Infect. Dis.* 2015.

28. **Collins, K. A., et al.** Enhancing protective immunity to malaria with a highly immunogenic virus-like particle vaccine. *Sci. Rep.* 2017.

29. **Datoo, M. S., et al.** Efficacy of a low-dose candidate malaria vaccine, R21 in adjuvant Matrix-M, with seasonal administration to children in Burkina Faso: a randomised controlled trial. *Lancet.* 2021.

30. **Martinsen, E. S., Perkins, S. and Schall, J. J.** A three-genome phylogeny of malaria parasites (Plasmodium and closely related genera): evolution of life-history traits and host switches. *Mol. Phylogenet. Evol.* 2008.

31. **Vincke, I. H. and Lips, M.** *Ann. Soc. Belge de Méa. Trop.* 1948.

32. **Jiménez-Díaz, M. B., et al.** Animal models of efficacy to accelerate drug discovery in malaria. . *Parasitology.* 2014.

33. **Oluwatobi Otun, S., et al.** Evaluation of Plasmodium berghei Models in Malaria Research. *J. Cell. Sign.* 2024.

34. **Escalante, A. A. and pacheca, M. A.** Malaria Molecular Epidemiology: An Evolutionary Genetics Perspective*. *Microbiol. Spectrum.* 2019.

35. **Bray, R. S.** Studies on malaria in chimpanzees. VI. Laverania falciparum. *Am. J. Trop. Med. Hyg.* 1958.

36. **Liu, W., et al.** Multigenomic Delineation of Plasmodium Species of the Laverania Subgenus Infecting Wild-Living Chimpanzees and Gorillas. *Genome Biol. Evol.* 2016.

37. **Pick, C., et al.** Phylogenomic analyses of malaria parasites and evolution of their exported proteins. *BMC Evol. Biol.* 2011.

38. **Sinden, R. E., et al.** Gametocyte and gamete development in Plasmodium falciparum. *Proc. R. Soc. Lond. B. Biol. Sci.* 1978.

39. **Maier, A. G., et al.** Plasmodium falciparum. *Trends Parasit.* 2019.

40. **Venugopal, K., et al.** Plasmodium asexual growth and sexual development in the haematopoietic niche of the host. *Nat. Rev. Microbiol.* 2020.

41. **Otun, O. and Achilonu, I.** Plasmodium yoelii as a model for malaria: insights into pathogenesis, drug resistance, and vaccine development. *Mol. Bio. Rep.* 2025.

42. **Sidjanski, S. and Vanderberg, J. P.** Delayed migration of Plasmodium sporozoites from the mosquito bite site to the blood. *Am. J. Trop. Med. Hyg.* 1997.

43. **Medica, D. L. and Sinnis, P.** Quantitative dynamics of Plasmodium yoelii sporozoite transmission by infected anopheline mosquitoes. *Infect. Immun.* 2005.

44. **Gueirard, P., et al.** Development of the malaria parasite in the skin of the mammalian host. *Proc. Natl. Acad. Sci.* 2010.

45. **Hopp, C. S., et al.** Comparative intravital imaging of human and rodent malaria sporozoites reveals the skin is not a species-specific barrier. *EMBO Mol. Med.* 2021.

46. **Pradel, G. and Frevert, U.** Malaria sporozoites actively enter and pass through rat Kupffer cells prior to hepatocyte invasion. *Hepatology.* 2001.

47. **Vreden, S. G. S.** The role of Kupffer cells in the clearance of malaria sporozoites from the circulation. *Parasitol. Today.* 1994.

48. **Mota, M. M., et al.** Migration of Plasmodium sporozoites through cells before infection. *Science.* 2001.

49. **Tavares, J., et al.** Role of host cell traversal by the malaria sporozoite during liver infection. *J. Exp. Med.* 2013.

50. **Frevert, U., et al.** Malaria Circumsporozoite Protein Binds to Heparan Sulfate Proteoglycans Associated with the Surface Membrane of Hepatocytes. *J. Exp. Med.* 1993.

51. **Cowan, G., et al.** Expression of thrombospondin-related anonymous protein in Plasmodium falciparum sporozoites. *Lancet.* 1992.

52. **Meis, J. F., et al.** Malaria parasites--discovery of the early liver form. *Nature.* 1983.

53. **Baer, K., et al.** Release of Hepatic Plasmodium yoelii Merozoites into the Pulmonary Microvasculature. *PLoS Pathog.* 2007.

54. **Vaughan, A. M., et al.** Complete Plasmodium falciparum liver-stage development in liver-chimeric mice. *J. Clin. Invest.* 2012.

55. **Vickerman, K. and Cox, F. E. G.** Merozoite formation in the erythrocytic stages of the malaria parasite Plasmodium vinckei. *Trans. R. Soc. Trop. Med. Hyg.* 1967.

56. **White, J. H. and Kilbey, B. J.** DNA replication in the malaria parasite. *Parasitol. Today.* 1996.

57. **Garg, S., et al.** Visualization and quantification of Plasmodium falciparum intraerythrocytic merozoites. *Sys. Syn. Biol.* 2015.

58. **Crutcher, J. M. and Hoffman, S. L.** Chapter 83 Malaria. *Medical Microbiology. 4th Edition.* Galveston (TX) : University of Texas Medical Branch at Galveston, 1996.

59. **Voss, T. S. and Brancucci, N. M.** Regulation of sexual commitment in malaria parasites - a complex affair. *Curr. Opin. Microbiol.* 2024.

60. **Nghoto, P., et al.** Revisiting gametocyte biology in malaria parasites. *FEMS Microbiol. Rev.* 2019.

61. **Smalley, M. E., Abdalla, S. and Brown, J.** The distribution of Plasmodium falciparum in the peripheral blood and bone marrow of Gambian children. *Trans. R. Soc. Trop. Med. Hyg.* 1981.

62. **Dash, M., et al.** Gametogenesis in Plasmodium: Delving Deeper to Connect the Dots. *Front. Cell. Infect. Microbiol.* 2022.

63. **Bennink, S., Kiesow, M. J. and Pradel, G.** The development of malaria parasites in the mosquito midgut. *Cell. Microbiol.* 2016.

64. **Nilsson, S. K., et al.** Targeting Human Transmission Biology for Malaria Elimination. *PLoS Pathog.* 2015.

65. **Ladda, R., Aikawa, M. and Sprinz, H.** Penetration of erythrocytes by merozoites of mammalian and avian malarial parasites. *J. Parasitol.* 1969.

66. **Goel, V. K., et al.** Band 3 is a host receptor binding merozoite surface protein 1 during the Plasmodium falciparum invasion of erythrocytes. *Proc. Natl. Acad. Sci.* 2003.

67. **Baldwin, M. R., et al.** Merozoite surface protein 1 recognition of host glycophorin A mediates malaria parasite invasion of red blood cells. *Blood.* 2015.

68. **Boyle, M. J., et al.** Interactions with heparin-like molecules during erythrocyte invasion by Plasmodium falciparum merozoites. *Blood.* 2010.

69. **Dvorak, J. A., et al.** Invasion of erythrocytes by malaria merozoites. *Science.* 1975.

70. **Breuer, W. V., Ginsgurg, H. and Cabantchik, Z. I.** An assay for malaria parasite invasion into human erythrocytes. The effects of chemical and enzymatic modification of erythrocyte membrane components. *Biochim. Biophys.* 1983.

71. **Camus, D. and Hadley, T. J.** A Plasmodium falciparum antigen that binds to host erythrocytes and merozoites. *Science.* 1985.

72. **Rayner, J. C., et al.** Two Plasmodium falciparum genes express merozoite proteins that are related to Plasmodium vivax and Plasmodium yoelii adhesive proteins involved in host cell selection and invasion. *Proc. Natl. Acad. Sci.* 2000.

73. **Tanabe, K., Mikkelsen, R. B. and Wallach, D. F. H.** Calcium transport of Plasmodium chahaudi-infected erythrocytes. *J. Cell Biol.* 1982.

74. **McCallum-Deighton, N. and Holder, A. A.** The role of calcium in the invasion of human erythrocytes by Plasmodium falciparum. *Mol. Biochem. Parasit.* 1992.

75. **Singh, S., et al.** Distinct External Signals Trigger Sequential Release of Apical Organelles during Erythrocyte Invasion by Malaria Parasites. *PLoS Pathog.* 2010.

76. **Alexander, D. L., et al.** Identification of the moving junction complex of Toxoplasma gondii: a collaboration between distinct secretory organelles. *PLoS Pathog.* 2005.

77. **Alexander, D .L., et al.** Plasmodium falciparum AMA1 binds a rhoptry neck protein homologous to TgRON4, a component of the moving junction in Toxoplasma gondii. *Eukaryot. Cell.* 2006.

78. **Srinivasan, P., et al.** Binding of Plasmodium merozoite proteins RON2 and AMA1 triggers commitment to invasion. *Proc. Natl. Acad. Sci.* 2011.

79. **Besteiro, S., Dubremetz, J. F. and Lebrun, M.** The moving junction of apicomplexan parasites: a key structure for invasion. *Cell. Microbiol.* 2011.

80. **Baum, J., et al.** A conserved molecular motor drives cell invasion and gliding motility across malaria life cycle stages and other apicomplexan parasites. *J. Biol. Chem.* 2006.

81. **Soldati-Favre, D.** Molecular dissection of host cell invasion by the apicomplexans: the glideosome. *Parasite.* 2008.

82. **Dobrowolski, J. M., Carruthers, V. B. and Sibley, L. D.** Participation of myosin in gliding motility and host cell invasion by Toxoplasma gondii. *Mol. Microbiol.* 1997.

83. **Green, J. L., et al.** Compositional and expression analyses of the glideosome during the Plasmodium life cycle reveal an additional myosin light chain required for maximum motility. *J. Biol. Chem.* 2017.

84. **Rees-Channer, R. R., et al.** Dual acylation of the 45kDa gliding-associated protein (GAP45) in Plasmodium falciparum merozoites. *Mol. Biochem. Parasitol.* 2006.

85. **Yeoman, J. A., et al.** Tracking Glideosome-associated protein 50 reveals the development and organization of the inner membrane complex of Plasmodium falciparum. *Eukaryot. Cell.* 2011.

86. **Bergman, L. W., et al.** Myosin A tail domain interacting protein (MTIP) localizes to the inner membrane complex of Plasmodium sporozoites. *J. Cell Sci.* 2003.

87. **Harding, C. R. and Meissner, M.** The inner membrane complex through development of Toxoplasma gondii and Plasmodium. *Cell. Microbiol.* 2014.

88. **Jewett, T. J. and Sibley, L. D.** Aldolase forms a bridge between cell surface adhesins and the actin cytoskeleton in apicomplexan parasites. *Mol. Cell.* 2003.

89. **Baum, J., et al.** Regulation of apicomplexan actin-based motility. *Nat. Rev. Microbiol.* 2006.

90. **Egarter, S., et al.** The toxoplasma Acto-MyoA motor complex is important but not essential for gliding motility and host cell invasion. *PLoS One.* 2014.

91. **Bichet, M., et al.** Genetic impairment of parasite myosin motors uncovers the contribution of host cell membrane dynamics to toxoplasma invasion forces. *BMC Biol.* 2016.

92. **Tardieux, I. and & Baum, J.** Reassessing the mechanics of parasite motility and host-cell invasion. *J. Cell Biol.* 2016.

93. **Dluzewski, A. R., et al.** Origins of the parasitophorous vacuole membrane of the malaria parasite, Plasmodium falciparum, in human red blood cells. *J. Cell Sci.* 1992.

94. **Ward, G. E., Miller, L. H. and Dvorak, J. A.** The origin of parasitophorous vacuole membrane lipids in malaria-infected erythrocytes. *J. Cell Sci.* 1993.

95. **Dasgupta, S., et al.** Membrane-wrapping contributions to malaria parasite invasion of the human erythrocyte. *Biophys. J.* 2014.

96. **Torii, M., et al.** Release of merozoite dense granules during erythrocyte invasion by Plasmodium knowlesi. *Infect. Immun.* 1989.

97. **Spillman, N. J., Beck, J. R. and Goldberg, D. E.** Protein export into malaria parasite-infected erythrocytes: mechanisms and functional consequences. *Annu. Rev. Biochem.* 2015.

98. **Gilson, P. R., et al.** Host cell remodelling in malaria parasites: a new pool of potential drug targets. *Int. J. Parasit.* 2016.

99. **de Rojas, M. O. and Wasserman, M.** Temporal relationships on macromolecular synthesis during the asexual cell cycle of Plasmodium falciparum. *Trans. R. Soc. Trop. Med. Hyg.* 1985.

100. **Langreth, S. G., et al.** Fine structure of human malaria in vitro. *J. Protozool.* 1978.

101. **Grüring, C., et al.** Development and host cell modifications of Plasmodium falciparum blood stages in four dimensions. *Nature Com.* 2011.

102. **Baumeister, S., et al.** Evidence for the involvement of Plasmodium falciparum proteins in the formation of new permeability pathways in the erythrocyte membrane. *Mol. Microbiol.* 2006.

103. **Gulati, S., et al.** Profiling the Essential Nature of Lipid Metabolism in Asexual Blood and Gametocyte Stages of Plasmodium falciparum. *Cell Host Micr.* 2015.

104. **Spielmann, T. and Gilberger, T-W.** Critical Steps in Protein Export of Plasmodium falciparum Blood Stages. *Trends Parasit.* 2015.

105. **Roth E., Jr.** Plasmodium falciparum carbohydrate metabolism: a connection between host cell and parasite. *Blood Cells.* 1990.

106. **Atamna, H., Pascarmona, G. and Ginsburg, H.** Hexose-monophosphate shunt activity in intact Plasmodium falciparum-infected erythrocytes and in free parasites. *Mol. Biochem. Parasitol.* 1994.

107. **Goldberg, D. E., et al.** Hemoglobin degradation in the malaria parasite Plasmodium falciparum: An ordered process in a unique organelle. *Proc. Natl. Acad. USA.* 1990.

108. **Slomianny, C.** Three-dimensional reconstruction of the feeding process of the malaria parasite. *Blood Cells.* 1990.

109. **Maurer, G.** Die Malaria perniciosa. *Centralblatt für Bakteriologie. Parasitenkunde und Infektionskrankheiten.* 1902.

110. **Trager, W., Rudzinska, M. A. and Bradbury, P. C.** The fine structure of Plasmodium falciparum and its host erythrocytes in natural malarial infections in man. . *Bull. World Health Organ.* 1966.

111. **Henrich, P., et al.** 3-D analysis of the Plasmodium falciparum Maurer's clefts using different electron tomographic approaches. *Biotechnol. J.* 2009.

112. **Bhattacharjee, S., et al.** Maurer's clefts of Plasmodium falciparum are secretory organelles that concentrate virulence protein reporters for delivery to the host erythrocyte. *Blood.* 2007.

113. **Leech, J. H., et al.** Identification of a strain-specific malarial antigen exposed on the surface of Plasmodium falciparum-infected erythrocytes. *J. Exp. Med.* 1984.

114. **Su, X. Z., et al.** The large diverse gene family var encodes proteins involved in cytoadherence and antigenic variation of Plasmodium falciparum-infected erythrocytes. . *Cell.* 1995.

115. **Francis, S. E., Sullivan, D. J. and Goldberg, D. E.** Hemoglobin metabolism in the malaria parasite Plasmodium falciparum. *Annu. Rev. Microbiol.* 1997.

116. **Stanojcic, S., et al.** Single-molecule analysis reveals that DNA replication dynamics vary across the course of schizogony in the malaria parasite Plasmodium falciparum. *Sci. Rep.* 2017.

117. **Klaus, S., et al.** Asynchronous nuclear cycles in multinucleated Plasmodium falciparum facilitate rapid proliferation. *Sci. Adv.* 2022.

118. **Voß, Y., et al.** Plasmodium schizogony, a chronology of the parasite's cell cycle in the blood stage. *PLoS Pathog.* 2023.

119. **Guttery, D. S., et al.** The molecular mechanisms driving Plasmodium cell division. *Biochem. Soc. Trans.* 2024.

120. **Evers, F., et al.** Composition and stage dynamics of mitochondrial complexes in Plasmodium falciparum. *Nature Com.* 2021.

121. **Arnot, D. E., Ronander, E. and Bengtsson, D. C.** The progression of the intra-erythrocytic cell cycle of Plasmodium falciparum and the role of the centriolar plaques in asynchronous mitotic division during schizogony. *Int. J. Parasitol.* 2011.

122. **Francia, M. E. and Striepen, B.** Cell division in apicomplexan parasites. *Nat. Rev. Microbiol.* 2014.

123. **Kono, M., et al.** Evolution and architecture of the inner membrane complex in asexual and sexual stages of the malaria parasite. *Mol. Biol. Evol.* 2012.

124. **Kono, M., et al.** Pellicle formation in the malaria parasite. *J. Cell Sci.* 2016.

125. **Rudlaff, R. M., et al.** An essential contractile ring protein controls cell division in Plasmodium falciparum. *Nature Com.* 2019.

126. **Clements, R. L., et al.** Identification of basal complex protein that is essential for maturation of transmission-stage malaria parasites. *Proc. Natl. Acad. Sci.* 2022.

127. **Morano, A. A., Rudlaff, R. M. and Dvorin, J. D.** A PPP-type pseudophosphatase is required for the maintenance of basal complex integrity in Plasmodium falciparum. *Nature Com.* 2023.

128. **Morano, A. A., Ali, I. and Dvorin, J. D.** Elucidating the spatio-temporal dynamics of the Plasmodium falciparum basal complex. *PLoS Pathogens.* 2024.

129. **Tan, M. S. Y. and Blackman, M. J.** Malaria parasite egress at a glance. *J. Cell Sci.* 2021.

130. **Dvorin, J. D. and Goldberg, D. E.** Plasmodium Egress Across the Parasite Life Cycle. *Annu. Rev. Microbiol.* 2022.

131. **Glushakova, S., et al.** Rounding precedes rupture and breakdown of vacuolar membranes minutes before malaria parasite egress from erythrocytes. *Cell Microbiol.* 2018.

132. **Glushakova, S., et al.** Membrane transformation during malaria parasite release from human red blood cells. *Curr. Biol.* 2005.

133. **Abkarian, M., et al.** A novel mechanism for egress of malarial parasites from red blood cells. *Blood.* 2011.

134. **Collins, C. R., et al.** The plasmodium falciparum pseudoprotease SERA5 regulates the kinetics and efficiency of malaria parasite egress from host erythrocytes. *PLoS Pathog*. 2017.

135. **Sinden, R. E.** The cell biology of sexual development in Plasmodium. *Parasitol*. 1983.

136. **Eichner, M., et al.** Genesis, sequestration and survival of Plasmodium falciparum gametocytes: parameter estimates from fitting a model to malariatherapy data. *Trans. R. Soc. Trop. Med. Hyg*. 2001.

137. **Cao, P., et al.** Modeling the dynamics of Plasmodium falciparum gametocytes in humans during malaria infection. *Elife*. 2019.

138. **Bruce, M. C., et al.** Commitment of the malaria parasite Plasmodium falciparum to sexual and asexual development. *Parasitol*. 1990.

139. **Silvestrini, F., Alano, P. and Williams, J. L.** Commitment to the production of male and female gametocytes in the human malaria parasite Plasmodium falciparum. *Parasitol*. 2000.

140. **Bancells, C., et al.** Revisiting the initial steps of sexual development in the malaria parasite Plasmodium falciparum. *Nat. Microbiol*. 2019.

141. **Dixon, M. W., et al.** Sex in Plasmodium: a sign of commitment. *Trends Parasitol*. 2008.

142. **Sinha, A., et al.** A cascade of DNA binding proteins for sexual commitment and development in Plasmodium. *Nature*. 2014.

143. **Kafsack, B. F. C., et al.** A transcriptional switch underlies commitment to sexual development in human malaria parasites. *Nature*. 2014.

144. **Kwon, S. H. and Workman, J. L.** The heterochromatin protein 1 (HP1) family: put away a bias toward HP1. *Mol. Cells*. 2008.

145. **Eksi, S., et al.** Plasmodium falciparum gametocyte development 1 (Pfgdv1) and gametocytogenesis early gene identification and commitment to sexual development. *PLoS Patho*. 2012.

146. **Brancucci, N. M. B., et al.** Heterochromatin protein 1 secures survival and transmission of malaria parasites. *Cell. Host. Microbe*. 2014.

147. **Filarsky, M., et al.** GDV1 induces sexual commitment of malaria parasites by antagonizing HP1-dependent gene silencing. *Science*. 2018.

148. **Josling, G. A., et al.** Dissecting the role of PfAP2-G in malaria gametocytogenesis. *Nature Com*. 2020.

149. **Trager, W. and Gill, G. S.** Enhanced gametocyte formation in young erythrocytes by Plasmodium falciparum in vitro. *J. Protozool*. 1992.

150. **Williams, J. L.** Stimulation of Plasmodium falciparum gametocytogenesis by conditioned medium from parasite cultures. *Am. J. Trop. Med.* 1999.

151. **Buckling, A., et al.** Chloroquine increases Plasmodium falciparum gametocytogenesis in vitro. *Parasitol.* 1999.

152. **Dietz, K-J. and Vogel, M. O.** AP2/EREBP transcription factors are part of gene regulatory networks and integrate metabolic, hormonal and environmental signals in stress acclimation and retrograde signalling. *Protoplasma*. 2010.

153. **Downs, W. G.** Infections of chicks with single parasites of Plasmodium gallinaceum Brumpt. *Am. J. Hyg.* 1947.

154. **Smith, T. G.** Sexual differentiation and sex determination in the Apicomplexa. *Trends Parasitol.* 2002.

155. **Tadesse, F. G., et al.** Gametocyte Sex Ratio: The Key to Understanding Plasmodium falciparum Transmission? *Trends Parasitol.* 2019.

156. **Khan, S. M., Franke-Fayard, B., et al.** Proteome Analysis of Separated Male and Female Gametocytes Reveals Novel Sex-Specific Plasmodium Biology. *Cell.* 2005.

157. **Grasso, F., et al.** A Comprehensive Gender-related Secretome of Plasmodium berghei Sexual Stages. *Mol. Cell. Proteomics*. 2020.

158. **Russell, A. J. C., et al.** Regulators of male and female sexual development are critical for the transmission of a malaria parasite. *Cell. Host Microbe.* 2024.

159. **Kass, L., et al.** Plasmodium Falciparum Gametocytes: Electron Microscopic Observations on Material Obtained by a New Method. *Am. J. Trop. Med. Hyg.* 1971.

160. **Aguilar, R., et al.** Molecular evidence for the localization of Plasmodium falciparum immature gametocytes in bone marrow. *Blood.* 2014.

161. **Hawking, F. and Wilson, M. E.** Evidence for cyclic development and short-lived maturity in the gametocytes of Plasmodium falciparum. *Trans. R. Soc. Trop. Med. Hyg.* 1971.

162. **Tiburcio, M., et al.** Early gametocytes of the malaria parasite Plasmodium falciparum specifically remodel the adhesive properties of infected erythrocyte surface. *Cell Microbiol.* 2013.

163. **Li, J., et al.** Repurposing the mitotic machinery to drive cellular elongation and chromatin reorganisation in Plasmodium falciparum gametocytes. *Nature Com.* 2022.

164. **Sinden, R. E. and Smalley, M. E.** Gametocytogenesis of Plasmodium falciparum in vitro: the cell-cycle. *Parasitology.* 1979, Vol. 79.

165. **Ferreira, J. L., et al.** The Dynamic Roles of the Inner Membrane Complex in the Multiple Stages of the Malaria Parasite. *Front. Cell. Infect. Microbiol.* January 2021.

166. **Meszoely, C. A. M., et al.** Plasmodium falciparum: Freeze-fracture of the gametocyte pellicular complex. *Exp. Para*. 1987.

167. **Parkyn Schneider, M., et al.** Disrupting assembly of the inner membrane complex blocks Plasmodium falciparum sexual stage development. *PLoS Pathog*. . 2017.

168. **Kaidoh, I., et al.** Novel structure in the pellicular complex of Plasmodium falciparum gametocytes. *J. Euka. Microbiol*. 1993.

169. **Dearnley, M. K., et al.** Origin, composition, organization and function of the inner membrane complex of Plasmodium falciparum gametocytes. *J. Cell Sci*. 2012.

170. *Variable microtubule architecture in the malaria parasite*. **Ferreira, J. L., et al.** 2023, Nature Com.

171. **Sinden, R. E.** Gametocytogenesis of Plasmodium falciparum in vitro: an electron microscopic study. *Parasitology*. 1982.

172. **Hanssen, E., et al.** Soft X-ray microscopy analysis of cell volume and hemoglobin content in erythrocytes infected with asexual and sexual stages of Plasmodium falciparum. *J. Struct. Biol*. 2012.

173. **Krungkrai, J., Prapunwattana, P. and Krungkrai, S. R.** Ultrastructure and function of mitochondria in gametocytic stage of Plasmodium falciparum-. *Parasite*. 2000.

174. **Evers, F., et al.** Comparative 3D ultrastructure of Plasmodium falciparum gametocytes. *Nature Com*. 2025.

175. **Hliscs, M., et al.** Organization and function of an actin cytoskeleton in Plasmodium falciparum gametocytes. *Cell. Microbiol*. 2014.

176. **Bannister, L. H., et al.** A brief illustrated guide to the ultrastructure of Plasmodium falciparum asexual blood stages. *Parasitol. Today*. 2000.

177. **Tremp, A. Z., Khater, E. I. and Dessens, J. T.** IMC1b is a putative membrane skeleton protein involved in cell shape, mechanical strength, motility, and infectivity of malaria ookinetes. *J. Biol. Chem*. 2008.

178. **Dixon, M. W. A. and Tilley, L.** Plasmodium falciparum goes bananas for sex. *Mol. Biochem. Parasitol*. 2021.

179. **Morrissette, N. S. and Sibley, L. D.** Cytoskeleton of Apicomplexan Parasites. *Microbiol. Mol. Biol. Rev*. 2002.

180. **Bullen, H. E., et al.** A novel family of Apicomplexan glideosome-associated proteins with an inner membrane-anchoring role. *J. Biol. Chem*. 2009.

181. **Agop-Nersesiam, C., et al.** Biogenesis of the inner membrane complex is dependent on vesicular transport by the alveolate specific GTPase Rab11B. *PLoS Pathog*. 2010.

182. **Smalley, M. E. and Sinden, R. E.** Plasmodium falcparum gametocytes: their longevity and infectivity. *Parasitology.* 1977.

183. **Gaskins, E., et al.** Identification of the membrane receptor of a class XIV myosin in Toxoplasma gondii. *J. Cell Biol.* 2004.

184. **Mann, T. and Beckers, C.** Characterization of the subpellicular network, a filamentous membrane skeletal component in the parasite Toxoplasma gondii . *Mol. Biochem. Parasitol.* 2001.

185. **Beck, J. R., et al.** A novel family of Toxoplasma IMC proteins displays a hierarchical organization and functions in coordinating parasite division. *PLoS Pathog.* 2010.

186. **Poulin, B., et al.** Unique apicomplexan IMC sub-compartment proteins are early markers for apical polarity in the malaria parasite. *Biol. Open.* 2013.

187. **Kumar, S., et al.** PfCDPK1 mediated signaling in erythrocytic stages of Plasmodium falciparum. *Nature Com.* 2017.

188. **Saini, E., et al.** Photosensitized INA-Labelled protein 1 (PhIL1) is novel component of the inner membrane complex and is required for Plasmodium parasite development. *Sci. Reports.* 2017.

189. **Wetzel, J., et al.** The role of palmitoylation for protein recruitment to the inner membrane complex of the malaria parasite. *J. Biol. Chem.* 2015.

190. **Chen, A. L., et al.** Novel components of the Toxoplasma inner membrane complex revealed by BioID. *mBio.* 2015.

191. **Chen, A. L., et al.** Novel insights into the composition and function of the Toxoplasma IMC sutures. *Cell. Microbiol.* 2017.

192. **Keeley, A. and Soldati, D.** The glideosome: a molecular machine powering motility and host-cell invasion by Apicomplexa. *Trends Cell Biol.* 2004.

193. **Vanderberg, J. P.** Studies on the motility of Plasmodium sporozoites. *J. Protozool.* 1974.

194. **Ryning, F. W. and Remington, J. S.** Effect of cytochalasin D on Toxoplasma gondii cell entry. *Infect. Immun.* 1978.

195. **Robson, K. J., et al.** A highly conserved amino-acid sequence in thrombospondin, properdin and in proteins from sporozoites and blood stages of a human malaria parasite. *Nature.* 1988.

196. **Russell, D. G. and Burns, R. G.** The polar ring of coccidian sporozoites: a unique microtubule-organizing centre. *J. Cell Sci.* 1984.

197. **Sun, S. Y., et al.** Cryogenic electron tomography reveals novel structures in the apical complex of Plasmodium falciparum. *mBio.* 2024.

198. **Khater, E. I., Sinden, R. E. and Dessens, J. T.** A malaria membrane skeletal protein is essential for normal morphogenesis, motility, and infectivity of sporozoites. *J. Cell Biol.* 2004.

199. **Gould, S. B., et al.** Alveolins, a new family of cortical proteins that define the protist infrakingdom alveolata. *Mol. Biol. Evol.* 2008.

200. **Tremp, A. Z., et al.** Morphogenesis of Plasmodium zoites is uncoupled from tensile strength. *Mol. Microbiol.* 2013.

201. **Tremp, A. Z. and Dessens, J. T.** Malaria IMC1 membrane skeleton proteins operate autonomously and participate in motility independently of cell shape. *J. Biol. Chem.* 2011.

202. **Kirschner, M. W. and Mitchison, T.** Microtubule dynamics. *Nature.* 1986.

203. **Hirokawa, N., et al.** Kinesin superfamily motor proteins and intracellular transport. *Nat. Rev. Mol. Cell Biol.* 2009.

204. **Zaytsev, A. V. and Grishchuk, E. L.** Basic mechanism for biorientation of mitotic chromosomes is provided by the kinetochore geometry and indiscriminate turnover of kinetochore microtubules. *Mol. Biol. Cell.* 2015.

205. **Gall, J. G.** Microtubule fine structure. *J. Cell Biol.* 1966.

206. **Nogales, E., Wolf, S. G. and Downing, K. H.** Structure of the alpha beta tubulin dimer by electron crystallography. *Nature.* 1998.

207. **Wade, R. H., Chretien, D. and Job, D.** Characterization of microtubule protofilament numbers. How does the surface lattice accommodate? *J. Mol. Biol.* 1990.

208. **Nogales, E., et al.** Structure of tubulin at 6.5 A and location of the taxol-binding site. *Nature.* 1995.

209. **Mitchison, T. and Kirschner, M.** Dynamic instability of microtubule growth. *Nature.* 1984.

210. **Dammermann, A., Desai, A. and Oegema, K.** The minus end in sight. *Curr. Biol.* 2003.

211. **Hendershott, M. C. and Vale, R. D.** Regulation of microtubule minus-end dynamics by CAMSAPs and Patronin. *Proc. Natl. Acad. Sci.* 2014.

212. **Lomakin, A. J., et al.** CLIP-170-dependent capture of membrane organelles by microtubules initiates minus-end directed transport. *Dev. Cell.* 2009.

213. **Vleugel, M., Kok, M. and Dogterom, M.** Understanding force-generating microtubule systems through in vitro reconstitution. *Cell Adh. Migr.* 2016.

214. **Dugina, V., Alieva, I., et al.** Interaction of microtubules with the actin cytoskeleton via cross-talk of EB1-containing +TIPs and γ-actin in epithelial cells. *Oncotarget.* 2016.

215. **Wiest, P. M., Johnson, J. H. and Flanigan, T. P.** Microtubule inhibitors block Cryptosporidium parvum infection of a human enterocyte cell line. *Infect. Immun.* 1993.

216. **Yvon, A. M. and Wadsworth, P.** Non-centrosomal microtubule formation and measurement of minus end microtubule dynamics in A498 cells. *Cell Sci*. 1997.

217. **Carlier, M. F. and Pantaloni, D.** Carlier, M. F.; Pantaloni, D. *Kinetic analysis of guanosine 5'-triphosphate hydrolysis associated with tubulin polymerization*. 1981 Biochemistry.

218. **Zheng, Y., et al.** Nucleation of microtubule assembly by a gamma-tubulin-containing ring complex. *Nature*. 1995.

219. **Bowne-Anderson, H., et al.** Microtubule dynamic instability: a new model with coupled GTP hydrolysis and multistep catastrophe. *BioEssays*. 2013.

220. **Simon, J. R. and Salmon, E. D.** The structure of microtubule ends during the elongation and shortening phases of dynamic instability examined by negative-stain electron microscopy. *J. Cell. Sci*. 1990.

221. **Chretien, D., Fuller, S. D. and Karsenti, E.** Structure of growing microtubule ends: two-dimensional sheets close into tubes at variable rates. *J. Cell Biol*. 1995.

222. **McIntosh, J. R., et al.** Microtubules grow by the addition of bent guanosine triphosphate tubulin to the tips of curved protofilaments. *J. Cell Biol*. 2018.

223. **Harding, C. R. and Frischknecht, F.** The Riveting Cellular Structures of Apicomplexan Parasites. *Trends Parasitol*. 2020.

224. **Morejohn, L.C. and Fosket, D.E.** The biochemistry of compounds with anti-microtubule activity in plant cells. *Pharmacol. Ther*. 1991.

225. **Soleihac, E., et al.** Specific Targeting of Plant and Apicomplexa Parasite Tubulin through Differential Screening Using In Silico and Assay-Based Approaches. *Int. J. Mol. Sci*. 2018.

226. **De Souza, W. and Attis, M.** Subpellicular Microtubules in Apicomplexa and Trypanosomatids. [book auth.] W. de Souza. *Structures and Organelles in Pathogenic Protists*. Berlin : Springer, 2010.

227. **Pouvelle, B., et al.** Taxol arrests the development of blood-stage Plasmodium falciparum in vitro and Plasmodium chabaudi adami in malaria-infected mice. *J. Clin. Invest*. 1994.

228. **Liu, J., et al.** An ensemble of specifically targeted proteins stabilizes cortical microtubules in the human parasite toxoplasma gondii. *Mol. Biol. Cell*. 2016.

229. **Chaaban, S. and Brouhard, G. J.** A microtubule bestiary: structural diversity in tubulin polymers. *Mol. Biol. Cell*. 2017.

230. **Bannister, L. H. and Mitchell, G. H.** he role of the cytoskeleton in Plasmodium falciparum merozoite biology: an electron-microscopic view. *Ann. Trop. Med. Parasitol*. 1995.

231. **Simon, C. S., et al.** An extended DNA-free intranuclear compartment organizes centrosome microtubules in malaria parasites . *Life Sci. Alliance*. 2021.

232. **Aikawa, M. and Beaudoin, R. L.** Studies on nuclear division of a malarial parasite under pyrimethamine treatment. *J. Cell Biol*. 1968.

233. **Schrevel, J., Asfaux-Foucher, J. G. and Bafort, J. M.** Ultrastructural study of multiple mitoses during sporogony of Plasmodium b. berghei. *J. Ultrastruct. Res*. 1977.

234. **Roostalu, J. and Surrey, T.** Microtubule nucleation: beyond the template. *Nat. Rev. Mol. Cell Biol*. 2017.

235. **Kollman, J. M., et al.** Microtubule nucleation by γ-tubulin complexes. *Nat. Rev. Mol. Cell Biol*. 2011.

236. **Sanchez, A. D. and Feldman, J. L.** Microtubule-organizing centers: from the centrosome to non-centrosomal sites. *Curr. Opin. Cell Biol*. 2016.

237. **Boveri, T.** Zellen-Studien: Ueber die Natur der Centrosomen. 1901.

238. **Liffner, B., et al.** Atlas of Plasmodium falciparum intraerythrocytic development using expansion microscopy . *Elife*. 2023.

239. **Fowler, R. E., et al.** Microtubule associated motor proteins of Plasmodium falciparum merozoites. *Mol. Biochem. Parasitol*. 2001.

240. **Sinden, R. E., et al.** The flagellum in malarial parasites. *Current Opinion in Microbio*. 2010.

241. **Dantas, T. J., Daly, O. M. and Morrison, C. G.** Such small hands: The roles of centrins/caltractins in the centriole and in genome maintenance. *Cell. and Mol. Life Sci*. 2012.

242. **Roques, M., et al.** Plasmodium centrin Pb CEN-4 localizes to the putative MTOC and is dispensable for malaria parasite proliferation. *Biol Open*. 2019.

243. **Talman, A. M., et al.** Proteomic analysis of the Plasmodium male gamete reveals the key role for glycolysis in flagellar motility . *Malar. J*. 2014.

244. **Francia, M. E., Dubremetz, J. F. and Morrissette, N. S.** Basal body structure and composition in the apicomplexans Toxoplasma and Plasmodium. *Cilia*. 2015.

245. **Marques, S. R., et al.** An essential role of the basal body protein SAS-6 in Plasmodium male gamete development and malaria transmission. *Cell Microbiol*. 2015.

246. **Zeeshan, M., et al.** Plasmodium SAS4: basal body component of male cell which is dispensable for parasite transmission. *Life Sci. Alliance*. 2022.

247. **Koreny, L., et al.** Molecular characterization of the conoid complex in Toxoplasma reveals its conservation in all apicomplexans, including Plasmodium species. *PLoS Biol*. 2021.

248. **Canning, E. U. and Sinden, R. E.** The organization of the ookinete and observations on nuclear division in oocysts of Plasmodium berghei. *Parasitol*. 1973.

249. *Cryoelectron tomography reveals periodic material at the inner side of subpellicular microtubules in apicomplexan parasites*. **Cyrklaff, M., et al.** 2007, Journal of experimental Medicine.

250. **Kaneko, I., et al.** Genome-wide identification of the target genes of AP2-O, a Plasmodium AP2-family transcription factor. *PLoS Pathog*. 2015.

251. **Engelberg, K., et al.** The apical annuli of Toxoplasma gondii are composed of coiled-coil and signalling proteins embedded in the inner membrane complex sutures. *Cell Microbiol*. 2020.

252. **Collier, S., et al.** Plasmodium falciparum formins are essential for invasion and sexual stage development. *nat. com. bio*. 2023.

253. *Identification of novel inner membrane complex and apical annuli proteins of the malaria parasite Plasmodium falciparum*. **Wichers, J. S., et al.** 2021, Cell. Micro.

254. *A Microtubule-Associated Protein Is Essential for Malaria Parasite Transmission*. **Wichers-Misterek, J. S., et al.** 2023, Molecular Biology.

255. **Birnbaum, J., et al.** A genetic system to study Plasmodium falciparum protein function. *Nat. Methods*. 2017.

256. *CRISPR/Cas9-engineered inducible gametocyte producer lines as a valuable tool for Plasmodium falciparum malaria transmission research*. **Boltryk, S. D., et al.** 2021, Nature Communication.

257. **May, D. G., et al.** Comparative Application of BioID and TurboID for Protein-Proximity Biotinylation. *Cells*. 2020.

258. **Alvarez-Jarreta, J., et al.** VEuPathDB: the eukaryotic pathogen, vector and host bioinformatics resource center in 2023. *Nucleic Acids Research*. 2024.

259. **Zeeshan, M., et al.** Kinesin-8B controls basal body function and flagellum formation and is key to malaria transmission. *Life Sc. All*. 2019.

260. **Zeeshan, M., et al.** Key roles for kinesin-13 and kinesin-20 in malaria parasite proliferation, polarity and transmission revealed by genome-wide functional analysis. *PLoS Biol*. . 2022.

261. **Yang, S., et al.** EB1 decoration of microtubule lattice facilitates spindle-kinetochore lateral attachment in Plasmodium male gametogenesis. *Nature Com*. 2023.

262. **Tran, J. Q., et al.** SPM1 stabilizes subpellicular microtubules in Toxoplasma gondii. *Eukar. Cell*. 2012.

263. **Schmidt, S., et al.** The Kelch13 compartment contains highly divergent vesicle trafficking proteins in malaria parasites. *PLoS Pathog*. 2023.

264. **Kumar, B., et al.** Metacaspase-3 of Plasmodium falciparum: An atypical trypsin-like serine protease. *Int. J. Biol. Macromol.* 2019.

265. **Zhang, Y.** Characterization of novel inner membrane complex suture proteins of Plasmodium falciparum. *Unpublished.* 2022.

266. **Winkler, W. C., et al.** Control of gene expression by a natural metabolite-responsive ribozyme. *Nature.* 2004.

267. **Prommana, P., et al.** Inducible knockdown of Plasmodium gene expression using the glmS ribozyme. *PLoS One.* 2013.

268. **Silvestrini, F., et al.** Protein Export Marks the Early Phase of Gametocytogenesis of the Human Malaria Parasite Plasmodium falciparum. *Mol. Cell. Proteomics.* 2010.

269. **Goncalves, J., Nolasco, S., et al.** TBCCD1, a new centrosomal protein, is required for centrosome and Golgi apparatus positioning. *EMBO Rep.* 2010.

270. **Stephan, A., et al.** n essential quality control mechanism at the eukaryotic basal body prior to intraflagellar transport. *Traffic* . 2007.

271. *Disrupting assembly of the inner membrane complex blocks Plasmodium falciparum sexual stage development.* **Schneider, M. P., et al.** 2017, PLoS Path.

272. **Tawk, L., et al.** Phosphatidylinositol 3-phosphate, an essential lipid in Plasmodium, localizes to the food vacuole membrane and the apicoplast. *Eukaryot. Cell.* 2010.

273. **Smith, R. C., Vega-Rodriguez, J. and Jacobs-Lorena, M.** The Plasmodium bottleneck: malaria parasite losses in the mosquito vector. *Mem. Inst. Oswaldo Cruz.* 2014.

274. **Joice, R., Nilsson, S. K. and Montgomery, J.** Plasmodium falciparum transmission stages accumulate in the human bone marrow. *Sci. Transl. Med.* 2014.

275. **Weingarten, M. D., et al.** A protein factor essential for microtubule assembly. *Proc. Natl. Acad. Sci.* 1975.

276. **Dehmelt, L. and Halpain, S.** The MAP2/Tau family of microtubule-associated proteins. *Gen. Biol.* 2004.

277. **Kumar, N., Aikawa, M. and Grotendorst, C.** Plasmodium gallinaceum: critical role for microtubules in the transformation of zygotes into Ookinetes. *Exp. Parasitol.* 1985.

278. **Fennell, B. J., et al.** Effects of the ntimitotic natural product dolastatin 10, and related peptides, on the human malarial parasite Plasmodium falciparum. *J. Antimicrob. Chemother.* . 2003.

279. **Fennell, B. J., et al.** Cellular and molecular actions of dinitroaniline and phosphorothioamidate herbicides on Plasmodium falciparum: Tubulin as a specific antimalarial target. *Mol. and Biochem. Parasitol.* 2006.

280. **Chawla, J., Oberstaller, J. and Adams, J. H.** Targeting Gametocytes of the Malaria Parasite Plasmodium falciparum in a Functional Genomics Era: Next Steps. *Pathogens*. 2021.

281. **Hentzschel, F., et al.** Microtubule inner proteins of Plasmodium are essential for transmission of malaria parasites. *Cell Bio*. 2025.

282. **Zeeshan, M., et al.** Plasmodium ARK2 and EB1 drive unconventional spindle dynamics, during chromosome segregation in sexual transmission stages. *Nature Com*. 2023.

283. **Liu, T., et al.** Mechanochemical tuning of a kinesin motor essential for malaria parasite transmission. *Nature Com*. 2022.

284. **Zeeshan, M., et al.** Genome-wide functional analysis reveals key roles for kinesins in the mammalian and mosquito stages of the malaria parasite life cycle. *PLoS Biol*. 2022.

285. **Kim, D. I., et al.** Probing nuclear pore complex architecture with proximity-dependent biotinylation. *Proc. Natl. Acad. Sci*. 2014.

286. **Rees-Channer, R. R., et al.** Dual acylation of the 45kDa gliding-associated protein (GAP45) in Plasmodium falciparum merozoites. *Mol. Biochem. Parasitol*. 2006.

287. **Frénal, K., et al.** Functional dissection of the apicomplexan glideosome molecular architecture. *Cell Host Microbe*. 2010.

288. **Bullen H. E., Tonkin, C. J., et al.** A novel family of apicomplexan glideosome-associated proteins with an inner membrane-anchoring role. *J. Biol. Chem*. 2009.

289. **Harding, C. R., et al.** Alveolar proteins stabilize cortical microtubules in Toxoplasma gondii. *Nature Com*. . 2019.

290. **Safavi, S. L.** Functional characterization of putative novel IMC suture proteins in Plasmodium. *Unpublished*. 2021.

291. **Qian, P., et al.** Inner membrane complex proteomics reveals a palmitoylation regulation critical for intraerythrocytic development of malaria parasite. *eLife*. 2022.

292. **Reiniger, L., et al.** An essential Aurora-related kinase transiently associates with spindle pole bodies during Plasmodium falciparum erythrocytic schizogony. *Mol. Biolo*. 2010.

293. **Voß, J., et al.** Malaria parasite centrins can assemble by Ca2+-inducible condensation. *PLoS Path*. 2023.

294. **R., Marques S., et al.** An essential role of the basal body protein SAS-6 in Plasmodium male gamete development and malaria transmission. *Cell Microbiol*. 2015.

295. **Qian, P., et al.** Apical anchorage and stabilization of subpellicular microtubules by apical polar ring ensures Plasmodium ookinete infection in mosquito. *Nature Com*. 2022.

296. **Slep, K.C.** The role of TOG domains in microtubule plus end dynamics. *Biochem. Soc. Trans.* 2009.

297. **Al-Bassam, J. and Chang, F.** Regulation of microtubule dynamics by TOG-domain proteins XMAP215/Dis1 and CLASP. *Trends Cell Biol.* 2011.

298. **Fox, J. C., et al.** The XMAP215 family drives microtubule polymerization using a structurally diverse TOG array. *Mol. Biol. Cell.* 2014.

299. **Usui, T., et al.** The XMAP215 homologue Stu2 at yeast spindle pole bodies regulates microtubule dynamics and anchorage. *EMBO J.* 2003.

300. **Hahn, I., et al.** Tau, XMAP215/Msps and Eb1 co-operate interdependently to regulate microtubule polymerisation and bundle formation in axons. *PLoS Genet.* 2021.

301. **Miller, M. P., Asbury, C. L. and Biggins, S.** A TOG protein confers tension sensitivity to kinetochore-microtubule attachments. *Cell.* 2016.

302. **Sabo, J., et al.** CKAP5 enables formation of persistent actin bundles templated by dynamically instable microtubules. *Curr. Biol.* 2023.

303. **Frenal, K., Krishnan, A. and Soldati-Favre, D.** The actomyosin systems in Apicomplexa. *Adv. Exp. Med. Biol.* 2020.

304. **Chen, C-T., et al.** Compartmentalized Toxoplasma EB1 bundles spindle microtubules to secure accurate chromosome segregation. *Mol. Biol. Cell.* 2015.

305. **Tirnauer, J. S. and Bierer, B. E.** EB1 proteins regulate microtubule dynamics, cell polarity, and chromosome stability. *J. Cell Biol.* 2000.

306. **Nehlig, A., et al.** Regulation of end-binding protein EB1 in the control of microtubule dynamics. *Cell. Mol. Life Sci.* 2017.

307. **Koarova, Y. A., et al.** Cytoplasmic linker proteins promote microtubule rescue in vivo. *J. Cell. Biol.* 2002.

308. **Mimory-Kiyosue, Y., et al.** CLASP1 and CLASP2 bind to EB1 and regulate microtubule plus-end dynamics at the cell cortex. *J. Cell. Biol.* 2005.

309. **Kruse, R., et al.** Characterization of the CLASP2 Protein Interaction Network Identifies SOGA1 as a Microtubule-Associated Protein. *Mol. Cell. Proteomics.* 2017.

310. **de Willige, D., et al.** Cytolinker Gas2L1 regulates axon morphology through microtubule-modulated actin stabilization. *EMBO Rep.* 2019.

311. **Jia, X., et al.** CLASP-mediated competitive binding in protein condensates directs microtubule growth. *Nature Com.* 2024.

312. **Majumdar, S., et al.** An isolated CLASP TOG domain suppresses microtubule catastrophe and promotes rescue. *Mol. Biol. Cell.* 2018.

313. **Gareil, N., et al.** An unconventional TOG domain is required for CLASP localization. *Curr. Biol.* 2023.

314. **Hur, E-M., et al.** GSK3 controls axon growth via CLASP-mediated regulation of growth cone microtubules. *Genes Dev.* 2011.

315. **Sayas, C. L., et al.** Distinct Functions for Mammalian CLASP1 and -2 During Neurite and Axon Elongation. *Front. Cell Neurosci.* 2019.

316. **Alder, A., et al.** Functional inactivation of Plasmodium falciparum glycogen synthase kinase GSK3 modulates erythrocyte invasion and blocks gametocyte maturation. *J. Biol. Chem.* . 2022.

317. **Ambrose, J. C., et al.** The Arabidopsis CLASP Gene Encodes a Microtubule-Associated Protein Involved in Cell Expansion and Division. *Plant Cell.* 2007.

318. **Zhang, L. and Ambrose, C.** CLASP balances two competing cell division plane cues during leaf development. *Nature Plants.* 2022.

319. **Al-Bassam, J., et al.** CLASP promotes microtubule rescue by recruiting tubulin dimers to the microtubule. *Dev. Cell.* 2010.

320. **Lindeboom, J. J., et al.** CLASP stabilization of plus ends created by severing promotes microtubule creation and reorientation. *J. Cell. Biol.* 2019.

321. **Morano, A. A., Ali, I. and Dvorin, J. D.** Elucidating the spatio-temporal dynamics of the Plasmodium falciparum basal complex. *PLoS Pathogens.* 2024.

322. **Saini, E., et al.** Plasmodium falciparum PhIL1-associated complex plays an essential role in merozoite reorientation and invasion of host erythrocytes. *PLoS Pathog.* 2021.

323. **Omorou, R., et al.** Protocols for Plasmodium gametocyte production in vitro: an integrative review and analysis. *Parasites Vectors.* 2022.

324. **Billker, O., et al.** Calcium and a calcium-dependent protein kinase regulate gamete formation and mosquito transmission in a malaria parasite. *Cell.* 2004.

325. **Downs, W. G.** Infections of chicks with single parasites of Plasmodium gallinaceum Brumpt. *Am. J. Hyg.* 1947.

326. **Paul, R. E. L., Brey, P. T. and Robert, V.** Plasmodium sex determination and transmission to mosquitoes. *Trends Prarasitol.* 2002.

327. **Tadesse, F. G., et al.** Gametocyte Sex Ratio: The Key to Understanding Plasmodium falciparum Transmission? *Trends Parasitol.* 2019.

328. **Bradley, J., et al.** Predicting the likelihood and intensity of mosquito infection from sex specific Plasmodium falciparum gametocyte density. *eLife.* 2018.

329. **James, S. P.** Some general results of a study of induced malaria in England. 1931.

330. **Reuling, I. J., et al.** A randomized feasibility trial comparing four antimalarial drug regimens to induce Plasmodium falciparum gametocytemia in the controlled human malaria infection model. *eLife.* 2018.

331. **Tiburcio, M., et al.** Specific expression and export of the Plasmodium falciparum Gametocyte EXported Protein-5 marks the gametocyte ring stage. *Malar. J.* 2015.

332. **Li, J., et al.** Disruption of Plasmodium falciparum kinetochore proteins destabilises the nexus between the centrosome equivalent and the mitotic apparatus. *Nature.* 2024.

333. *Expansion microscopy of Plasmodium gametocytes reveals the molecular architecture of a bipartite microtubule organisation centre coordinating mitosis with axoneme assembly.* **Rashpa, R. and Brochet, M.** 2022, PLOS Pathogens.

334. **Chaaban, S. and Brouhard, G. J.** A microtubule bestiary: structural diversity in tubulin polymers. *Mol. Biol. Cell.* 2017.

335. **Wade, R. H., Chretien, D. and D., Job.** Characterization of microtubule protofilament numbers: How does the surface lattice accommodate? *J. Mol. Biol.* 1990.

336. **Donhauser, Z. J., Jobs, W. B. and Binka, E. C.** Mechanics of Microtubules: Effects of Protofilament Orientation. *Biophys. J.* . 2010.

337. **Mani, N., Wijeratne, S. S. and Subramanian, R.** Micron-scale geometrical features of microtubules as regulators of microtubule organization. *eLife.* 2021.

338. **Hanahan, D.** Studies on transformation of Escherichia coli with plasmids. *J. Mol. Biol.* 1983.

339. **Sambrook, J., Fritsch, E. F. and Maniatis, T.** *Molecular cloning: a laboratory manual.* US : University of Texas South Western Medical Center, 1989.

340. **Mesén-Ramírez, P., et al.** Malaria parasite HOPS/CORVET complexes are critical for endocytosis and invasion organelles function. *PloS.* 2025.

341. **BioLabs, New England.** Restriction Digest Protocol. [Online] New England BioLabs, Januar 2025. https://www.neb.com/en/protocols/2018/07/30/restriction-digest-protocol?srsltid=AfmBOooShbEjlxoHhf6RhVV2e3-bYhGE8wfqqpRZyq9ykixJmxlqIOt-.

342. **Trager, W. and Jensen., J. B.** Human malaria parasites in continuous culture. *Science.* 1976.

343. **Wu, Y., et al.** Transfection of Plasmodium falciparum within human red blood cells. *PNAS.* 1995.

344. **Moon, R. W., et al.** Adaptation of the genetically tractable malaria pathogen Plasmodium knowlesi to continuous culture in human erythrocytes. *PNAS.* 2012.

345. **Ganesan, S. M., et al.** Yeast dihydroorotate dehydrogenase as a new selectable marker for Plasmodium falciparum transfection. *Mol Biochem Parasitol.* 2011.

346. **SOP University Edinburgh:** Culturing Plasmodium falciparum. 2007.

347. Lambros, C. and Vanderberg, J. P. Synchronization of Plasmodium falciparum erythrocytic stages in culture. *J Parasitol.* 1979.

348. Malleret, B., et al. A rapid and robust tri-color flow cytometry assay for monitoring malaria parasite development. *Sci Rep*. 2011.

349. Wiśniewski, J. R. Filter-Aided Sample Preparation for Proteome Analysis. *Methods Mol Biol*. 2018.

350. Giemsa, G. Eine vereinfachung und vervollkommnung meiner Methylenazur-Methylenblau-Eosin-Färbemethode zur Erzielung der Romanowsky-Nocht'schen Chromatinfärbung. *Zentralblatt für Bakteriologie, Parasitenkunde, Infektionen und Hygiene*. 1904.